RESEARCH LABORATORIES
Air Resources Laboratories
Silver Spring, Maryland
December 1967

Atmospheric Transport and Diffusion in the Planetary Boundary Layer

Technical Memorandum RLTM-ARL 3

U.S. DEPARTMENT OF COMMERCE / ENVIRONMENTAL SCIENCE SERVICES ADMINISTRATION

U.S. DEPARTMENT OF COMMERCE
ENVIRONMENTAL SCIENCE SERVICES ADMINISTRATION
RESEARCH LABORATORIES

Research Laboratories Technical Memorandum -ARL 3

ATMOSPHERIC TRANSPORT AND DIFFUSION IN THE PLANETARY BOUNDARY LAYER

Semiannual Research Program Review
January - June 1967
for the Division of Reactor Development and Technology
U. S. Atomic Energy Commission

ENVIRONMENTAL METEOROLOGY BRANCH
TECHNICAL MEMORANDUM NO. 3

SILVER SPRING, MARYLAND
DECEMBER 1967

Table of Contents

Preface

In accordance with the letter of agreement of June 29, 1966, with the U. S. Atomic Energy Commission, Division of Reactor Development and Technology, Environmental and Sanitary Engineering Branch, the Air Resources Laboratories have continued their study of atmospheric transport and diffusion in the planetary boundary layer, micrometeorology, diffusion climatology, and the application of this work to the disposal of radioactive waste gases to the atmosphere. The research is technically administered and supervised through the Air Resources Environmental Laboratory of the Air Resources Laboratories. The work is performed at the Air Resources Laboratories Headquarters in Silver Spring, Maryland, and at the Air Resources Idaho Falls Laboratory, National Reactor Testing Station, Idaho. Any inquiry on the research being performed should be directed to the editor, Isaac Van der Hoven, Chief, Air Resources Environmental Laboratory, Air Resources Laboratories, Environmental Science Services Administration, 8060 13th. Street, Silver Spring, Maryland 20910.

ATMOSPHERIC TRANSPORT AND DIFFUSION

IN THE PLANETARY BOUNDARY LAYER

AIR RESOURCES LABORATORIES SEMIANNUAL RESEARCH PROGRAM REVIEW
FOR THE ENVIRONMENTAL AND SANITARY ENGINEERING BRANCH
DIVISION OF REACTOR DEVELOPMENT AND TECHNOLOGY
U. S. ATOMIC ENERGY COMMISSION

JANUARY - JUNE 1967

1.0 RESEARCH AT AIR RESOURCES LABORATORIES HEADQUARTERS, SILVER SPRING, MD.

1.1 Low Altitude Constant Volume Balloon (Tetroon)Trajectories

(This program is a joint effort carried out by personnel of the Air Resources Laboratories in Silver Spring, Md., and in field offices. Support is provided jointly by the Atomic Energy Commission and the Public Health Service.)

A paper, based on the tetroon position data obtained during the field experiments in Idaho in 1966, entitled "A Preliminary Lagrangian Study of Helical Circulations in the Planetary Boundary Layer," is undergoing external review. The crux of the paper is that at the National Reactor Testing Station (NRTS) during the afternoon counter-rotating longitudinal roll vortices, or helices, of about 2-km diameter frequently exist. These helices appear to be driven primarily by buoyancy. Work will continue on an analysis of the development of these circulations during the morning hours.

The report on the New York City tetroon experiment of 1965 has been completed. Emphasis in this paper is on the vertical velocities derived from the tetroon flights over the metropolitan area, including the magnitude of the vertical velocity as a function of stability, the variation of the vertical-velocity periodicity with stability, and the vertical diffusion derived through the use of Taylor's expression.

A summarization has been prepared of continuous and instantaneous point source diffusion as derived from the available sequential and simultaneous tetroon releases to date. For downwind distances from 5 to 50 km the instantaneous and continuous point source lateral diffusion is proportional, respectively, to the 0.8 and 0.9 power of distance. The continuous lateral diffusion is proportional to the release interval in hours to the 0.3 power. It is also shown that on this scale at this height, the horizontal eddy diffusivity varies from 10^6 to 10^7 cm^2 sec^{-1} and the eddy dissipation averages 1 cm sec^{-3}.

A study of tetroon ascent rates up to the mean floating level yields drag coefficients in the range of 0.5 to 1.0 and appears to vary with Reynolds number. The applicability of the squared power of the velocity in the expression for drag coefficient is under question.

Preliminary work is being carried out on a pressure element for attachment to the transponder. A "Clark Variable Resistor" has been subjected to force tests. Performance is only fair in that the repeatability is poor and there is some hysteresis.

1.2 Natural Radioactivity (Radon) Diffusion Studies

(Support for this work is provided jointly by the Atomic Energy Commission and the Public Health Service).

Radon measurements, at the U. S. Naval Laboratory (urban) in Washington, D. C., and at the Tysons Corner tower facility (suburban) and at Sterling (rural) in Virginia, were terminated in March 1967. This will complete the data acquisition in the Washington area for this project.

An analysis of diurnal, monthly, and seasonal mean atmospheric concentrations of radon, at three sites at four different heights above ground up to 91 m, indicates a homogeneity of horizontal distribution of radon over a distance of 32 km during much of the daytime period. Seasonal and annual mean radon concentrations expressed in picocuries per cubic meter of air (p Ci m^{-3}) are shown in table 1 for the three sampling sites.

Further analysis of the temporal-spatial variations of radon concentration, with respect to meteorological conditions, indicates that the concentration of radon in air near the ground is most responsive to atmospheric dilution-specifically, vertical mixing. The effects of advection, changes in radon emanation from the ground, and atmospheric scavenging processes pose a problem for evaluating vertical mixing or general atmospheric dilution only during certain unique meteorological conditions over relatively short time periods. In general these studies have supported the contention that by utilizing appropriate averaging and sampling periods measurements of the atmospheric content of natural radioactivity can provide a reliable and inexpensive means for assessing mesoscale vertical mixing rates and dilution in the lower atmosphere. A report of the radon measurements taken in the urban-rural environment of Washington, D. C., has been submitted for editorial review.

TABLE 1. Seasonal and Annual Mean Radon Concentrations (pCi m^{-3}) for Washington, D. C., Area Stations

Site	Height Above Ground (meters)	Winter	Spring	Summer	Fall	Annual
U. S. Naval Research Lab. Washington, D. C.	7	December 1965 - February 1967				
0900 LST		201	103	222	219	191
1200 LST		144	74	144	153	132
1500 LST		129	65	114	118	109
Sterling, Virginia	15	December 1965 - February 1967				
0900 LST		199	111	253	216	208
1200 LST		124	66	144	111	113
1500 LST		109	45	101	85	85
Tysons Corner, Virginia	1	September 1963 - January 1966				
0900 LST		138	84	147	161	139
1200 LST		114	54	96	127	99
1500 LST		133	---	115	63	(105)
Tysons Corner, Virginia	91	September 1963 - January 1966				
0900 LST		108	71	126	127	113
1200 LST		92	44	88	108	86
1500 LST		69	---	98	42	(74)

( ) denotes average of only three seasons

The vertical profile data observed at the Tysons Corner tower facility will be analyzed next. Following this, a correlation of radon concentrations and air quality data will be made to substantiate that high atmospheric concentrations of natural radioactivity can be an index of air pollution potential conditions in the atmosphere.

1.3 Atmospheric Transport and Diffusion at Coastal Sites

A study was made to determine the effect of adjacent land and large water surfaces upon atmospheric transport and diffusion of effluents released at the boundary between the two surfaces. An evaluation of the appropriate literature indicated that overland atmospheric diffusion rates were three times more rapid on the average than overwater diffusion when the water is colder than air temperatures over land. The transport didstance required to complete the transition from overwater to overland diffusion was found to be a function of initial plume height, wind speed, and vertical temperature profile. Figure 1 is a graphical representation of the relationship with the height (H) in meters, wind speed ($\bar{u}$) in meters/second and the vertical potential temperature profile within the inversion over the water ($\Delta\theta$) in ^{o}C. This empirical relationship fits very well the recent measurements at the Millstone Point site reported by Collins and Bowne (1967) where for 17 cases of onshore gradient, the height of the mixed inland turbulent layer reached the stack height (125 m) at an average distance of 3000 m from the beach with an average value of $\bar{u} = 4.5$ m/sec and $\Delta\theta = 2.5^{o}C$.

It was concluded that the computation of air trajectories from fixed-point wind measurements at the coastal site is largely indeterminate when the large-scale pressure gradient is weak and local effects such as a sea breeze circulation predominate. A uniform coastline such as the Florida coast tends to produce consistent trajectory reversals as opposed to the more complex trajectories observed off the Los Angeles coast. Strong large-scale pressure gradients tend to result in straight-line trajectories and can be estimated more reliably from fixed-point wind measurements.

1.4 Boundary Layer Turbulence

A study of the structure of the vertical-wind component turbulence was conducted during October 1966 at the C. W. Thornthwaite and Associates marsh site near Bridgeton, N. J. This study was under the supervision of Professors Blackadar and Panofsky of the Pennsylvania State University. Three main objectives were established for investigation: the first was a direct comparison of the Thornthwaite propeller anemometer, (Thornthwaite et al., 1961) and a continuous-wave ultrasonic

anemometer of the type proposed by Kaimal (1963); the second was to compare turbulence statistics measured in the boundary layers of the cut ($\sim$4 cm) and uncut ($\sim$40 cm) grass. The third objective was to examine the intermittent structure of the boundary zone separating the two flow regimes. The marsh area was essentially flat with a uniform grass cover in all directions for at least 800 m. This measurement program also served as a final field check for this particular ultrasonic anemometer (UA 2/3) before its shipment to ARFRO, NRTS, Idaho, where it is to be used in the CERT program.

Analysis of the data, taken to satisfy the first two objectives, has been completed, and an interim report is being prepared. In the four cases where the propeller anemometer was compared with the sonic anemometer the standard deviations of the vertical wind velocity computed from the propeller anemometer were approximately one-half the value derived from the sonic. Power spectrum estimates of both signals showed the largest differences to exist at frequencies above 0.5 Hz. An average Richardson number (1 m) of -0.01 was computed for the four examples. The average value of the ratio of the standard deviation to the mean wind speed at the level of measurement ($\sigma_w/\bar{u}$) for sonic anemometer measurements was 0.098, which agrees well with the value of .090 computed from Brookhaven tower data (Deacon, 1959), and 0.096 computed using a reference level wind at 2 m (Pasquill, 1962).

Power spectra estimates were calculated from all data over a frequency band bounded by 0.01 Hz and 8 Hz. A negative 5/3 power law was observed in five of 10 cases (fig. 2). The low frequency extent of this region was approximately 0.8 normalized frequency ($nz/\bar{u}$) units where n is the frequency (Hz), $\bar{u}$ is the mean wind speed (cm sec^{-1}) at the height of the wind observations z (cm). This value was larger than the value of .5 given by MacCready (1962). Further statistical analysis will be carried out to distinguish the situations in which a negative 5/3 law was observed from those where it was not.

Analysis of the intermittency will be evaluated by calculating the statistical distributions and the higher moments of the measured vertical velocity values at two heights. Further studies, using wind and temperature measurements made at NRTS (summer of 1965) are planned to define the appropriate sampling and averaging time for accurate determinations of the stress and heat flux. Our effort will concentrate on the low frequency end of this problem, and it is our hope that in the near future Fast Fourier Transform techniques can be used to obtain more accurate power spectrum estimates.

2.0 RESEARCH AT NATIONAL REACTOR TESTING STATION, IDAHO

2.1 EBR-II Diffusion Studies

In the event of an accidental release of airborne material from a reactor, measurements of concentration immediately downwind from the reactor complex are necessary to determine the effect of the complex on the diffusion. Two types of experiments are possible: field studies using a tracer mate ial and wind tunnel scale model tests. A wind tunnel scale model approach to this problem was carried out by Halitsky et al. (1963).

A field study program was conducted at the NRTS, in which the dispersion of a fluorescent tracer from a height of 1 m downwind of a reactor complex was measured. This study was designed to give direct and reliable data. The principal purpose was to determine diffusion patterns around the EBR-II reactor from a release location on the surface of the containment vessel. The reactor complex consists of a reactor containment building, plus a number of smaller buildings throughout the area (figure 3). The building height variation is from 4 to 38 m; the power plant and containment dome are 38 and 29 m high, respectively. A total of 15 surface tracer releases and nine stack releases was made. Eight surface releases were conducted in unstable atmospheres and seven during inversion conditions. The tracer material was collected and analyzed at 90 sampling stations for 30-min periods. The effects of the reactor complex upon the horizontal and vertical wind direction variances were also measured.

A series of six 6-m towers were located at 600 m upwind and 50, 100, 200, 400 and 600 m downwind. A NRTS bivane and a Beckman and Whitley cup anemometer were installed at the 6-m level of each tower. The tower at 50 m also had temperatures and dew-points at 1/2, 1, and 2 m. A 74-m tower is also located at the right edge of the 400-m arc with wind velocity and direction sensors at 6, 46, and 74 m and temperature elements at the 2-, 15-, 46-, and 74-m levels.

A meteorological summary of the 15 releases is shown in table 2. Eight tests were conducted during lapse conditions and seven tests with an inversion. Wind speeds ranged from a minimum of 1.7 m/sec at the 50-m arc to a maximum of 10.5 m/sec at the 600-m arc during the tests. There is evidence of a heat island near the reactor complex since the tower at 50 m indicated only lapse to neutral conditions. This can also be indicative as to the amount of diffusion measured at the intermediate arcs.

Table 2 . Meteorological Data for EBR-II Diffusion Tests at 6-m Height (30-min Samples)

Tower	Test 2 σ_θ	σ_ϕ	$\bar{u}$	ΔT	ΔT_1	Test 3 σ_θ	σ_ϕ	$\bar{u}$	ΔT	ΔT_1	Test 4 σ_θ	σ_ϕ	$\bar{u}$	ΔT	ΔT_1
600_U	5.7	3.6	5.1	-3.4	-0.6	8.9	4.2	6.0	-1.5	-0.8	11.3	3.2	5.8	+1.7	-0.9
50_D	57.0	16.9	1.8			21.6	11.8	2.0			37.1	13.9	3.3		
100_D	30.5	14.6	2.8			14.2	10.1	4.1			26.6	13.7	3.9		
200_D	8.9	8.3	4.8			10.9	7.6	5.1			15.2	7.5	4.6		
400_D	6.2	5.5	4.8			9.1	4.5	6.1			11.8	3.8	5.5		
600_D	5.8	3.5	5.0			9.0	4.1	6.1			11.12	3.4	5.7		
	Test 5					Test 6					Test 7				
600_U	7.3	3.7	6.0	-0.3	-0.7	9.4	3.9	5.7	-0.2	-0.2	5.9	3.5	8.0	+0.9	-0.4
50_D	22.9	10.8	3.5			53.5	14.4	2.8			35.0	16.8	3.7		
100_D	16.4	10.3	4.3			27.9	13.3	3.5			17.6	15.1	5.5		
200_D	11.1	7.4	5.4			11.0	6.7	5.2			11.4	7.5	5.8		
400_D	7.3	4.5	6.1			9.4	4.6	5.5			7.2	5.3	7.2		
600_D	7.2	3.8	6.2			9.3	4.0	5.6			6.0	3.5	8.0		

σ_θ - Horizontal wind direction standard deviation (degrees)

σ_ϕ - Vertical wind direction standard deviation (degrees)

$\bar{u}$ - Wind speed (m/sec^{-1})

ΔT - (°F) temperatures at 400-m arc (74 m - 2 m)

ΔT_1 - (°F) temperatures at 50-m arc (6 m - 1/2 m)

M - Missing

U - Upwind

D - Downwind

Table 2 . (Continued) Meteorological Data for EBR-II Diffusion Tests at 6-m Height (30-min Samples)

	Test 8					Test 9					Test 10				
Tower	σ_θ	σ_ϕ	$\bar{u}$	ΔT	ΔT_1	σ_θ	σ_ϕ	$\bar{u}$	ΔT	ΔT_1	σ_θ	σ_ϕ	$\bar{u}$	ΔT	ΔT_1
600_U	8.1	3.9	6.1	+0.8	-0.5	8.6	4.4	4.2	+0.5	-0.7	6.9	4.3	5.9	+0.7	-0.6
50_D	17.2	13.2	3.7			27.6	11.7	2.2			15.8	11.1	3.7		
100_D	14.7	12.0	4.3			13.9	9.2	2.7			11.6	9.5	4.3		
200_D	M	M	5.1			M	M	3.1			M	M	5.0		
400_D	8.1	4.3	5.7			8.5	4.1	3.8			6.6	4.2	5.6		
600_D	8.0	4.0	6.0			8.7	4.5	4.0			6.9	4.2	5.8		
	Test 11					Test 12					Test 13				
600_U	11.9	4.0	9.7	-5.0	-1.4	10.8	4.1	9.8	-4.3	-0.9	11.4	3.6	10.5	-3.8	-0.7
50_D	30.9	13.2	5.4			33.0	13.9	4.7			29.7	13.2	5.5		
100_D	19.7	10.9	6.5			21.9	11.0	6.2			19.8	9.4	6.9		
200_D	11.8	6.7	7.9			11.4	6.5	8.0			11.0	6.0	8.6		
400_D	10.6	4.0	9.0			10.9	3.7	9.4			11.5	4.0	9.3		
600_D	12.1	4.0	9.6			10.9	4.1	9.7			11.5	3.7	10.4		

σ_θ - Horizontal wind direction standard deviation (degrees)

σ_ϕ - Vertical wind direction standard deviation (degrees)

$\bar{u}$ - Wind speed (m/sec^{-1})

ΔT - (°F) temperatures at 400-m arc (74 m - 2 m)

ΔT_1 - (°F) temperatures at 50-m arc (6 m - 1/2 m)

M - Missing

U - Upwind

D - Downwind

Table 2 . (Continued) Meteorological Data for EBR-II Diffusion Tests at 6-m Height (30-min Samples)

	Test 14					Test 15					Test 16				
Tower	σ_θ	σ_ϕ	$\bar{u}$	ΔT	ΔT_1	σ_θ	σ_ϕ	$\bar{u}$	ΔT	ΔT_1	σ_θ	σ_ϕ	$\bar{u}$	ΔT	ΔT_1
600_U	9.3	4.1	10.3	-3.0	-0.7	16.6	2.7	4.0	+6.7	0.0	4.6	4.0	6.5	+1.0	-0.7
50_D	25.2	11.9	5.0			24.7	12.6	1.7			31.2	15.3	2.1		
100_D	11.3	8.2	6.6			20.0	7.9	2.2			18.2	12.4	3.2		
200_D	9.4	4.4	7.7			16.7	5.4	2.7			9.1	7.6	3.6		
400_D	10.2	4.8	7.6			19.8	3.8	3.4			6.0	3.6	4.9		
600_D	9.4	4.2	10.2			16.7	2.8	3.9			4.6	3.9	6.4		

σ_θ - Horizontal wind direction standard deviation (degrees)

σ_ϕ - Vertical wind direction standard deviation (degrees)

$\bar{u}$ - Wind speed (m/sec^{-1})

ΔT - ($^\circ F$) temperatures at 400 m arc (74 m - 2 m)

ΔT_1 - ($^\circ F$) temperatures at 50 m arc (6 m - 1/2 m)

M -Missing

U - Upwind

D - Downwind

Meteorological data for the various tests include standard deviations of horizontal and vertical wind direction, σ_θ or σ_φ, mean wind speed, $\bar{u}$, and difference in temperature between the 2- and 74-m heights.

The data in table 2 show a marked reduction of wind direction standard deviation and average wind speed as one proceeds downwind from the reactor area. The wind speed generally increased by a factor of two from 30 to 600 m downwind. It appears that the towers at 400 m and 600 m have wind speeds and turbulence conditions nearly the same as the upwind location.

A sampling grid was installed with arc widths of 249, 150, 60, 60 and 60°, respectively, at distances of 30, 100, 200, 400, and 600 m from the reactor dome. The positions of the arcs and spacing between samples were discussed in the previous semiannual report on this work.

One can estimate the increased atmospheric dilutions anticipated due to the buildings by forming the ratio of the term $\sigma_\theta \sigma_\varphi \bar{u}$ measured downwind versus the value upwind of the building complex. These "dilution ratios" were calculated for 5-, 10-, and 30-min periods. Figures 4 and 5 show a mean decrease in dilution ratio from at least a factor of 21 for 5-min periods to 5.5 for 30-min periods under lapse conditions and a factor of 28 decreasing to 8.7 for the same time periods under inversion conditions at 50 m downwind. The aerodynamic turbulence shows a steady decrease to approximately 600 m. Dilution ratios between the two sides of EBR-II can exceed a factor of 10 on occasion for 30-min average periods and even greater factor for shorter time periods.

The dilution ratios for 5-min periods shown in figures 4 and 5 are applicable for estimating short-period concentrations or or doses. However, these values cannot be compared to the measured tracer concentrations since a 30-min sampling period was necessary for the tracer collection.

The simplest form of diffusion equation for use near buildings and other obstacles is

$$\frac{\chi \bar{u}}{Q} = \frac{K}{L^2} \quad , \tag{1}$$

where L^2 is the projected area of the buildings normal to the prevailing wind and K is a coefficient that is dependent on meteorological conditions. A general review of diffusion formulae relating rate of discharge of a pollutant to concentration downwind from stacks and built-up areas has been made recently by Barry (1964). He states that K may be defined as that portion

of Q entering the volume defined by $L^2\bar{u}$ per second. In recent literature several authors have shown that the above form of the equation is representative and they suggested values of K that vary from 0.5 to 2.0 at 100 m.

The cross section of the EBR-II complex is rather irregular. The area, L^2, used in this study was 665 m^2. The average values of K are shown in figures 6 and 7 for lapse and inversion conditions and the extremes of K for each stability class are shown in figures 8 through 11. The measured tracer concentrations were used and (1) solved for K. The K values range up to a value of 1.1 at 100 m. These numbers seem to be in fair agreement with values recommended by previous authors. Wind tunnel tests by Halitsky et al. (1963) for the same reactor complex have shown similar values of K for neutral atmospheres (fig. 12).

The lateral particle dispersion, σ_y, was computed from air concentration distributions along the 30-, 100-, 200-, 400-, and 600- m arcs. In addition, the crosswind integrated air concentration (CIC) for each arc was calculated.

Lateral bivane fluctuations σ_θ, were tested as a predictor of σ_y through the NRTS empirical relationship $\sigma_y = 0.035\sigma_\theta x^{0.87}$, where σ_θ (deg.) is measured at x (m). The best relationship between measured and empirically calculated values was obtained by using a 9-sec averaging time in the computation of σ_θ. A scattergram of this relationship is shown for all arcs of all tests in (fig. 13). As shown, the regression line between measured and calculated values of σ_y had an average slope of 0.98 and the correlation coefficient between the values was 0.83. Therefore, the σ_y as calculated by the empirical relationship for all tests was averaged and plotted for each arc distance and compared to the average measured values (fig. 14). Also the results of another method of σ_y calculations using the peak concentration along the arc (χ_p) and the CIC are shown in the figure. All three relationships correspond reasonably well on the average.

Average measured σ_y variation with distance downwind for lapse and inversion conditions was compared (fig. 15) to NRTS (Grid III) open terrain curves as defined by stability classes by Yanskey et al. (1966) in their figure 3.5. The lapse curve approached the class C stability (slight unstable) curve for open terrain at 600 m and the inversion curve approached the class E (slightly stable) stability curve also at 600 m. The aerodynamic (building) turbulence contribution to lateral dispersion appeared to be the same during lapse and inversion conditions as indicated by the same average values of σ_y found at 100 m downwind during both conditions. Although vertical diffusion was not measured, computations of effective σ_z from ground-level air concentrations

could be made from all runs from the Gaussian formula

$$\sigma_z = \frac{2}{\pi} \frac{Q}{\bar{u}\ CIC} \quad . \tag{2}$$

For inversion cases, figure 16 of σ_z versus distance downwind showed a marked departure from the class E and F stability of the open terrain tests (Grid III).

The measured air concentrations along the mean plume axis are shown in figures 17 and 18 for lapse and inversion conditions. The measured mean data are represented by the heavy line. The measured plume-center air concentrations can fit quite well to a straight-line plot on log-log paper to 600 m. The best fit assuming this power law relationship to downwind distances gave slopes of -0.60 (i.e. $x^{-0.6}$) for both lapse and inversion conditions.

A comparison of χ_p was made between the open terrain and building complex. The preliminary results are shown in table 3. The dilution ratio values presented are the computed centerline concentrations of the undisturbed flow (open terrain) divided by the measured concentrations in the disturbed (by building complex) flow.

Table 3. Average Dilution Ratios

Distance	Lapse (7 cases, $\bar{u}$ = 7.6 m/sec)	Inversion (6 cases, $\bar{u}$ = 6.3 m/sec)
100	4.4	3.5
200	2.8	4.2
400	1.8	3.9
600	1.4	3.2

Excellent agreement was found between the horizontal wind direction standard deviation and horizontal particle dispersion after smoothing the wind direction record by appropriate averaging times and using the empirical relationship $\sigma_y = 0.035\sigma_\theta x^{0.87}$, where σ_θ is measured at the distance, x.

During lapse cases a four-fold reduction in peak concentration (i.e., increase in dilution) from a release of effluent downwind of the containment vessel in the EBR-II reactor complex at 1 m in height could be expected on the average due to aerodynamic turbulence caused by the buildings. This conclusion is

based on comparisons to measured diffusion from a continuous point source over flat open terrain during similar meteorological conditions. Individual tests show this reduction can vary from factors of 2 to 15 at 100 m from release point. The aerodynamic turbulence effect of buildings seems to disappear between 500 and 600 m downwind in both stable and unstable atmospheres. These results apply to tracer releases of 30 min. Turbulence measurements using bivanes and anemometers on both sides of the buildings can be related to actual concentration measurements.

2.2 Deposition and Effluent Cloud Depletion Studies

2.2.1 Meteorological Studies of Deposition of Gaseous Effluents

The Controlled Environmental Radioiodine Tests (CERT) provided a unique source of data for the study of turbulent transfer characteristics of radioiodine effluents from air to natural grass surfaces. The first step in this study was the comparison of measured values of deposition velocity to predictions by two models.

The major factors involved in the transfer of suspended material from air to natural surfaces are (1) turbulent transfer through the lowest layer of the atmosphere above the vegetation canopy, (2) surface sublayer transfer within and slightly above the vegetation canopy, and (3) the biological, chemical, and physical receptiveness of the vegetation itself. With these factors in mind, two models have been developed for predicting deposition.

First is the flux-gradient model suggested by Sheppard (1958) and based on the equation,

$$K \frac{\partial \chi}{\partial z} = V_{d_o} \chi_o \ (= \text{deposition rate}) \ , \qquad (3)$$

where K = eddy diffusivity (L^2/T), $\partial\chi/\partial z$ = vertical concentration gradient (units/L^4), V_{d_o} = deposition velocity at the interface (L/T), χ_o = air concentration at the interface (units/L^3). Integrating and solving for $V_{d_{(z)}}$ where $V_{d_o}\chi_o = V_{d(z)}\chi_{(z)}$ and $K = (ku_*z) + D$, we obtain

$$V_{d(z)} = \frac{ku_*}{\ln(ku_*zD^{-1})} \left[1 - \frac{\chi_o}{\chi_{(z)}} \right] \qquad (4)$$

for $z > o$ and $D << ku_*z$,

where D = molecular diffusivity of effluent material (L^2/T), k = von Karman's constant, u_* = friction velocity (L/T), and z = height above zero plane (L). The portion of (4) in brackets equals 1 for a perfect sink material because theoretically $\chi_o = 0$. The assumptions in this formulation are: (1) momentum flux equals mass flux in the atmospheric boundary layer, (2) molecular diffusion becomes the controlling factor for transfer close to the surface, i.e., in the surface sublayer, and (3) the deposition velocity is proportional to the relative sink capacity of the surface.

The second approach as presented by Chamberlain (1966) utilizes the three factors or stages of transfer from air-to-natural surfaces in an electrical resistance analogy form (depicted in figure 19), which is,

$$R_{T_{(z)}} = R_{BL_{(z)}} + R_{SS} + R_S \quad , \tag{5}$$

where $R_{T_{(z)}}$ = total resistance ($1/V_{d_{(z)}}$) at reference height, $R_{BL_{(z)}}$ = atmospheric boundary layer resistance at reference height, z, R_{SS} = surface sublayer resistance, R_S = biological, chemical, and physical resistance at the surface of deposition. The atmospheric boundary layer resistance, R_{BL}, is taken as the momentum transfer resistance or $R_{BL} = \rho\bar{u}_{(z)}/\tau = \bar{u}_{(z)}/u_*^2$, where ρ is the density of air and τ is the stress. The surface sublayer resistance formulation was derived from wind tunnel work pertaining to heat transfer to bluff-type roughness surfaces (Owen and Thomson, 1963). This formulation is:

$$R_{SS} = (u_* B)^{-1} \tag{6}$$

where, $B^{-1} = \rho Re^m Pr^n = \alpha \left(\frac{u_* z_o}{\nu}\right)^m \left(\frac{\nu}{D}\right)^n$,

in which α = a function of surface roughness elements, Re = Reynolds number = $u_* z_o/\nu$, Pr = Prandtl number = ν/D, ν = kinematic viscosity of air, D = molecular diffusivity of diffusing substance. An empirical determination of the constants, m and n, by Owen and Thomson led to the values 0.45 and 0.8, respectively. The parameter, α, was determined by Chamberlain (1965) from experimental data to be about 0.08 for short grass. The interface resistance, R_S, has not been evaluated for partial sink grass (fibrous type) surface.

First, measured carbon plate (a biologically inert bluff-type surface) deposition velocities were compared to Sheppard's flux-gradient model without the portion in the

brackets and assuming that the molecular diffusivity of gaseous elemental iodine is 0.08 cm^2/sec. A scattergram of this relationship is shown as figure 20. The line of best fit is $V_d(carbon)=0.278V_d$ (Sheppard) and there is a significant correlation between the two.

The resistance analogy model was also tested, using the measured carbon plate deposition velocities. The boundary layer resistance, $\bar{u}/u_*^2$, was subtracted from the reciprocal of the measured deposition velocity for each test and the difference was plotted against the surface sublayer resistance as defined by Owen and Thomson without the correction for surface roughness, α (fig. 21). The line of best fit by the statistical logarithmic least squares method had a slope of near one and an intercept value of 3. The intercept value is equivalent to the α value in the surface sublayer resistance term. This α value of 3 is in good agreement with the values found by Owen and Thomson for faces of similar character. The Reynolds numbers during inversion conditions were usually below those required for fully rough flow but this did not seem to affect the results. A significant correlation between calculated and observed V_d was found and the scattergram of the comparison is shown in figure 22.

For grass deposition, the testing of models is not as straightforward because grass is a semirigid fibrous type of surface, which is quite different from the bluff type of surface for which the models were developed. Also grass deposition velocities were found to be significantly related to grass density. A scattergram of deposition velocity versus grass density ($g(dry\ matter)/m^2$) for one of the releases, in which the grass density over the pasture varied by a factor of 5, demonstrates this relationship (fig. 23). The data from this test permitted a comparison between soil deposition under the grass and grass deposition. Generally the soil deposition was at least a factor of 4 less than the grass deposition and was inversely related to grass density, but grass density remained proportional to total deposition.

Because a linear empirical relationship was found between deposition velocity and grass density, each measurement of V_d in each test was normalized by dividing by grass density and the medians of these normalized values were used to represent the tests. The normalized V_d values were compared to the boundary layer transfer velocity $u_*^2/\bar{u}$ (fig. 24) and were found to be highly correlated. It is interesting to note that the two cases with the highest normalized V_d's occurred during inversion conditions. The wind speed profiles during these two cases indicated a stagnant layer to a depth of 9.4 m and gradients of wind velocity above this layer were indicative of typical inversion profiles.

Since a significant linear relationship was found between normalized V_d and boundary layer transfer velocity, conformance to the boundary layer resistance model was tested. First, to achieve dimensional consistency, reciprocals of the normalized grass V_d values for each test were arbitrarily divided by the average grass density for all

field tests and the boundary layer resistance values were subtracted from these normalized V_d reciprocals. These differences were then compared with the surface sublayer resistances (fig. 25). With the two anomalous inversion values eliminated from the scattergram, the line of best fit yielded an α value of 1.8, which is an order of magnitude higher than the findings of other investigators. Also it was found that there was no significant improvement in the prediction when the surface sublayer resistance was added to the boundary layer resistance.

The average ratios of momentum transfer from the wind profile to mass transfer from the concentration profile were found to be 0.9 in stable and 1.4 in unstable conditions. These averages are significantly different.

The total amount of radioiodine deposited on the pasture was calculated for six of the releases for which there was sufficient field data and the results are shown as a percentage of the total amount released in table 4. The ranges of distances downwind between which these total deposition values were measured are also shown.

Table 4. Percent of Total Amount of Radioiodine on Pasture

Test No.	% of Total	Distance Range (m)	V_d(cm/sec)	u_*(m/sec)	Stability
1	1.06	100-300	0.72	0.60	Unstable
2	1.07	100-380	0.61	0.58	Unstable
4	0.70	50-100	0.15	0.12	Stable
5	1.33	50-300	0.10	0.36	Stable
7	2.97	100-380	1.02	0.43	Unstable
19	1.04	100-380	1.23	0.64	Unstable

The data have demonstrated two important aspects of the turbulent transfer of gaseous radioiodine effluents from air to a natural surface (i.e., grass).

(1) Because good results were obtained via the Chamberlain resistance analogy model for carbon plate deposition velocities, and because the boundary layer transfer velocity, $u_*^2/\bar{u}$, showed a good empirical relationship to normalized grass deposition velocities, the boundary layer transfer term in the equation appears to be adequate. This term, however, will be more theoretically correct if changes in the profile of concentration due to the nonperfect sink characteristic of the iodine are taken into account. Therefore, a need exists for the determination of fractional retention factors for this substance.

(2) The two models tested were found to be inadequate for the region very close to a grass surface. The necessity of normalizing grass deposition velocities for grass density demonstrated the need for some measure of total effective surface area instead of plane area available for deposition on fiberous type surfaces. Also, the scavenging of material by the grass blades is volumetric rather than planar and, therefore, may depend on the material's residence time in the grass. This indicates the need for more research on the microturbulence structure within a grass canopy before a fundamentally sound model of the surface sublayer can be formulated.

A hot-wire anemometry system has been ordered for use in future CERT field tests to study the structure of turbulence at grass top and in the grass canopy. It is expected to arrive in November 1967.

2.2.2 Parametric Evaluation of a Plume Depletion Model

At present there are no field study data available from which total cloud depletion can be evaluated over a wide range of distances. Therefore, due to operational necessity, reasonable depletion estimates via theoretical approaches tempered with existing fragmentary knowledge of deposition mechanisms are necessary.

Assuming that diffusion is adequately described by the K-theory approach if the vertical profiles of K and $\bar{u}$ can be defined, numerical solutions of the equation can be obtained by a computer program for conditions representative of the three general stability classes: stable, unstable, and neutral. The complex variations of $\bar{u}$ and K with height do not allow accurate estimates of concentration, and therefore of deposition, to be made from analytic solutions of the two-dimensional (x,z) equation with appropriate boundary conditions.

The computer program used in this study was adapted from a program originally designed to make heat conduction calculations with time in one direction between two boundaries (Wagner, 1965). Resolution for the magnitude of the input parameters was achieved by adjusting grid point spacing for the computer program's finite difference calculations. Time was converted to distance and the direction was considered to be the vertical (z) with the boundaries being the ground level and the depth of mixing.

Profiles of K, from ground level to 100 m, representative of the three stability categories, were derived from measurements reported by Geiger (1965) and Wong and Brundidge (1966) and adapted to represent average conditions over the desert-type terrain of the NRTS in Idaho. The resulting K profiles are shown in figure 26. Wind velocity profiles were determined through the use of the log-linear velocity profile law and are consistent in the low levels (region of constant stress) with the similarity theory relationship

$$u_*^2 = K \frac{d\bar{u}}{dz} \quad , \tag{7}$$

where u_* is the friction velocity. These wind velocity profiles are shown in figure 27. Above 100 m, K and $\bar{u}$ were held constant.

Computer calculations to 10^5 m were made assuming complete reflection of material from the ground (no deposition) and from the depth of mixing height, L, for each of the stability classes. The assumed values of L were 200 m for stable conditions, and 2000 m for neutral and unstable conditions. Effective standard deviations of vertical effluent concentrations, σ_z, were computed, for comparison with experimentally measured values, through use of the Gaussian relationship

$$\sigma_z = \sqrt{\frac{2}{\pi}} \frac{Q}{\bar{u}_e \chi_{z=o}} \quad , \tag{8}$$

where Q = source strength,

$\bar{u}_e$ = effective wind speed, and

$\chi_{z=o}$ = air concentration at ground level.

These σ_z calculations were compared against measured σ_z values (Yanskey, Markee, and Richter, 1966) derived from diffusion experiments at the NRTS and extrapolations to longer distances (fig. 28). The calculated σ_z values using K-theory generally are not different from the measured σ_z values by more than a factor of 2 at all distances. Therefore it is assumed that the K and $\bar{u}$ profiles used in the calculation adequately described vertical diffusion. These profiles were used for all subsequent plume depletion calculations.

As mentioned previously, there are two boundary conditions that can be used at ground level for an effluent material which deposits by adsorption at the ground surface. Both of these conditions were used in this parametric evaluation of plume depletion.

For a partial sink, V_d and K had to be evaluated at ground level. Empirical data from the CERT Project at the NRTS have shown an approximately linear relationship between the deposition velocity, V_d, measured for a 1-m reference height, and u_* ($V_d = 0.012 1 u_*$). This relationship was used to determine V_d from the u_* values used in determining the K and $\bar{u}$ profiles for each stability class; K at ground level was assumed to be equal to the value calculated for a 5-cm height from the K profiles. The calculations for total retention (perfect sink) represent the upper limit of plume depletion.

Calculations were made for partial and total retention during the three stability conditions. The unstable conditions included three separate calculations for different depths of the mixed layer, L, of

200, 500, and 2000 m. These different L values represent the minimum L value during the daytime and average daytime L values in winter and summer, respectively, at the NRTS. The L values for stable and neutral conditions were 200 and 2000 m, respectively. For the total retention assumption, calculations were made for source heights, h, of 0.25 and 9 m. A source height of 0.25 m was assumed for all partial retention calculations. The maximum distance for which the calculations were made was 10^5 m.

Values of calculated total plume depletion factors (i.e., amount of material released/amount of material remaining airborne at distance (x) at selected downwind distances) are shown in table 5 for the partial retention assumption and in table 6 for the total retention assumption. At distances beyond 10^4 m the resultant plume depletion factors assuming total retention are significantly affected by the depth of the mixed layer as shown for the unstable condition. In fact, the depletion values for L = 200 m under unstable conditions exceed those for stable conditions at 10^5 m. This may be explained by the fact that after a depositing effluent has travelled to some distance, diffusion is predominantly in the downward direction due to the reflection of the effluent at the top of the mixed layer. Therefore, at longer distances the rate of transfer of effluent to ground level is increased and the deposition rate is amplified. The same trends are indicated for the partial retention cases but the change is not as dramatic as in the total retention cases.

As indicated in table 6, plume depletion changes rapidly with initial source height. An increase of less than 9 m in source height lowers the depletion factors by more than a factor of two except in the neutral case.

The other aspect of the plume depletion problem is the resultant reduction in air concentration. Figures 29, 30, and 31 show the variations with height and distance by stability class of the ratios of effluent concentration assuming no deposition to effluent concentration for perfect sink deposition. The greatest change of concentration reduction with height was found during stable conditions and the least change during neutral conditions. These reduction factors always exceeded the total plume depletion factors in the lower levels, which demonstrates the fact that vertical profiles of air concentration are distorted by deposition.

The concentration reduction factors for selected distances are shown in table 7 for a source height of 0.25 m at heights of 0.1 and 1 m. Note that these reduction factors change with height by greater than a factor of two for perfect sink deposition and they exhibit very little

Table 5. Calculated Plume Depletion Factors - Partial Sink - h = 0.25 m.

Distance Downwind(m)	Stable V_d=0.12cm/s L=200 m	Neutral V_d=1.11cm/s L=2000 m	Unstable V_d=1.81cm/s L=200 m	Unstable V_d=1.81cm/s L=500 m	Unstable V_d=1.81cm/s L=2000 m
1.10×10^2	1.08	1.18	1.08	1.08	1.08
1.11×10^3	1.19	1.32	1.13	1.13	1.13
1.01×10^4	1.61	1.48	1.20	1.17	1.17
3.01×10^4	2.25	1.59	1.36	1.23	1.20
1.00×10^5	3.95	1.78	2.10	1.46	1.26

Table 6. Calculated Plume Depletion Factors - Perfect Sink

Distance Downwind(m)	Stable L=200 m h=0.25	Stable L=200 m h=9.0	Neutral L=2000 m h=0.25	Neutral L=2000 m h=9.0	Unstable L=200 m h=0.25	Unstable L=200 m h=9.0	Unstable L=500 m h=0.25	Unstable L=500 m h=9.0	Unstable L=2000 m h=0.25	Unstable L=2000 m h=9.0
1.10×10^2	2.09	1.00	1.65	1.01	2.13	1.03	2.13	1.03	2.13	1.03
1.11×10^3	3.78	1.13	2.16	1.23	2.69	1.20	2.69	1.20	2.69	1.20
1.01×10^4	11.6	2.79	2.71	1.63	3.69	1.64	3.18	1.41	3.13	1.39
3.01×10^4	24.6	5.43	3.12	1.92	7.25	3.21	4.10	1.81	3.58	1.58
1.00×10^5	50.4	11.5	3.90	2.50	76.7	34.1	9.88	4.38	4.50	1.99

change for partial sink deposition. This change in concentration reduction factors with height results in an elevation of the height of the maximum concentration in the vertical direction with distance. The heights of the maximum concentration for perfect sink deposition are plotted in figure 32.

It appears that the K-theory parabolic diffusion equation, solved numerically, provides realistic vertical concentration profiles and, consequently, reasonable plume depletion estimates. The magnitude of the plume depletion factors for a partial sink is, however, somewhat surprising because the values are so low. This may be due to the fact that either the deposition velocity estimates are too low or the K values at the ground are too high. A slight change in either of these parameters can alter the depletion factors considerably.

Table 7. Air Concentration Reduction Factors

Stability	Distance Downwind(m)	Partial Sink z=0.1 m	Partial Sink z=1 m	Perfect Sink z=0.1 m	Perfect Sink z=1 m
Stable	1.10×10^2	1.17	1.09	5.91	2.52
	1.11×10^3	1.38	1.28	15.3	6.58
	1.01×10^4	2.14	1.99	100	43.4
	1.00×10^5	9.20	8.58	1800	776
Neutral	1.10×10^2	1.18	1.07	4.68	2.18
	1.11×10^3	1.47	1.29	8.15	3.82
	1.01×10^4	1.87	1.65	12.2	5.75
	1.00×10^5	2.61	2.28	21.7	10.2
Unstable L=200 m	1.10×10^2	1.20	1.13	6.61	3.08
	1.11×10^3	1.33	1.25	11.4	5.32
	1.01×10^4	1.39	1.30	13.8	6.45
	1.00×10^5	2.42	2.27	286	134
Unstable L=500 m	1.10×10^2	1.20	1.13	6.61	3.08
	1.11×10^3	1.33	1.25	11.4	5.34
	1.01×10^4	1.37	1.29	12.7	5.94
	1.00×10^5	1.70	1.60	39.2	18.4
Unstable L=2000 m	1.10×10^2	1.20	1.13	6.61	3.08
	1.11×10^3	1.33	1.25	11.4	5.35
	1.01×10^4	1.38	1.29	13.2	6.23
	1.00×10^5	1.54	1.45	22.2	11.4

2.3 Radar-Tetroon-Transponder System

2.3.1 Trajectories

Two tetroon flights were initiated from the Test Reactor Area

during the mornings of June 1 and 2, 1967, in connection with the ATR-ARCO revaluation of meteorology program. The first trajectory record was terminated on the southwest boundary of the NRTS where it descended so low it was lost behind a ridge. The second trajectory record was terminated after about 2-hr flight time when the transponder failed.

2.3.2 Transponders

Cordin Company, TTX series, solid-state transponders were static tested under various temperature and voltage conditions. One unit was flight tested. General characteristics were all satisfactory and the unit flight tested performed well out to the full range of the radar. Also transponders from Dave Hobart, ESSA, and Roy Booker, Weather Science Inc., Norman, Oklahoma, were tested. The latter had a strong signal, but excessive frequency variation. The former performed satisfactorily.

2.3.3 Tetroon Determined Estimates of Relative Dispersion Characteristics

The position and velocity data from the tetroon flights during the month of July 1966 at the NRTS were used to determine some characteristics of relative dispersion in the earth's boundary layer. The synoptic conditions during the period of testing were such that the wind carried the majority of the tetroons in a north-northeast to northeasterly direction with average velocities from 5 to 15 m/sec. Since this general condition provided the largest sample of trajectory pairs, those few cases not falling into this category were not included in this study.

Considering the available data, we believe the ideal situation would be study the dispersion as it is represented by the behavior of a cluster of four tetroons as shown in figure 33. However, a preliminary analysis of those clusters released during the predominant synoptic situation indicated that the 30-min delay in the release of the second pair plus an early loss of one of the four tetroons reduced the number of samples, with barely over 1-hr concurrent flight time, to two. For this reason, only data from pairs of tetroons are considered in this study. The data available for this period contained 10 pairs of tetroon trajectories, which were released in the predominant flow pattern and were in excess of 105-min tracking time without missing data. It is these 10 trajectories that were used in this study. A case study of the dispersion of clusters of four particles has been initiated and will be reported later.

To study dispersion parameters in the along- and cross-wind direction, we found it necessary to rotate the coordinate axes in such a way that the x-axis was oriented along the mean wind and the y-axis was perpendicular to the mean wind for each pair. The direction of the mean wind for each flight was assumed to be along a line connecting the midpoints of the first and last observed pair position. The position and velocity data for each pair were then determined in the new coordinate system. The relative displacements and velocities for each pair were then computed.

The mean auto-correlation functions for the along-, cross-wind, and vertical component of the relative velocity are computed and are respectively shown as $R_{u_r u_r}(\tau)$, $R_{v_r v_r}(\tau)$, and $R_{w_r w_r}(\tau)$ in figure 34. The auto-correlation function for the along-wind component of the relative velocity shows a monotonic decreasing characteristic, where the auto-correlation functions for the relative cross-wind and vertical velocities show a wavy behavior for time lag greater than 10 min. All three auto-correlation functions converge at about 40 min.

The mean normalized power spectra for the along-, cross-wind, and vertical component of the relative velocity, denoted as $F_{u_r u_r}(n)$, $F_{v_r v_r}(n)$, and $F_{w_r w_r}(n)$, are computed with the use of the Blackman-Tukey smoothing formula (Blackman and Tukey, 1958).

$$FF_k = 0.54\ F_k + 0.23\ (F_{k-1} + F_{k+1}) \quad , \tag{9}$$

where

$$F_K = 4 \int_0^{T_M} R(\tau)\ \cos\ 2\pi n\tau\ d\tau \tag{10}$$

is calculated by trapezoidal integration with $n = 0.5\ k/T_m$, $k = 1,=,....,$ $T_m/\Delta t$.

The three normalized power spectra are shown in figure 35. It is interesting to note that all three spectra practically coincide with each other in the frequency range $> 1.4 \times 10^{-3}$ c/sec . Because the power spectra for the large-scale relative velocity is more or less proportional to k^{-3} (Kao and Gain, 1967), a line of k^{-3} is drawn in figure 35 for comparison. For frequency lower than 1.4×10^{-3} c/sec the turbulent kinetic energy of the along- and cross-wind component of the relative velocity increase with decreasing frequency; however, the spectrum for the along-wind component shows a steeper slope than that for the cross-wind component. The spectrum for the relative vertical velocity shows an energy peak at frequency 3.4×10^{-4} c/sec.

The power spectra were computed up to the folding frequency of 8.33×10^{-3} c/sec. Because of the three point smoothing of the trajectory positions in the analysis, which is equivalent to a 3-min running mean of the velocity, spectral values for frequencies greater than 5.5×10^{-3} c/sec are unrepresentative, and were, therefore, not shown in figure 35.

To obtain the power spectra of the relative along-, cross-wind, and vertical velocities, the normalized power spectra need to be multiplied

with the variances of the respective components of the relative velocity. The variances of these velocity components are listed as follows:

$\overline{u_r^2}$	$\overline{v_r^2}$	$\overline{w_r^2}$	
8.91	6.49	5.51	$(10^4\ cm^2\ sec^{-2})$.

The seemingly high value of the variance of the relative vertical velocity is likely due to the effects of the thermal and forced convections over the paths of the flights.

To examine the characteristics of the anisotropy of the field of relative turbulence and diffusion, the cross-correlation functions and normalized cross-spectra are computed and shown in figures 36 and 37, respectively. The cross-correlation function for the along- and cross-wind relative velocities is mostly positive for time lag smaller than 20 min, but negative for time lag $>$ 20 and $<$ 35 min. The cross-correlation function for the relative along-wind and vertical velocities shows mostly positive in the range of time lag from 15 to 35 min, but negative outside of the range, whereas the cross-correlation function for the vertical and cross-wind velocities shows an alternate positive and negative distribution. Figure 37 shows that the rate of the along-wind transport of cross-wind momentum is mostly negative for the high frequency range but positive for the low frequency range, whereas that of the vertical momentum is mostly negative for all frequencies. The rate of the vertical transport of the cross-wind momentum appears not appreciably positive or negative in any frequency range. The effect of the cross-spectra on the degree of anisotropy of turbulence and diffusion may be seen from figure 37 showing three spectral curves. In general, for small diffusion times, the degree of anisotropy of turbulent diffusion is affected by the cross-spectrum of all frequencies, but primarily by that of the low frequency for large diffusion times.

As a measure of the relative along-, cross-wind, and vertical separations of particles as a function of time, the mean squares of these separations are computed at 1-min intervals. These mean squares of particle separation are plotted in figure 38. It is seen from this figure that the rate of change of the mean square of the relative along-wind separation is about five times greater than that of the relative cross-wind separation, whereas the latter is about an order of magnitude greater than that of the relative vertical separation. The mean square of the along-wind particle separation generally increases with time up to about 70 min, after that it shows a slight wavy oscillation and then a substantial decrease. In examining the trajectories of these tetroon flights we found that at about 70 min after the launch of the tetroon some of them approached the mountain range to the north of the launch site. This mountain range could cause a convergence in the direction of the mean wind and, therefore, the decrease in the mean square of the relative along-wind separation.

Figure 38 shows that the mean squares of particle separation for this sample behave more or less linear with time in the first 70 min. Applying the expression for the large diffusion times,

$$\overline{x_{r_i}^2}(t) \quad 2K_{x_i x_i} t \tag{11}$$

to the curves in figure 38, the following eddy diffusivities were found

$$K_{xx} \quad 5 \times 10^7 \text{ cm}^2/\text{sec}$$

$$K_{yy} \quad 10^7 \text{ cm}^2/\text{sec} \quad .$$

To further examine the degree of anisotropy of the field of turbulence and diffusion, we computed the covariance of particle separation in the horizontal plane and the angle between the principal axis of diffusion and the direction of the mean wind, shown in figure 39. The covariances of particle separation involving the vertical displacement are generally small compared with the covariance of the separation here. It is seen from figure 39 that the values of the covariance and angle α in the horizontal plane are negative for the first 25 min, then become positive for the rest of the time, which indicates that the principal axis of diffusion tends to make a positive angle with the direction of the mean wind for comparatively large diffusion times. It is interesting to note that the mean covariances of the relative velocities are:

$\overline{u_r v_r}$	$\overline{u_r w_r}$	$\overline{v_r w_r}$	
-0.20	-0.46	-0.09	$(10^4 \text{ cm}^2/\text{sec}^2)$.

In the sample of 10 pairs used in this investigation, eight of the 10 were oriented in such a way that their lines of separation were practically parallel to the mean wind for the duration of the trajectories. It would seem that the small rate of cross-wind dispersion as compared to the rate of along-wind dispersion was somewhat influenced by the predominance of this orientation in the sample used. Since the representation of puff dispersion by pairs of particles requires a large number of separate trajectory pairs, it seems advisable to carry out some experiments with at least three tetroons at a time.

2.4 Meso-Micro Studies

Although weather map types of various schemes have long been used, it was not until the development of high-speed computers that linear correlation could be applied to the derivation of types. The method is a straightforward linear correlation of data points from the synoptic weather map of one time to the corresponding data points of a synoptic weather map of some other time. If each map from a sample is correlated to every other map in the sample, and a count is made of the number of significant correlations to each map, the maps having the most other

maps significantly correlated to them are readily picked as the type maps. To avoid ambiguity in the system of selection, the following set of rules was utilized:

1) Find the map having the most other maps significantly correlated to it.

2) Designate this map as type A, and remove from the sample all maps significantly correlated to map type A.

3) From the remaining maps find the one map having the most other maps significantly correlated to it.

4) Designate this map as type B, and remove from the sample all maps significantly correlated to map type B.

5) Repeat the process until a sufficient number of map types have been selected.

The level of significance is usually taken to be 0.70. As an arbitrary level of significance 0.70 forces sufficient contrast between the map types to make identification of types reasonably easy by visual scanning. The ease of detecting types in an independent sample by visual scanning is clouded by the fact that about one-half the maps will be a combination of two or more types. Other values for the level of significance may be used as dictated by the application to which the types are to be put.

When climatologies for each of several stations within a sub-synoptic scale region are derived for each map type, an important application results. Average differences between a key station and each of the other stations for continuous variables such as temperature, relative humidity and winds may be determined. These average differences may be checked for reliability by finding the standard deviations of the differences. A forecast need be made for only one station, and values for all other stations are determined objectively from the derived differences. A test was made in western Washington where maximum temperatures and minimum relative humidity forecasts were objectively made for a number of U. S. Forest Service ranger stations based upon the subjective forecast for Olympia. The results displayed the objective forecasts to be as good as, or better than the subjective forecasts made for the ranger stations.

The climatologies of events such as abnormal winds, classes of stability, thunderstorms, or precipitation are of great value to forecasting when derived according to map types, because the derived probabilities of occurrence reflect variations brought about by changing flow patterns.

Map types may also be used as a method of stratifying a dependent set of data for forecasting studies. Separate forecast equations or

diagrams are derived for each of the distinctive flow patterns implied by the map types.

The application of this tool should prove valuable in supplementing climatological data and research forecasting effectiveness at the NRTS.

2.5 Technical Support to Reactor Projects

2.5.1 Advanced Test Reactor (ATR)

In response to the Environmental Branch, Health Services Laboratory, Idaho Operations Office, request for assistance with the evaluation of ATR dose calculations for off-site locations, the meteorological conditions affecting the problem have been re-examined. As requested, the revaluation for the city of Arco has been given first priority and the results of this study are presented.

Estimates of $\overline{\chi/Q}$ values that could arrive at Arco have been made for three potential trajectories and four observed tetroon flights. All calculations of $\overline{\chi/Q}$ were made using a modification of the LOFT puff diffusion technique described in IDO-12059, "Meteorology for the Loss of Fluid Test Reactor" (Dickson et al, 1967).

The modified diffusion model yielded relative dose factor estimates, $\overline{\chi/Q}$, (units-hr/m^3), at the end of each minute during the transport toward Arco. A source term of unity with a 1-min duration was adopted as requested. Since the effluent release was to be treated as a single puff, the Hilsmeier-Gifford (1962) values of σ_y as a function of distance have been used; the Markee values of σ_z were adopted as most representative for the NRTS. In addition, diurnal variation of the vertical depth of the turbulent mixed boundary layer of the atmosphere was included.

The three potential trajectories were selected for estimating fields of $\overline{\chi/Q}$ near Arco. Trajectories #1 and #2 are based on an analysis of wind data from on-site wind stations and tetroon flights initiated near EBR-I during the mornings of July 7 and 11, 1966. These combinations of an on-site Eulerian trajectory and a Lagrangian off-site tetroon trajectory are judged realistic, documented transports from ATR to Arco. Trajectory #3 represents straight-line flow from ATR to Arco.

Calculations of $\overline{\chi/Q}$ have been made along trajectory #3 for the six NRTS diffusion categories using a mean wind speed of 4 mph. Calculations have been made for summer and winter seasons for straight-line flow. Only the summer season has been examined for flow along trajectories #1 and #2. For straight-line flow (trajectory #3) under inversion conditions (stability categories E and F) the calculated fields of $\overline{\chi/Q}$ are the same in winter as in summer because σ_z never grows large enough to be influenced by the different values of the depth of the mixed layer. Therefore the summer season calculations will be presented.

The strong lapse condition has not been calculated for winter because it is extremely unlikely to persist long enough to permit flow to Arco. Table 8 summarizes the 21 potential diffusion regimes according to season of the year, amount of cloud cover, time of day and general weather conditions. The first letter of the regime identifier denotes the season by a W or a S. The middle number identifies the trajectory, and the last letter denotes the particular NRTS stability category. Plume depletion was not included in these calculations. For flow to Arco the best available theoretical value for depletion is a factor of 3.5.

Four other important cases were presented, which were documented transport toward Arco during typical June and July mornings. The observed diffusion categories and depths of the mixed layer were used for this series of calculations.

Table 9 lists the date and time of the four observed cases of transport toward Arco. Cases S10 and S20 occurred on clear July mornings; cases S30 and S40 occurred on partly cloudy to cloudy June mornings.

Table 9. Observed Cases of Effluent Flow Toward Arco

Case	Begin	End	Remarks
S10	0845	1405	7/7/66, FLT 4B meshed with site tower winds
S20	0815	1235	7/11/66, FLTS 21 & 22 meshed with site tower winds
S30	0925	1125	ATR #1, 6/1/67, flow toward Arco, showers over mountains
S40	0828	1023	ATR #2, 6/2/67, flow toward craters of the Moon, mostly cloudy

Table 10 summarizes the mean wind speeds, the times of day of the test cases, and the accumulated values of relative dose factor, $\overline{\chi/Q}$ ARCO.

IDO-12025, "An Eight Year Summary of the Temperature Gradient Below 250-ft at the National Reactor Testing Station" (Johnson and Dickson, 1962), summarizes temperature information for the period 1953 through 1960. The longest observed durations of inversion conditions during each month of this period of record are tabulated for Central Facilities. These tabulations show that inversion conditions seldom persist 24 hr or longer. A further examination of inversion periods lasting 24hr or longer revealed that only once in 8 years did a class F stability condition persist 24 hr or more. In this instance, however, the wind directions

Table 8. Stability Test Cases for ATR Effluent Flow to Arco

Case	Begin	End	Remarks
W3A	----	----	Unlikely except 1200-1300
W3B	1000	1920	Mostly clear 1000-1600, P/C and Class F 1700-1920
W3C	0900	1820	Generally P/C 1000-1800, Class F 1600-1820
W3D	0800	1720	Overcast, Class F 1600-1720
S3A	0900	1820	Mostly clear
S3B	0700	1620	Clear 0700-0900, P/C 0900-1620
S3C	0600	1520	P/C 0600-0900, overcast 0900-1520
S3D	0600	1520	Overcast, not too likely without PCPN in area
S3E	2000	0420	Overcast, not too likely without PCPN in area
S3F	2000	0420	Partly cloudy
S2A	1100	1520	Mostly clear
S2B	0900	1320	Partly cloudy
S2C	0600	1020	Partly cloudy 0600-0900, overcast 0900-1020
S2D	0600	1020	Overcast, Class C 0900-1020, PCPN PSBL in area
S2E	2000	0020	Overcast, not too likely without PCPN in area
S2F	2000	0020	Partly cloudy
S1A	1100	1640	Mostly clear
S1B	0900	1440	Partly cloudy
S1C	0600	1140	Partly cloudy 0600-0900, overcast 0900-1140
S1D	0600	1140	Overcast, Class C 0900-1140, PCPN PSBL in area
S1E	2000	0140	Overcast, not too likely without PCPN in area
S1F	2000	0140	Partly cloudy

Note: P/C - Partly cloudy; PCPN PSBL - Precipitation possible

were such that it is extremely improbable that effluent would flow continuously from ATR to Arco for the duration of the inversion. In fact, the transport of effluent to Arco from ATR under moderate to strong inversion conditions (class F) seems to be a rare occurrence.

Table 10. Summary of Wind Speed, Times and $(\chi/Q)_{Arco}$.

Case	$\bar{u}$	Time	$(\chi/Q)_{Arco}$
W3B	4.0 mph	1000-1920	5.7×10^{-11}
W3C	4.0 mph	0900-1820	9.0×10^{-11}
W3C	4.0 mph	0800-1720	1.5×10^{-10}
S1A	9.6 mph	1100-1640	1.8×10^{-12}
S1B	9.6 mph	0900-1440	6.0×10^{-12}
S1C	9.6 mph	0600-1140	2.1×10^{-11}
S1D	9.6 mph	0600-1140	3.1×10^{-11}
S1E	9.6 mph	2000-0140	7.6×10^{-11}
S1F	9.6 mph	2000-0140	6.0×10^{-10}
S2A	7.6 mph	1100-1520	3.2×10^{-12}
S2B	7.6 mph	0900-1320	1.2×10^{-11}
S2C	7.6 mph	0600-1020	3.9×10^{-11}
S2D	7.6 mph	0600-1020	6.2×10^{-11}
S2E	7.6 mph	2000-0020	2.1×10^{-10}
S2F	7.6 mph	2000-0020	1.9×10^{-9}
S3A	4.0 mph	0900-1820	7.1×10^{-11}
S3B	4.0 mph	0700-1620	2.7×10^{-11}
S3C	4.0 mph	0600-1520	7.0×10^{-11}
S3D	4.0 mph	0600-1520	1.1×10^{-10}
S3E	4.0 mph	2000-0420	4.2×10^{-10}
S3F	4.0 mph	2000-0420	2.8×10^{-9}
S1O	9.6 mph	0845-1405	4.5×10^{-12}
S2O	7.6 mph	0815-1235	1.1×10^{-11}
S3O	12.3 mph	0925-1125	4.1×10^{-12}
S4O	12.0 mph	0828-1023	$<1.0\times10^{-20}$

Eulerian wind measurements are being recorded at Arco following installation of a wind station this summer. As more data become available, transport from ATR to Arco can be examined in greater detail. However, for the present, so little data exist that it is impractical to develop statistical data regarding the shortest travel times and distances for transport to Arco and the frequencies of these transports.

Plans are currently being formulated to locate several wind

stations throughout the Upper Snake River Plain so that the type of flow patterns and their frequencies of occurrence can be determined for Arco, Pocatello, Blackfoot, and Idaho Falls.

2.5.2 Loss of Fluid Test (LOFT) Reactor

A climatological study of wind persistence up to 8 hr was completed during the semiannual period. The computer program for this study is outlined in section 2.6.1 of this report. The purpose of the study was to define wind direction persistence probabilities so that the best start times for reactor testing at LOFT may be selected in order to effect the lowest off-site doses of radioactive material.

2.5.3 Transient Reactor Test Facility (TREAT)

A modification of the nomogram in NRTS Meteorological Information Bulletin, Number 2 was made for TREAT personnel so that they could make whole body gamma dose calculations from source strength, wind speed, and atmospheric stability classifications. It was agreed that the meteorological data would be furnished by ARFRO on request and that they would make their own source term estimates. Table 11 and figure 40 are the set of instructions and the nomogram, respectively, that the TREAT personnel are using.

2.6 Computer Program

2.6.1 Wind Direction Persistence Program

In connection with the revaluation of meteorological conditions for LOFT this program has been developed to compute statistics of the persistence of wind direction under various conditions. The input data for the program are hourly wind speed and direction (based on a 16-point compass), hourly precipitation amounts and temperature recorded at two levels. The program is designed to consider the data for two 12-hr periods (1800 MST to 0500 MST and 0600 MST to 1700 MST) on a monthly basis. Up to five separate persistence duration periods (1, 2, 4, 6 and 8 hr) may be considered in one execution of the program. Two classes of lateral wind variation are allowed in the computation. Under one class, persistence is considered to have occurred during the specified duration period if the lateral variation is only plus or minus one compass point. Under the second class the lateral variation is allowed to be as much as plus or minus two compass points. For a given month, persistence duration period, and 12-hr periods, the frequency and percentage of persistence periods are computed and printed out in tabular form. The program considers the direction and speed for each hour of the 12-hr period as an initial condition and then checks only the direction of the following hours to see if the lateral variation tolerences are satisfied for the given duration periods. An occurrence of calm winds is considered to be a break in persistence. Also cases in which precipitation has occurred for a specified number of hours prior to the initial hour or during the

persistence period are eliminated. The program also has the capability to consider specified stability classes as determined by the temperature difference at the two levels.

Table 11. Instructions for Using Nomogram for Environmental Radiological Calculations for TREAT

Procedure:

1. Obtain wind and stability forecast from Atmospheric Sciences (Extension 2329) for proposed time of off-gas release. This forecast will include wind direction (in degrees), wind speed (in mph) and atmospheric stability class (A,B,C,D,E,F).

2. Enter nomogram at intersection of appropriate stability class curve and selected distance downwind (in meters) from the TREAT area based on the wind direction. Note: Wind direction limits within which the effluent is expected to affect selected areas of interest are labeled on the nomogram at their appropriate distances downwind.

3. Read and record ordinate axis value (air concentration x wind speed/source strength).

4. Proceed laterally from initial intersection point to intersection with external cloud dose curve and read and record abscissa axis value at the top of nomogram (external cloud dose x wind speed/source strength).

5. Multiply both recorded values by the source strength (in C_i) and divide them by the wind speed (in mph). The value resulting from step 3 will be the time integrated air concentration (C_i-sec/m^3) and result from step 4 will be the external cloud dose (mr).

2.6.2 Precipitation Duration and Probability Program

This program is designed to compute the hourly frequencies of precipitation, frequencies of duration and the probability of occurrence of precipitation for the next 12-, 24-, and 36-hr periods based on the number of consecutive "wet" or "dry" 12-hr periods prior to the forecast time. Also computed are tables of probability for the continuation of precipitation or no precipitation for N days based on the past M consecutive days of occurrence or non-occurrence of precipitation. The computations are carried out on a seasonal basis for the 12-hr time periods 0000Z to 1200Z and 1200Z to 0000Z. Input data for the program are the standard Weather Bureau hourly precipitation cards punched two per day for each precipitation day. The data has been batched onto magnetic tape for more efficient and economical handling.

2.6.3 Dye Analysis Program

This program will compute the dye concentrations for as many as 25 sample stations on each arc of a test grid and as many as six arc per grid. The standard deviation of the distribution of the dye concentration along each arc is computed. Each sampler concentration is multiplied by a factor $\bar{u}Q^{-1}$, where $\bar{u}$ is the integrated wind speed along the centerline and Q is the release rate in gm/sec^{-1}. Input data for this program consists of the flow rate at each sampler, length of release, amount of dye released, and the fluorometer reading of each sample.

2.6.4 Linear Least Squares Fitting and Partial Correlation Program

This program will compute independent correlations of as many as 10 groups of data with up to 500 data points in each group. The matrix of simple correlation coefficients is inverted with a separate subroutine and the partical correlations between the variables are then computed. Several options are available in the computational scheme of the program as well as in the printout section.

2.6.5 Analysis of Concentration Fields and Display of Isolines on Printer

This program is a modification of a program that provides a contour analysis of any function when its values are known at discrete points on a rectangular grid. The modifications include the option of using a logarithmic interpolation in placing the isolines of concentration and the insertion of a feature that yields a reasonable analysis at the boundary of the concentration field. The analysis is printed out with each isoline represented by a distinct set of symbols. As an aid to pattern visualization the spaces between isolines may be filled with different sets of symbols. The symbols for the isolines and those used to fill the spaces between are specified by the user. The analysis is superimposed over a grid represented by dots printed at a specified spacing and numbered on the left side and the top of the diagram. The values associated with the isolines are printed at the top of the diagram along with the symbols that represent them. Sample printouts are shown in figure 41.

Use of this program has eliminated considerable time and expense in representing graphically the results of the ATR-Arco Revaluation of Meteorology Computations. The program is general enough that it can be used as a subroutine with any program of this type in which the immediate graphical display of results is important.

2.6.6 Auto- and Cross-Correlation Computations

This program has been designed to compute the variance, covariance, cross-covariance, auto- and cross-correlation functions of a variable number of time series each of variable length. Options are available that allow the computation of the average of the above

functions as well as the individual vector auto-correlation and its average. Another option allows the auto- and cross-correlation results to be punched on cards for later use in spectral calculations.

2.6.7 Power Spectra Computations

This program uses the correlation functions of time series data to compute the power spectra for this data. The computation is simply the finite difference approximation of the cosine transform of the correlation functions. An option is available that allows the use of any or all of three lag windows. The first is the rectangular window, which is equivalent to truncation of the correlation function at a specified lag. The other two windows available are equivalent to the "hanning" and "hamming" smoothing. The program also contains a correction function that adjusts the relative high and low frequency ends of the computed spectra.

3.0 REVIEW OF REACTOR SAFETY ANALYSIS REPORT

The Air Resources Laboratory in Silver Spring, Maryland, and the Field Office in Idaho have continued to take an active part in the review of reactor safety analysis reports as well as consultations with regard to the preparation of the reports. In addition, written comments have been prepared for the Division of Reactor Licensing through the Division of Reactor Development and Technology as follows:

1. Midwest Fuel Recovery Plant, General Electric Company Nuclear Energy Division, Design and Analysis Report, dated November 23, 1966.

2. Preliminary Safety Analysis Report, Fort St. Vrain Nuclear Generating Station, Volumes I and II, dated September 1966.

3. Vermont Yankee Nuclear Power Station, Plant Design and Analysis Report, Volumes I, II, and III, dated December 2, 1966.

4. Oconee Nuclear Station Units 1 and 2, Duke Power Company Preliminary Safety Analysis Report, Volumes I and II, dated December 1, 1966.

5. Point Beach Nuclear Power Plant, Wisconsin Michigan Power Company, dated February 3, 1967.

6. Burlington Nuclear Generating Station #1, Preliminary Safety Description and Analysis Report, Volumes 1, 2, 3, dated December 13, 1966.

7. Diablo Canyon Site, Pacific Gas and Electric Company, Preliminary Safety Analysis Report, Volumes I and II, dated January 18, 1967.

8. Oyster Creek Unit #1, Jersey Central Power & Light Company, Facility Description Safety Analysis Report, dated January 18, 1967, Volumes I and II.

9. Peach Bottom Atomic Power Station Units #2 and #3, Philadelphia Electric Company, Preliminary Safety Report.

10. Oconee Nuclear Station Units 1 and 2, Duke Power Company, Preliminary Safety Analysis Report, Amend. #2 dated April 18, 1967.

11. Midwest Fuel Recovery Plant, Application for Licenses, Amendment #1, dated April 17, 1967.

12. Surry Power Station Units 1 and 2, Virginia Electric & Power Company, Preliminary Safety Report, dated March 20, 1967.

13. Fort Calhoun Station - Unit #1, Omaha Public Power District, Facility Description Analysis, dated April 18, 1967.

14. Oconee Nuclear Station Units 1, 2, and 3, Duke Power Company, Preliminary Analysis Amend. #4, dated May 25, 1967.

15. Three Mile Island Nuclear Station, Unit 1, Metropolitan Edison Company, Preliminary Safety Report, Volumes 1, 2, 3. Dated June 6, 1967.

16. Fort St. Vrain Nuclear Generating Station, Public Service Company of Colorado, Application for Construction Permit, Amend. #2, dated May 24, 1967.

4.0 PUBLICATIONS AND TALKS

1. Bernstein, A. B. (1967), "A note on the use of cup anemometers in wind profile experiments," J. Appl. Met. 6(2), 280-286.

2. U. S. Dept. of Commerce (1966), "A catalog of radar-positioned constant-volume balloon (tetroon) flights," Technical Paper No. 58, Environmental Science Services Administration (Gov't. Printing Office, Washington, D. C.).

3. Angell, J. K., D. H. Pack, and C. R. Dickson, "A Lagrangian study of helical circulations in the planetary boundary layer." Paper presented at the 268th National Meeting of the American Meteorological Society, Washington, D. C., April 17-20, 1967.

4. Van der Hoven, I. "Atmospheric Transport and diffusion at coastal sites." Paper presented at the National Health Physics Society Meeting, Washington, D. C., June 19-22, 1967.

5.0 LABORATORY PERSONNEL

5.1 Silver Spring, Maryland

Charles R. Hosler, Meteorologist transferred to the Air Resources Cincinnati Laboratory, Cincinnati, Ohio, on June 30, 1967.

Pauline W. Fuhr, Meteorological Technician transferred to the Naval Oceanographic Office, Washington, D. C., on March 25, 1967.

Ralph R. Soller, Meteorological Technician transferred to the Air Resources Cincinnati Laboratory, Indiana, Pennsylvania.

5.2 National Reactor Testing Station, Idaho

Delbert Sharp transferred to Interoceanic Canal Project, Panama Canal Zone, in April.

John Kearns transferred to Wake Island in May.

Larry Wendell, new Principal Assistant, and Gerald L. Young, Electronic Technician, entered on duty June 30, 1967.

David Bjorem, Research Meteorologist, entered on duty June 30, 1967.

Norman Ricks and Jack Simonds entered on duty for the summer as Meteorological Technicians.

6.0 REFERENCES

Barry, P. J. (1964), "Estimation of downwind concentration of airborne effluents discharged in the neighbourhood of buildings," talk presented to Advisory Committee on the Safety of Particle Accelerators of the Atomic Energy Control Board, Sept. 1963. Atomic Energy of Canada, Limited, Chalk River, Ontario.

Blackman, R. B., and J. W. Tukey (1958), "The measurement of power spectra" (Dover Publications, Inc., New York).

Chamberlain, A. C. (1965), "Deposition." Conference on AEC Meteorological Activities, May 19-22, 1964, BNL 914 (C-42), I. A. Singer, M. E. Smith, and E. W. Bierly, Eds., 125-132, (Brookhaven National Laboratory, Upton, N. Y.).

Chamberlain, A. C. (1966), "Transport of gases to and from grass and grass-like surfaces," Proc. Roy. Soc., Series A-Math and Phys. Sci. 290, 236-265.

Collins, G. F. and N. E. Bowne (1967), "Summary report of summer pilot balloon and woresonde observations at Millstone Point," Travelers Res. Ctr. Serv., Hartford, Conn.

Deacon, E. L. (1959), "The problem of atmospheric diffusion," Int. J. Air Poll., 2(1), 92-108.

Dickson, C. R., G. E. Start, E. H. Markee, Jr., A. P. Richter, and J. Kearns (1967), "Meteorology for the Loss of Fluid Test Reactor, Progress Report," U. S. Atomic Energy Commission, IDO-12059, Idaho Falls, Idaho.

Geiger, R. (1965), "The Climate Near the Ground," (Harvard University Press Cambridge, Massachusetts.)

Halitsky, James, J. Golden, P. Halpern, P. Wu (1963), "Wind tunnel tests of gas diffusion from a leak in the shell of a nuclear power reactor and from a nearby stack,"" New York University, Dept. of Met. & Oceanography, Geophysical Sciences Laboratory Report No. 63-2, Weather Bureau Contract No. CWB-10321.

Hilsmeier, W. F. and F. A. Gifford, Jr. (1962), "Graphs for estimating atmospheric dispersion," ORO-545, U. S. Weather Bureau, Oak Ridge, Tennessee.

Johnson, Otis J. and C. Ray Dickson (1962), "An eight-year summary of the temperature gradient below 250-feet at the National Reactor Testing Station," IDO-12025, USWB, National Reactor Testing Station, Idaho Falls, Idaho.

Kaimal, J. C. (1963), "A simplified sonic anemometer for measuring the vertical component of wind velocity," AFCRL-63-203, Air Force Cambridge Research Laboratories, Office of Aerospace Research, U. S. Air Force, L. G. Hanscom Field, Mass.

Kao, S. K., and A. A. Gain (1967), "Dispersion of particles in the troposphere," U. S. Atomic Energy Commission, Division of Biology and Medicine, Contract AT(11-1)-1585).

MacCready, P. B., Jr. (1962), "The inertial subrange of atmospheric turbulence," J. Geophys. Res., 67(3), 1051-1059.

Owen, P. R. and W. R. Thomson (1963), "Heat transfer across rough surfaces," J. Fluid Mech. 15, 321-334.

Pasquill, F. (1962), "Recent broad-band spectral measurements of turbulence in the lower atmosphere," J. Geophys. Res., 67(8), 3025-3028.

Sheppard, P. A. (1958), "Turbulent transfer through the earth's surface and through the air above," Quart. J. Roy. Meteorol. Soc., 84, 205-216.

Thornthwaite, C. W., W. J. Superior, J. R. Mather, and F. K. Hare (1961), "The measurement of vertical winds and momentum flux," Climatology, Vol. XIV (1) (C. W. Thornthwaite Assoc., Centerton, N. J.).

Wagner, R. J. (1965), "Heat Conduction Code No. 1, "Computer Program PPCo 40.0190, Computer Center, National Reactor Testing Station, Idaho.

Wong, E. Y. J., and K. C. Brundidge (1966), "Vertical and temporal distribution of the heat conductivity and flux," J. Atmospheric Sci. 23, 167-178.

Yanskey, G. R., E. H. Markee, Jr., and A. P. Richter (1966), "Climatology of the National Reactor Testing Station," U. S. Atomic Energy Commission, IDO-12048, Idaho Falls, Idaho.

7.0 FIGURE CAPTIONS

Figure	Caption
1.	Maximum height of vertical mixing due to surface heating as a function of overland travel distance and speed and initial overwater vertical stability.
2.	Vertical wind component spectra for N. J. marsh study (Oct. 1966).
3.	EBR II Complex
4.	Mean dilution ratio.
5.	Mean dilution ratio.
6.	K-Mean isopleths of effluent release through containment building.
7.	K-Mean isopleths of effluent release through containment building.
8.	K-Max isopleths of effluent release through containment building.
9.	K-Min isopleths of effluent release through containment building.
10.	K-Max isopleths of effluent release through containment building.
11.	K-Min isopleths of effluent release through containment building.
12.	Halitsky wind tunnel K-isopleths for neutral release.
13.	Measured vs. computed lateral particle standard deviation for all cases.

14. Comparison of averaged σ_y computations with distance downwind.

15. Measured lateral particle standard deviation vs. downwind distance.

16. Computed vertical particle standard deviation vs. downwind distance.

17. Peak concentration vs. downwind distance.

18. Peak concentration vs. downwind distance.

19. Electrical resistance analogy.

20. Relationship between median carbon plate deposition velocities and Sheppard model calculations.

21. Relationship between measured and calculated surface sublayer resistance - carbon plates.

22. Comparison between carbon plate V_d and V_d calculated from the resistance analogy model.

23. Relationship between grass deposition velocity and grass density during one release.

24. Relationship between normalized grass V_d and boundary layer transfer velocity.

25. Relationship between measured and calculated surface sublayer resistance - grass.

26. Eddy diffusivity, K, profiles by stability class.

27. Wind velocity profiles by stability class.

28. Comparison of σ_z values by stability class and distance downwind.

29. Air concentration reduction factor variation with height for selected distances downwind - stable - perfect sink.

30. Air concentration reduction factor variation with height for selected distances downwind - neutral - perfect sink.

31. Air concentration reduction factor variation with height for selected distances downwind - unstable - perfect sink.

32. Height of the maximum air concentration with distance downwind by stability class.

33. Dispersion of a cluster of four tetroons in space and time.

34. Mean auto-correlation functions of the vertical, along- and cross-wind components of the relative velocities.

35. Mean normalized power-spectra of the vertical, along- and cross-wind components of the relative velocities.

36. Mean cross-correlation functions of the vertical, along- and cross-wind components of the relative velocities.

37. Mean normalized cross-spectra of the vertical, along- and cross-wind components of the relative velocities.

38. Variances of vertical, along- and cross-wind components of the relative displacements.

39. Covariance of the along- and cross-wind components of the relative displacements, and the angle between the principal axis of diffusion and the direction of the mean wind.

40. Nomogram for environmental radiological calculations for TREAT.

41. Sample printout of computer analyzed concentration field.

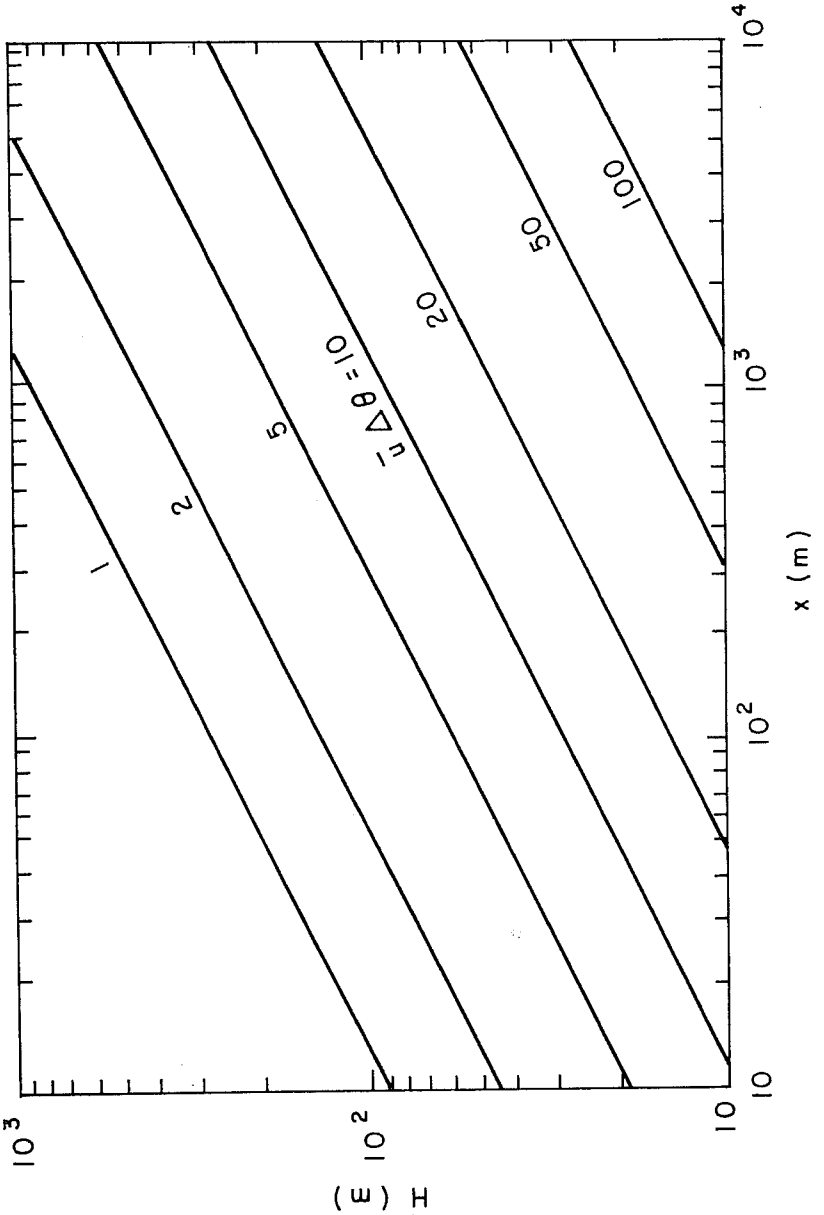

Fig. 1. Maximum height of vertical mixing due to surface heating as a function of overland travel distance and speed and initial overwater vertical stability.

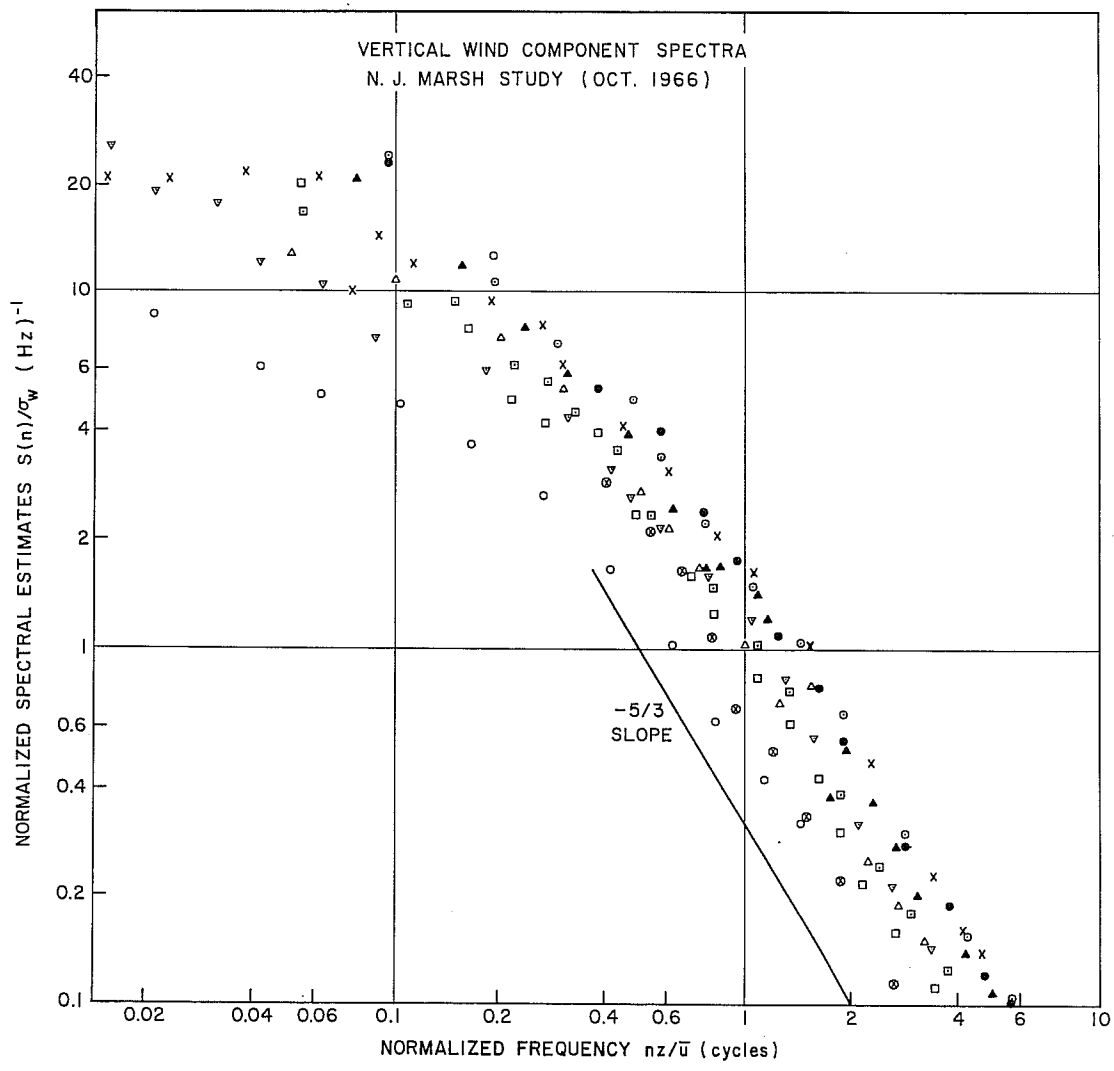

Fig. 2. Vertical wind component spectra for N. J. marsh study (Oct. 1966).

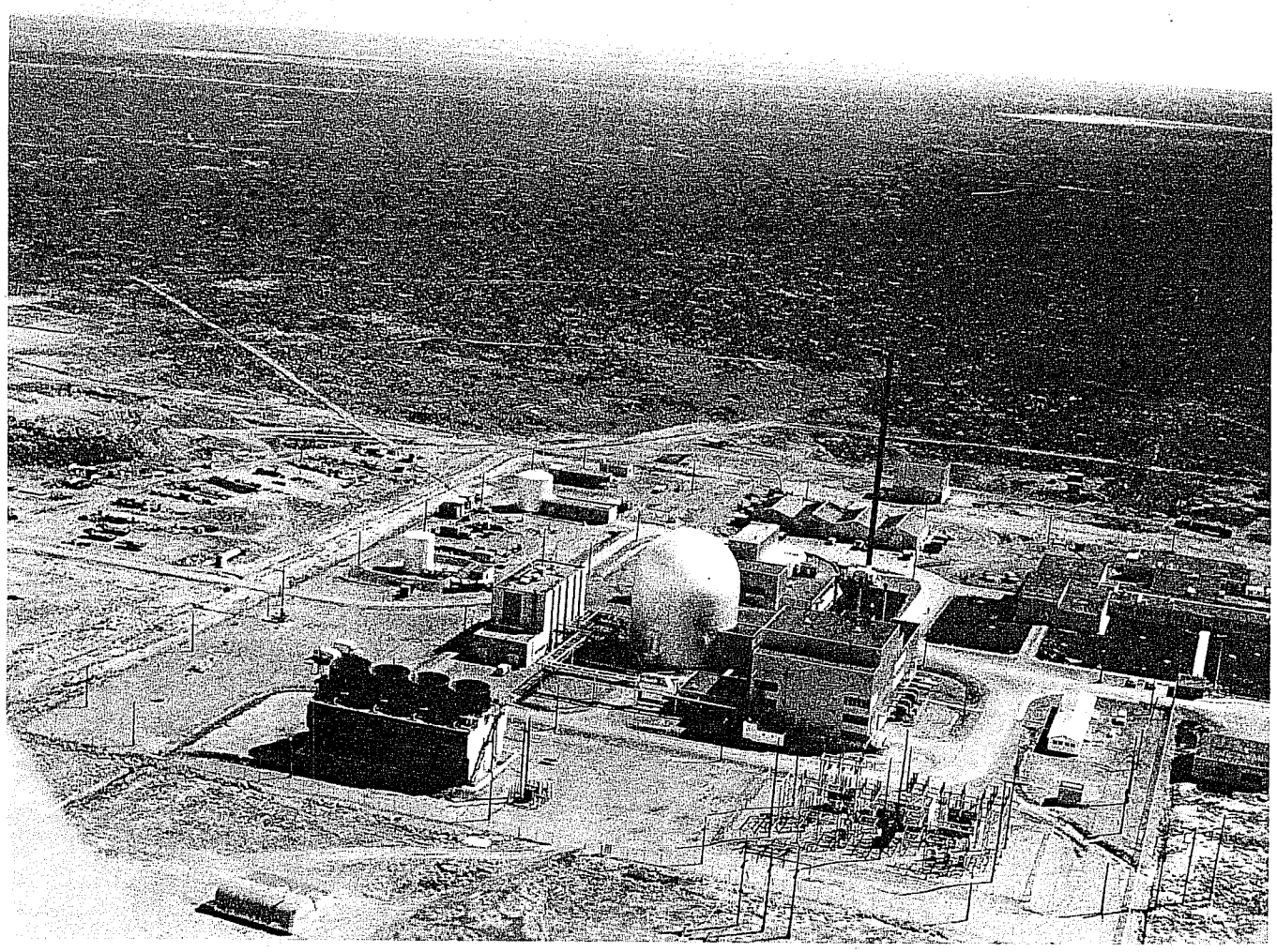

Fig. 3. EBR II Complex.

B- 72369

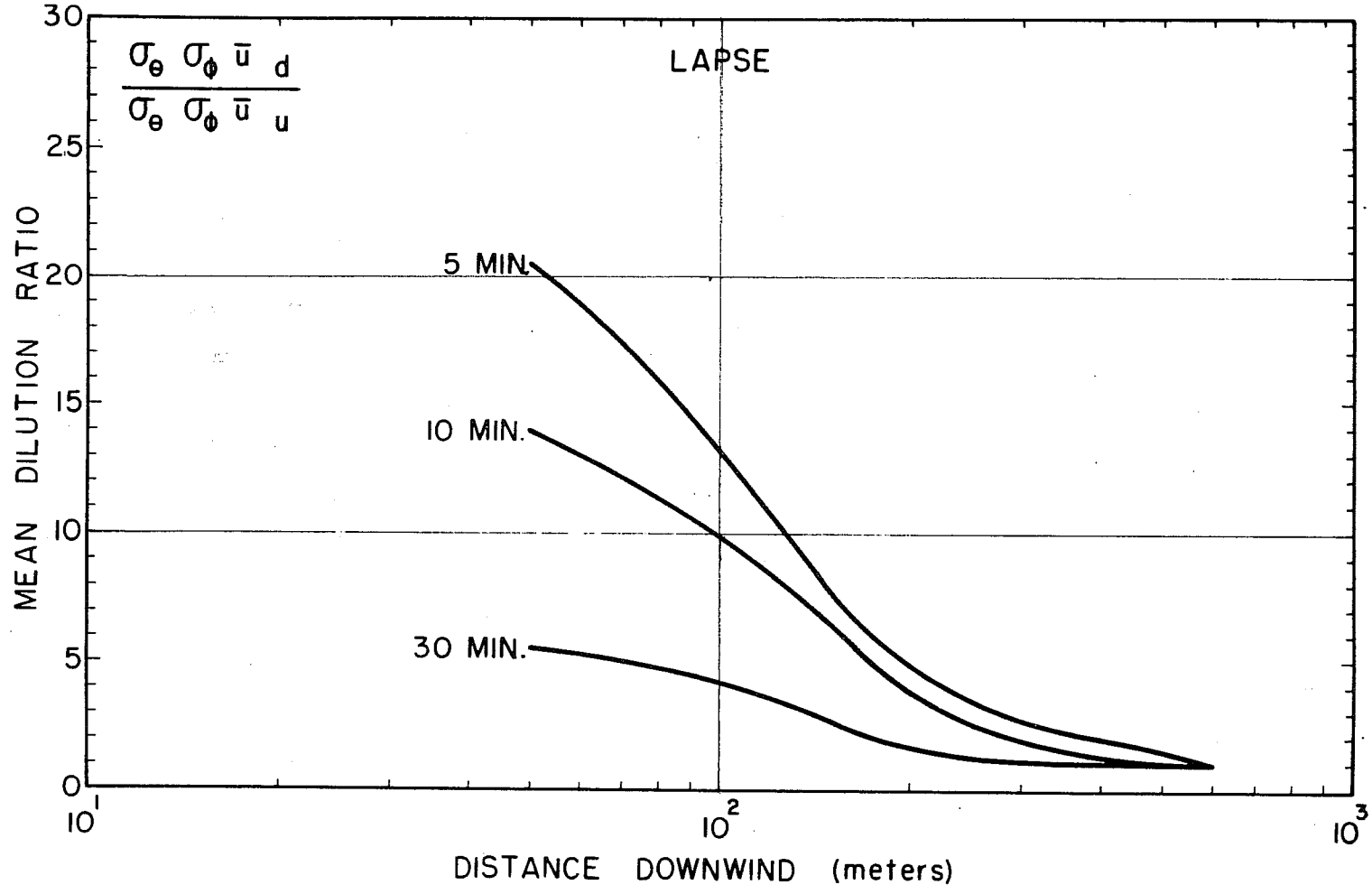

Fig. 4. Mean dilution ratio.

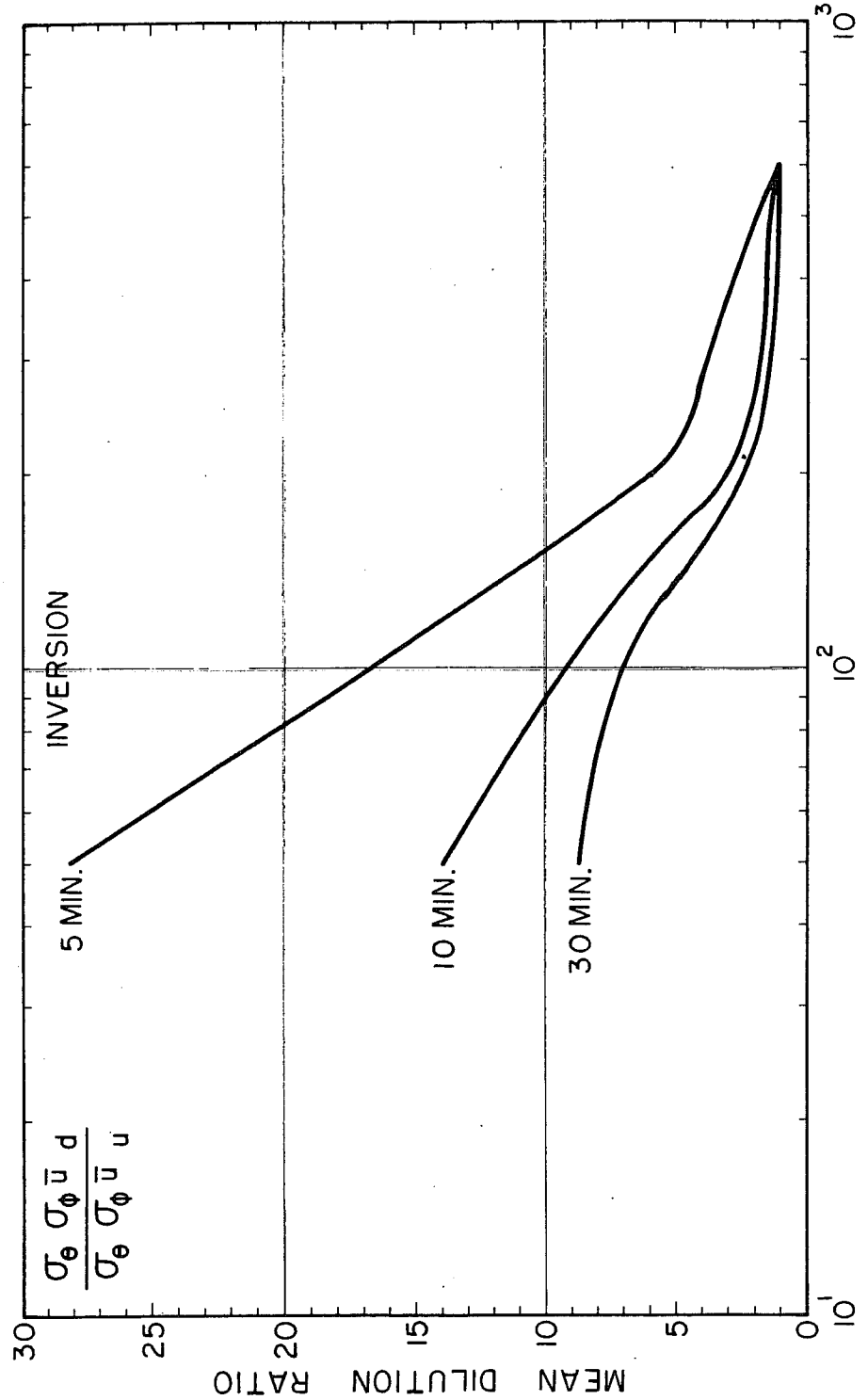

Fig. 5. Mean dilution ratio.

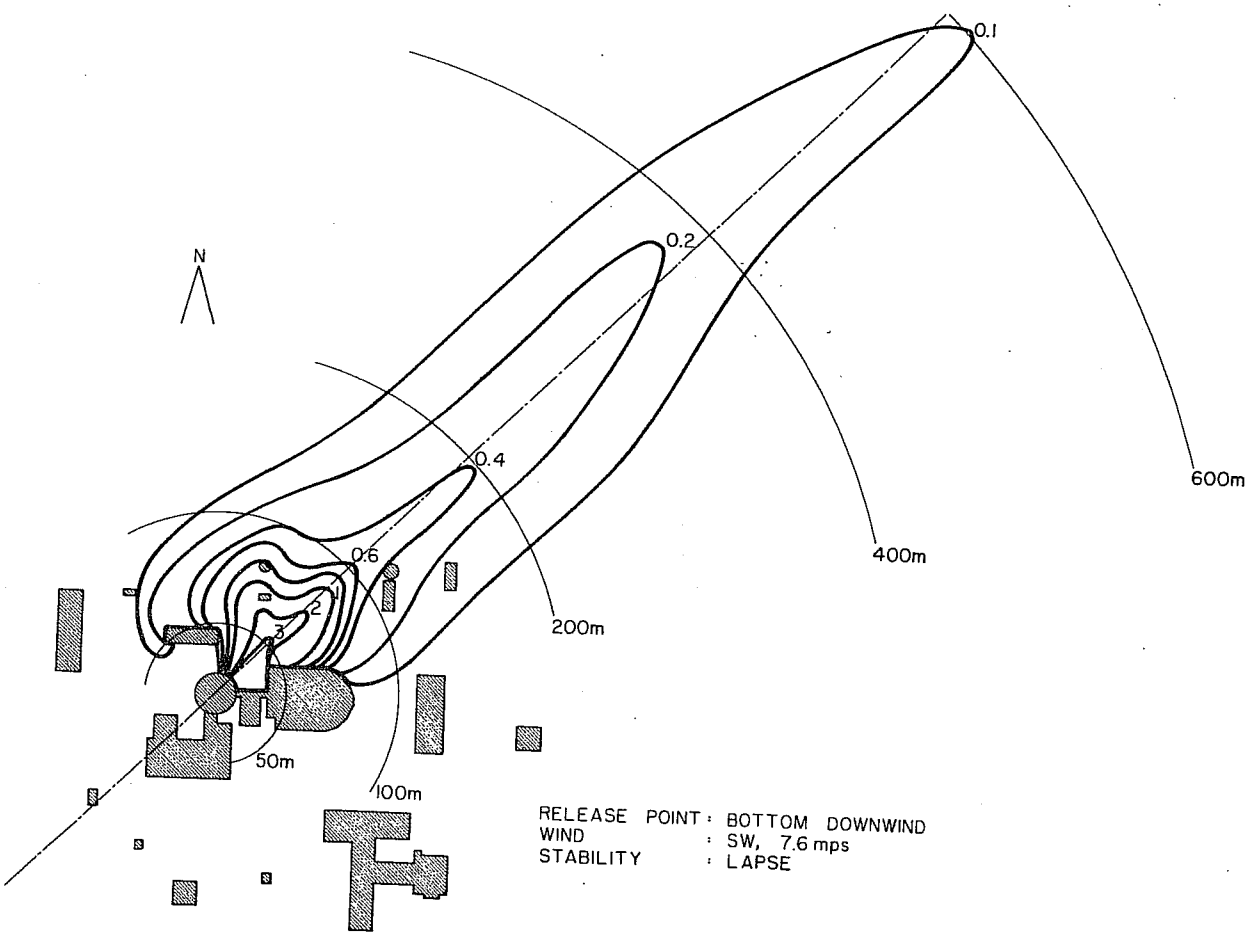

Fig. 6. K-Mean isopleths of effluent release through containment building.

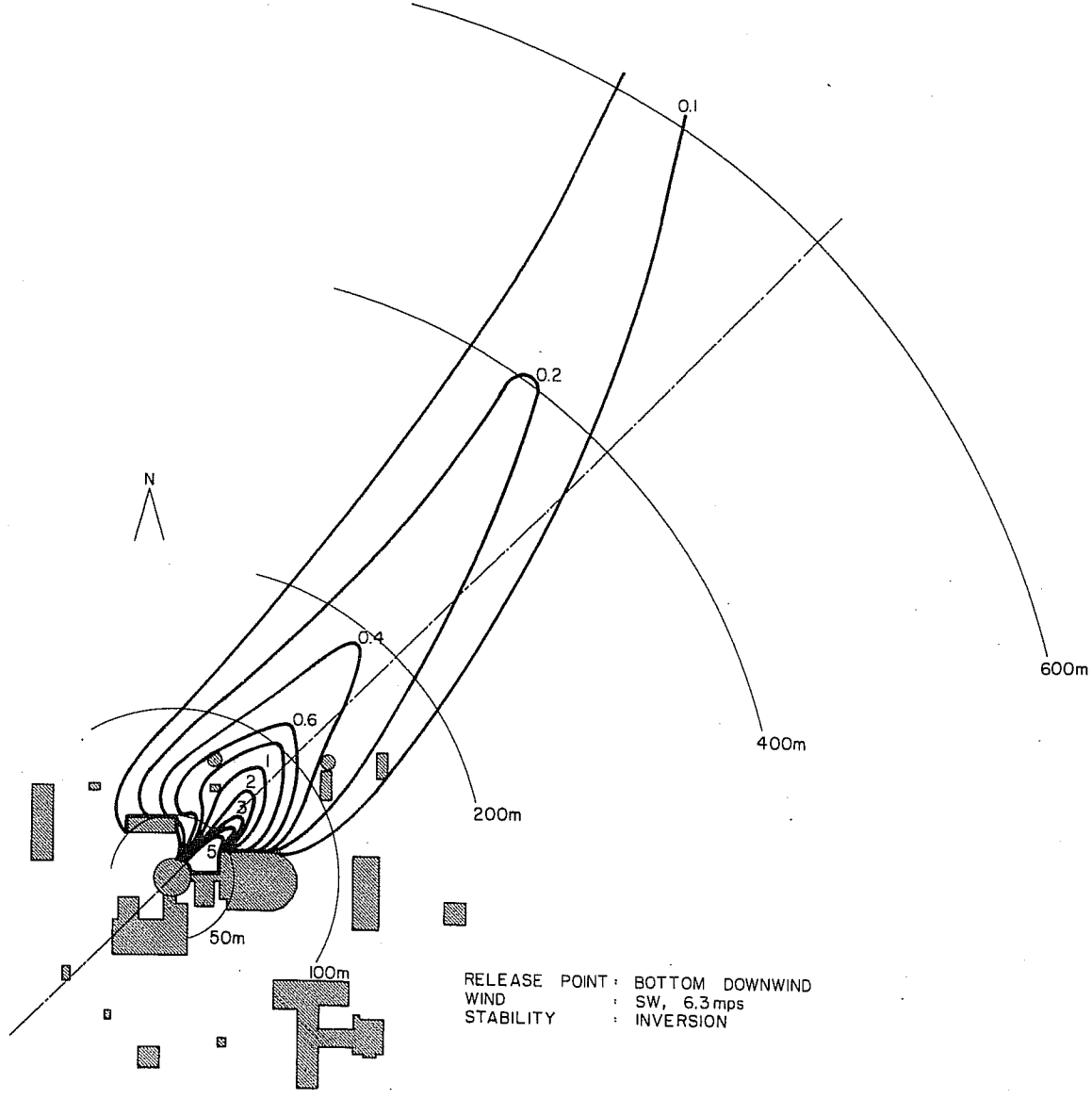

Fig. 7. K-Mean isopleths of effluent release through containment building.

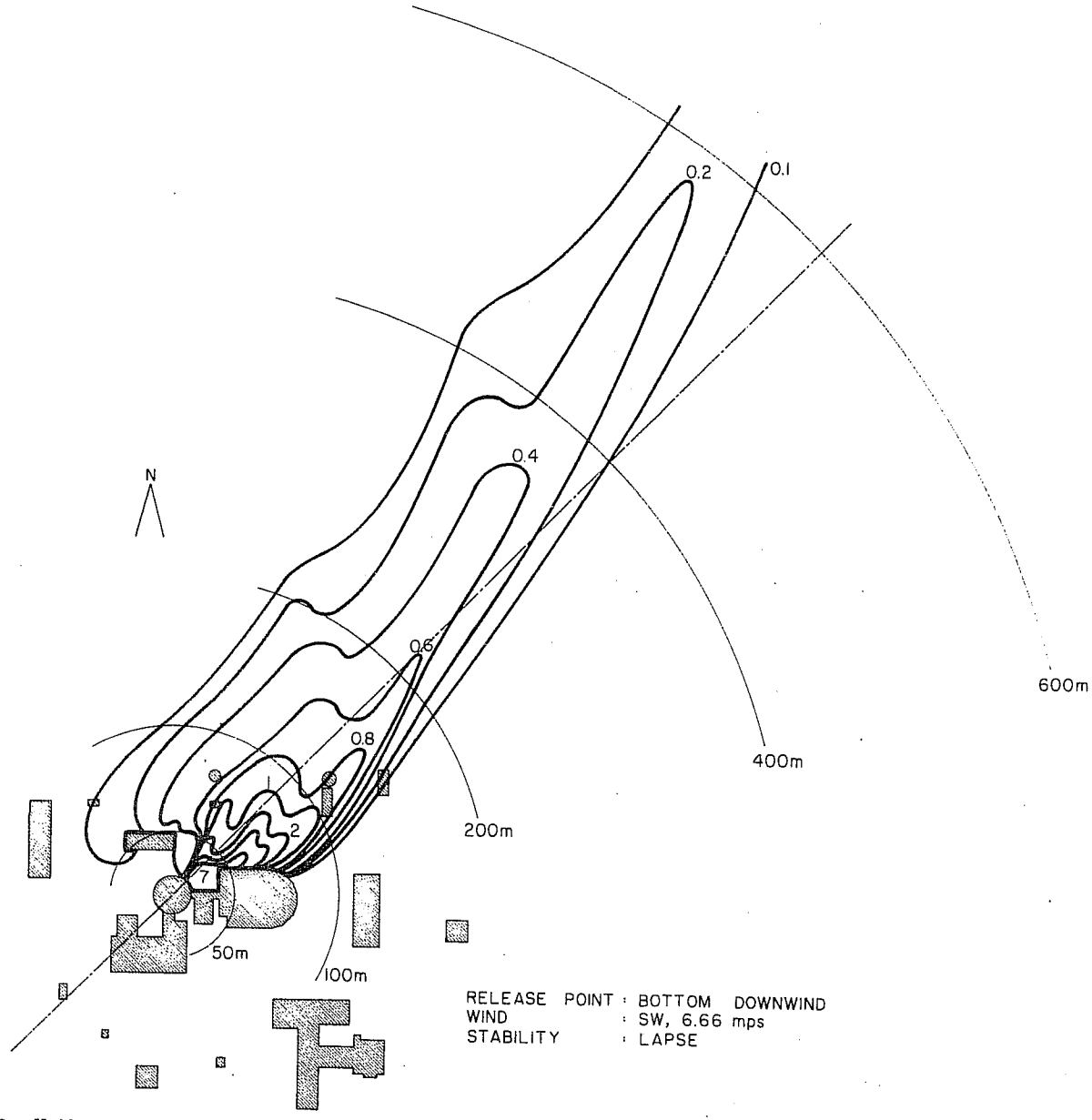

Fig. 8. K-Max isopleths of effluent release through containment building.

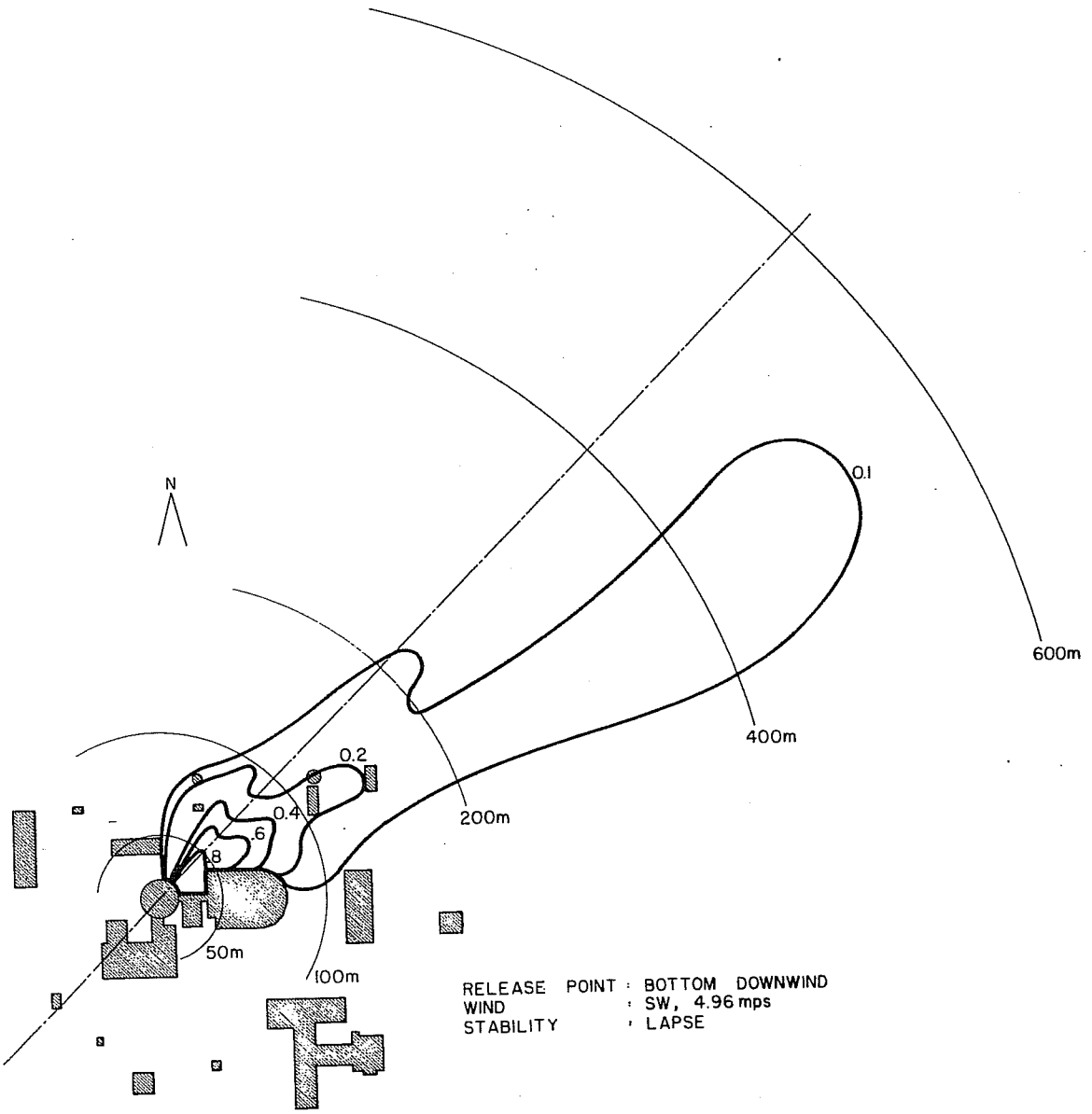

Fig. 9. K-Min isopleths of effluent release through containment building.

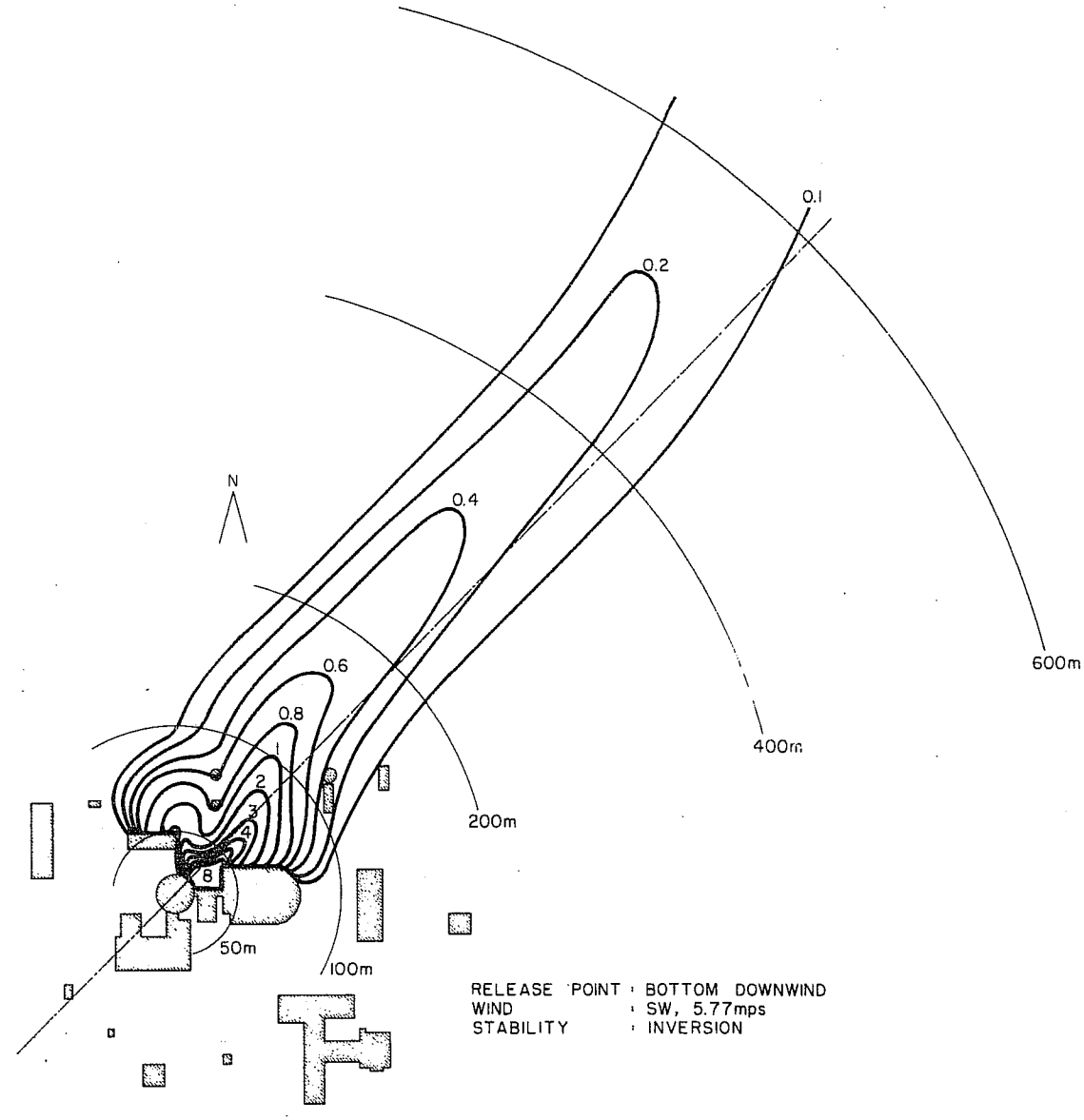

Fig. 10. K-Max isopleths of effluent release through containment building.

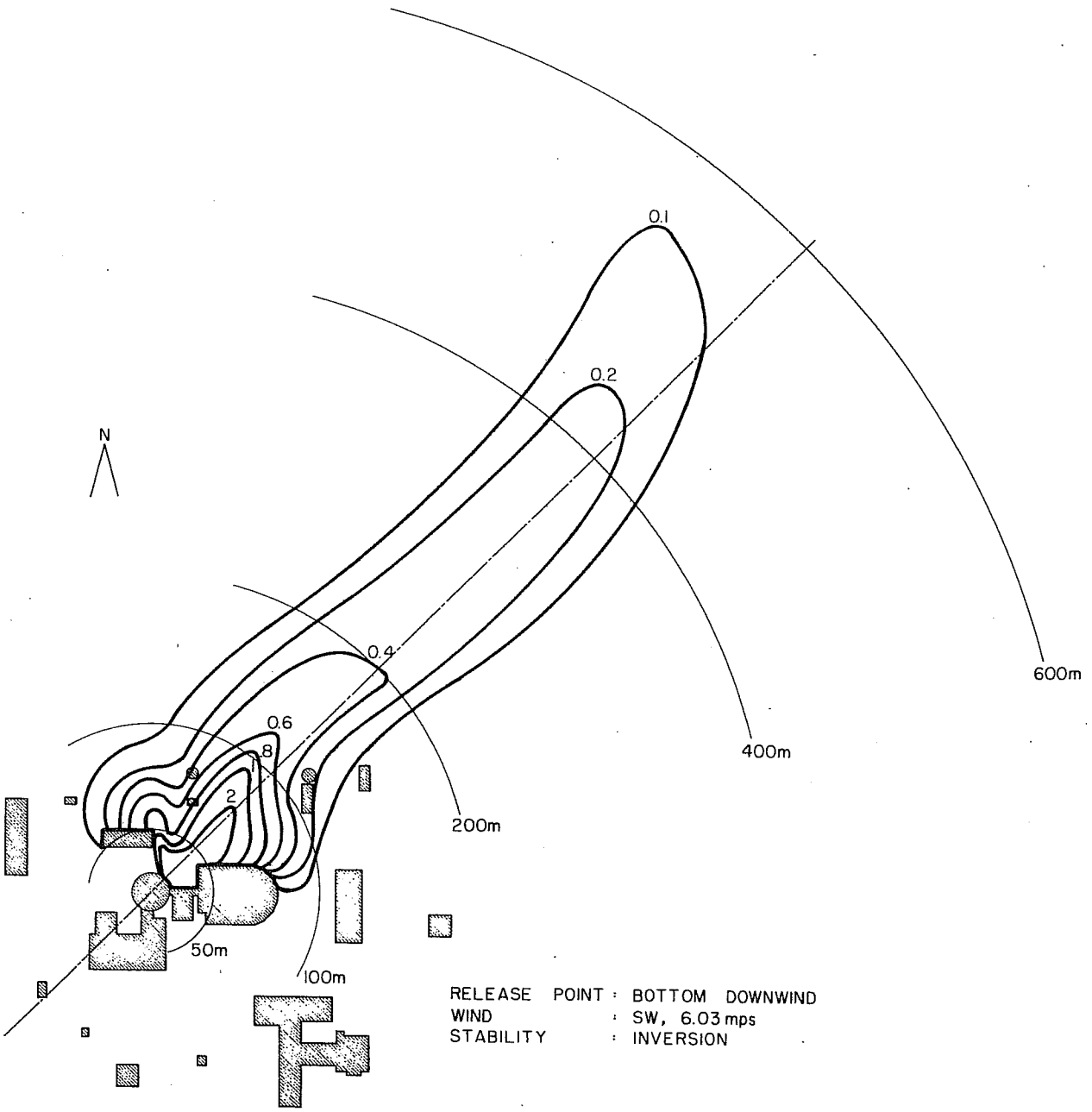

Fig. 11. K-Min isopleths of effluent release through containment building.

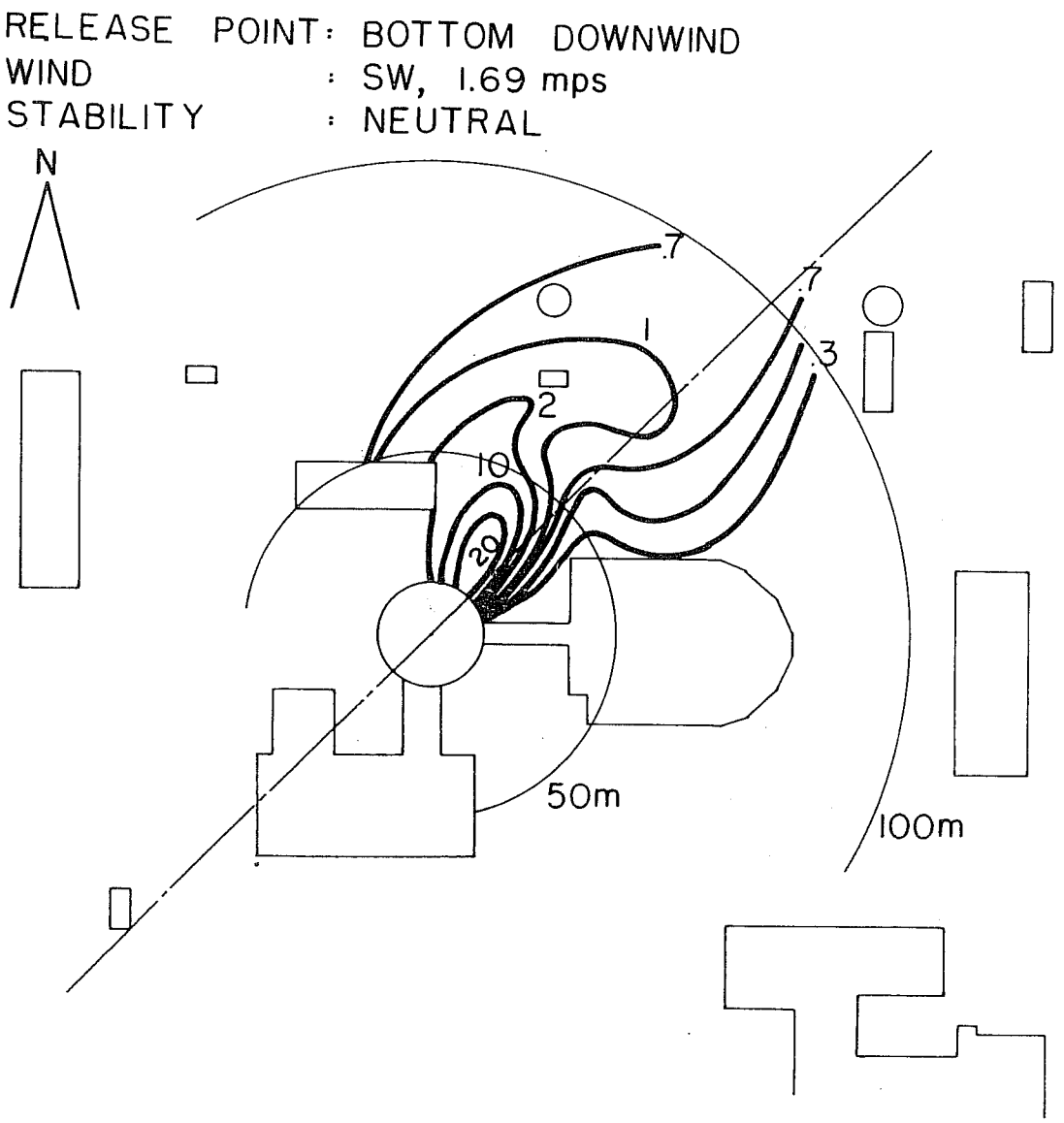

Fig. 12. Halitsky wind tunnel K-isopleths for neutral release.

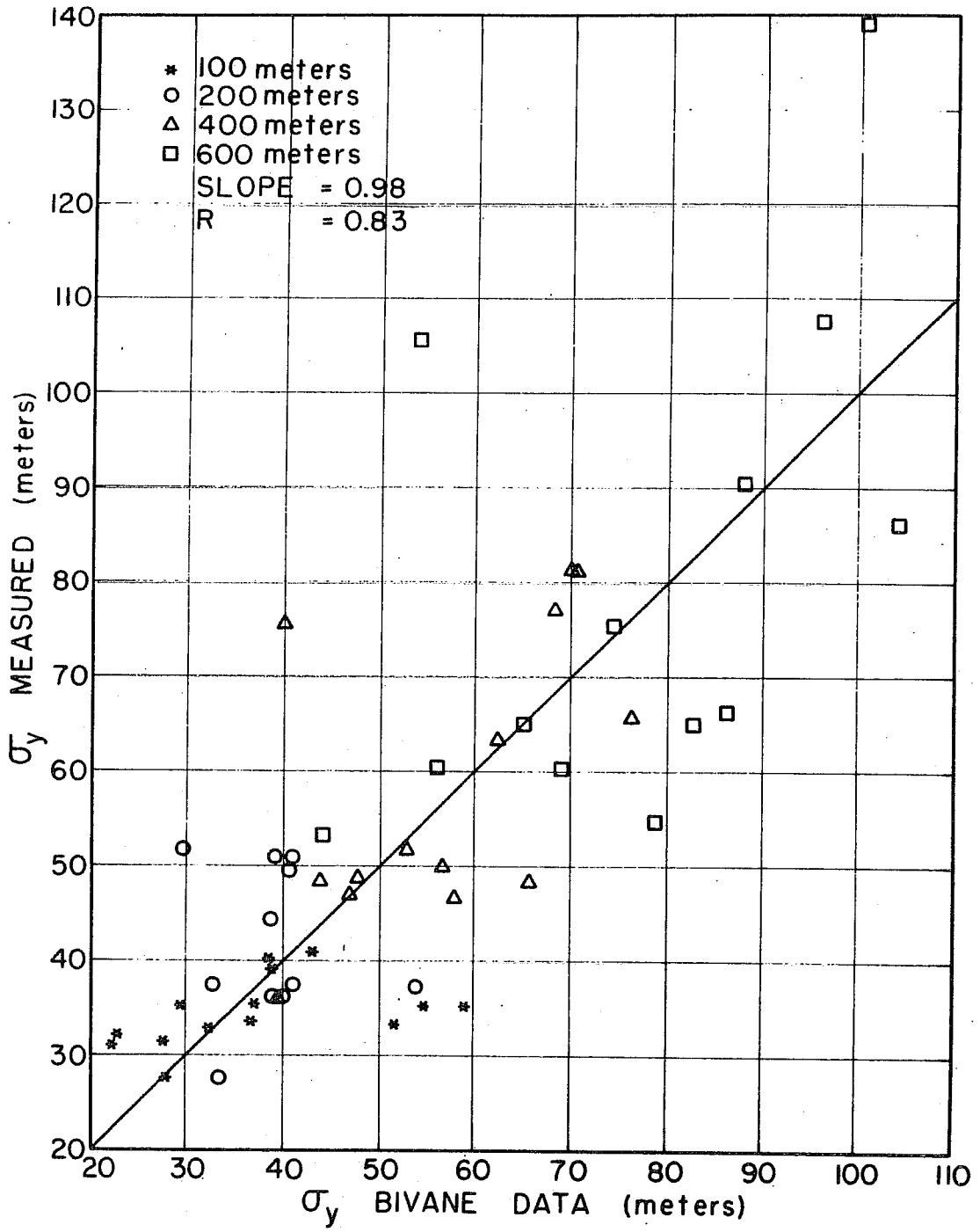

Fig. 13. Measured vs. computed lateral particle standard deviation for all cases.

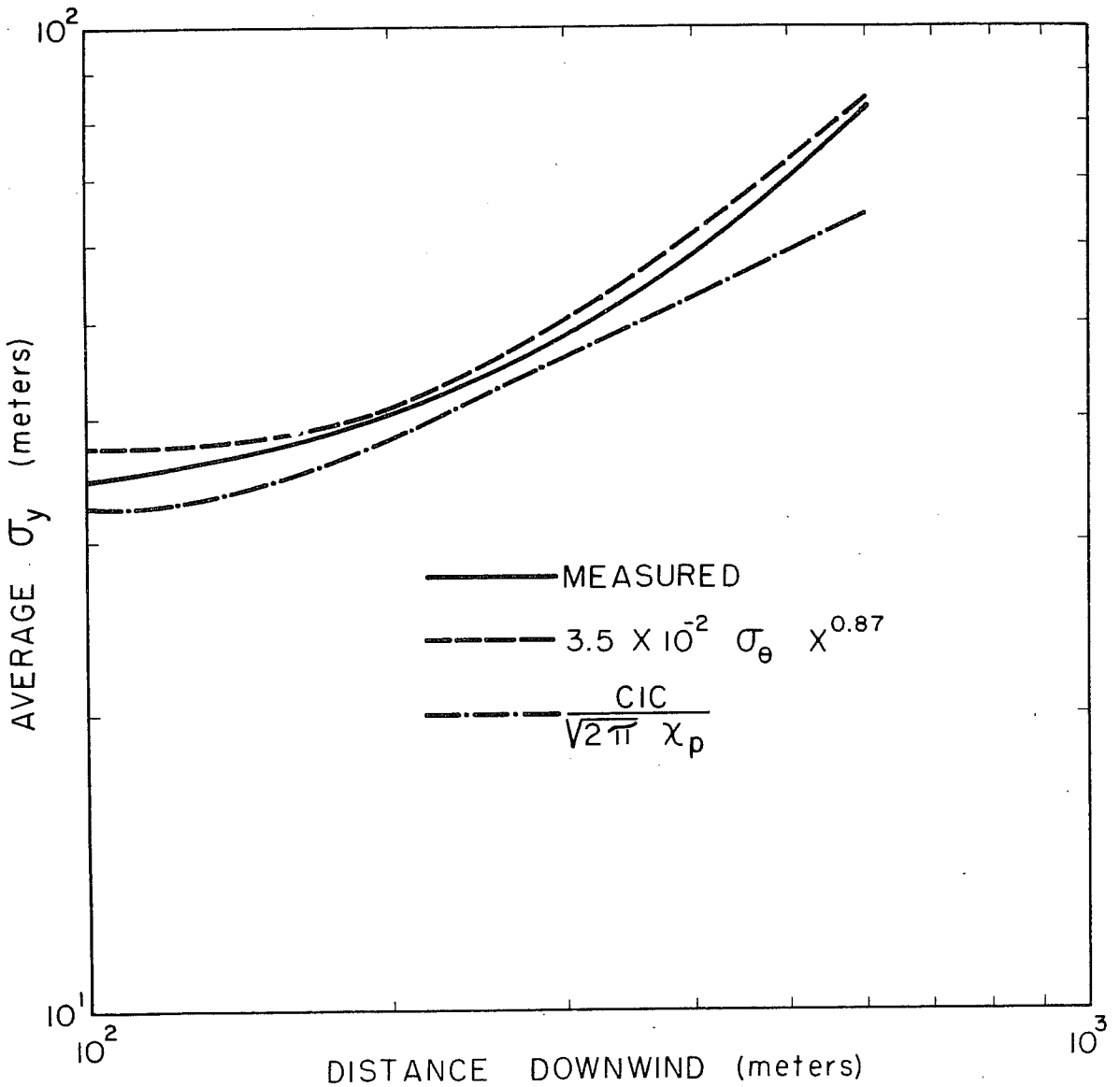

Fig. 14. Comparison of averaged σ_y computations with distance downwind.

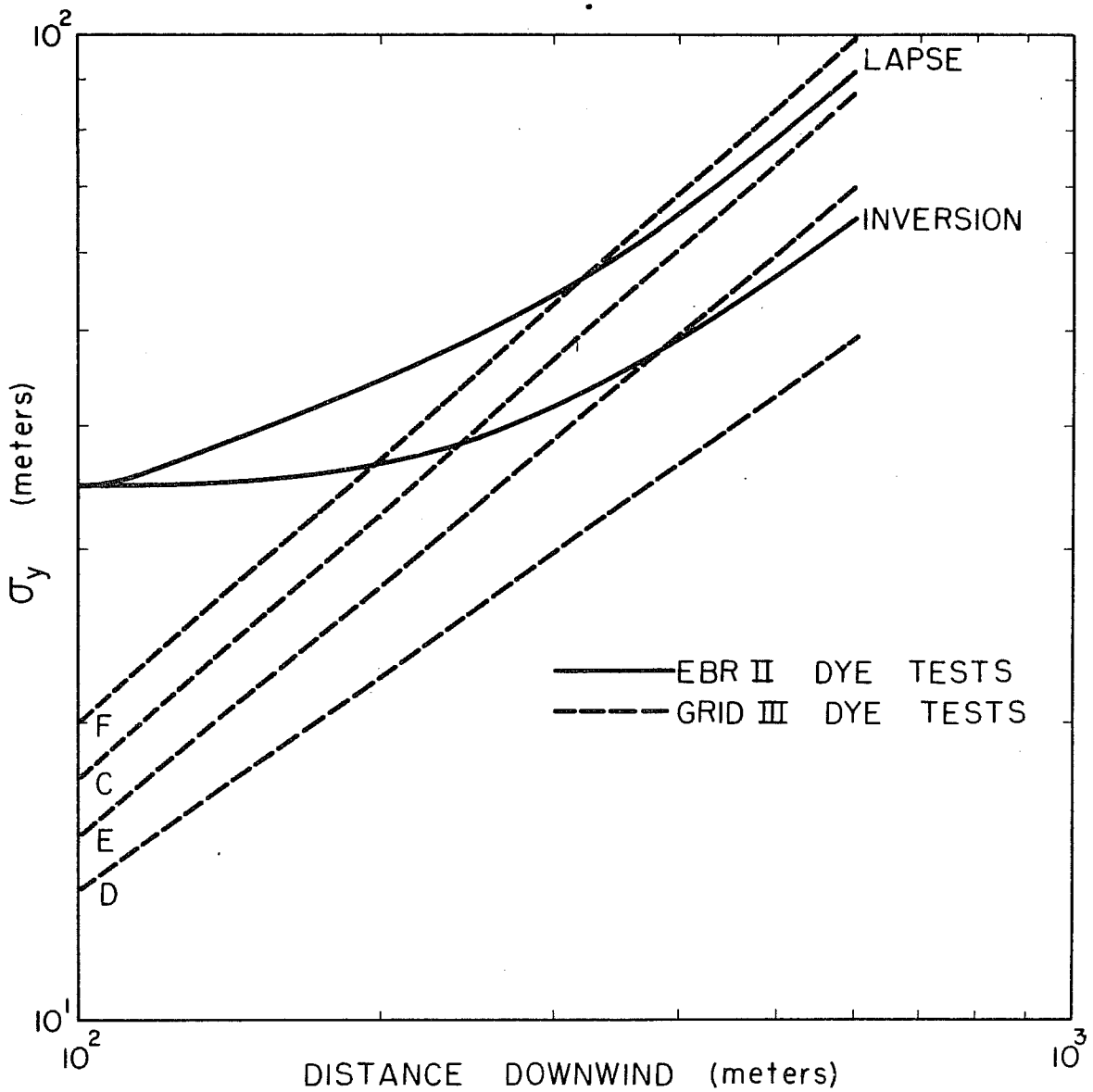

Fig. 15. Measured lateral particle standard deviation vs. downwind distance.

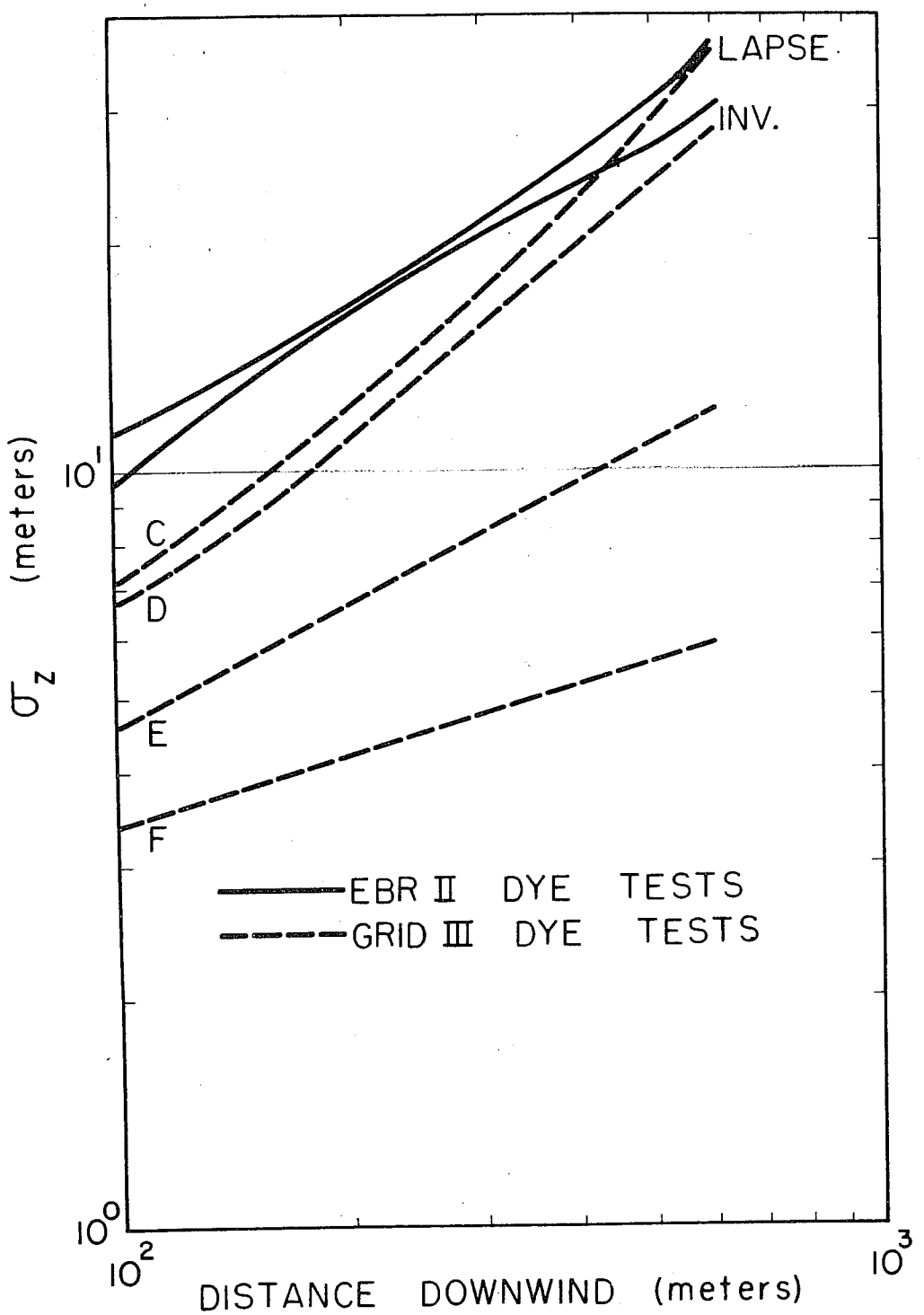

Fig. 16. Computed verticle particle standard deviation vs. downwind distance.

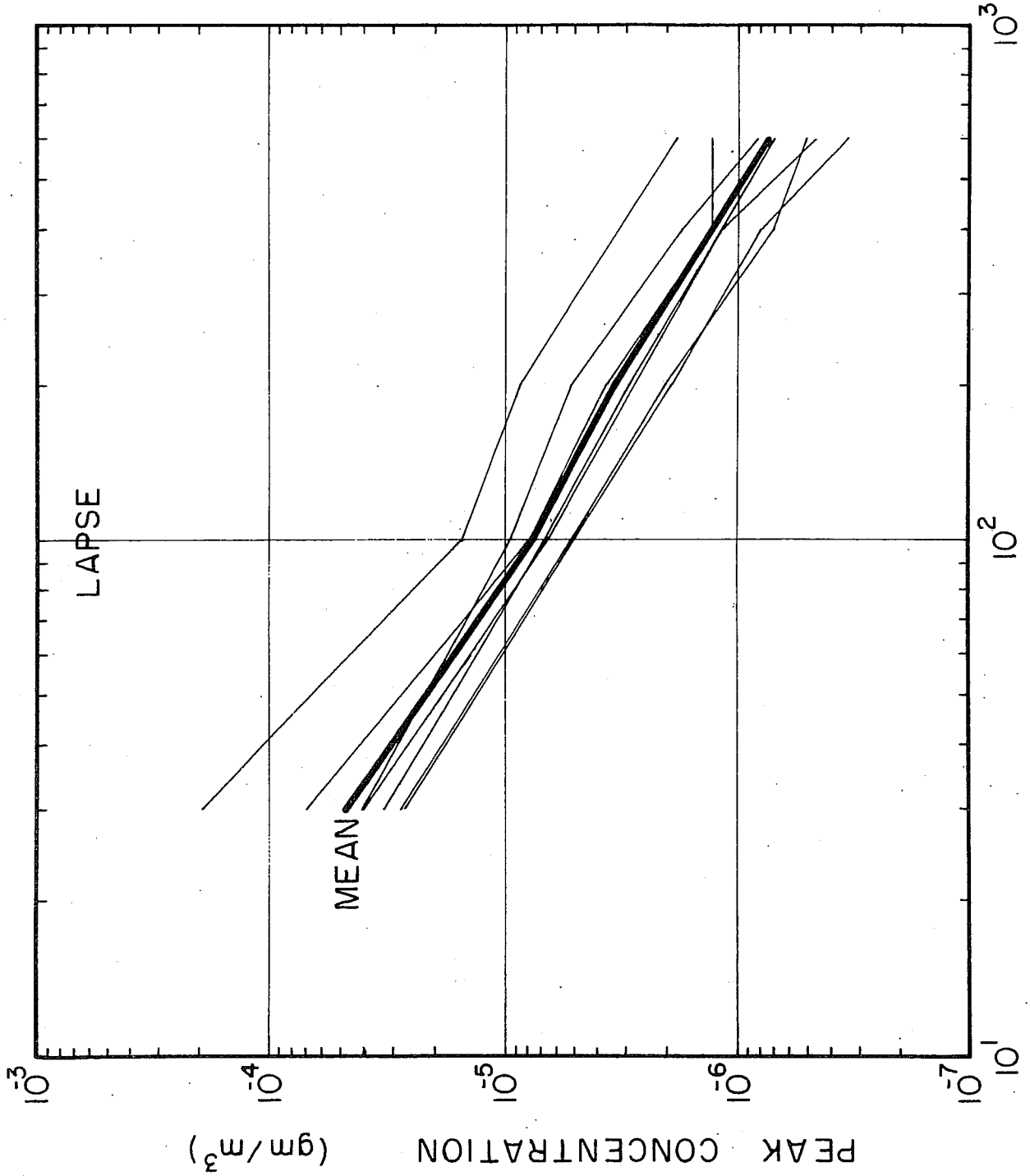

Fig. 17. Peak concentration vs downwind distance.

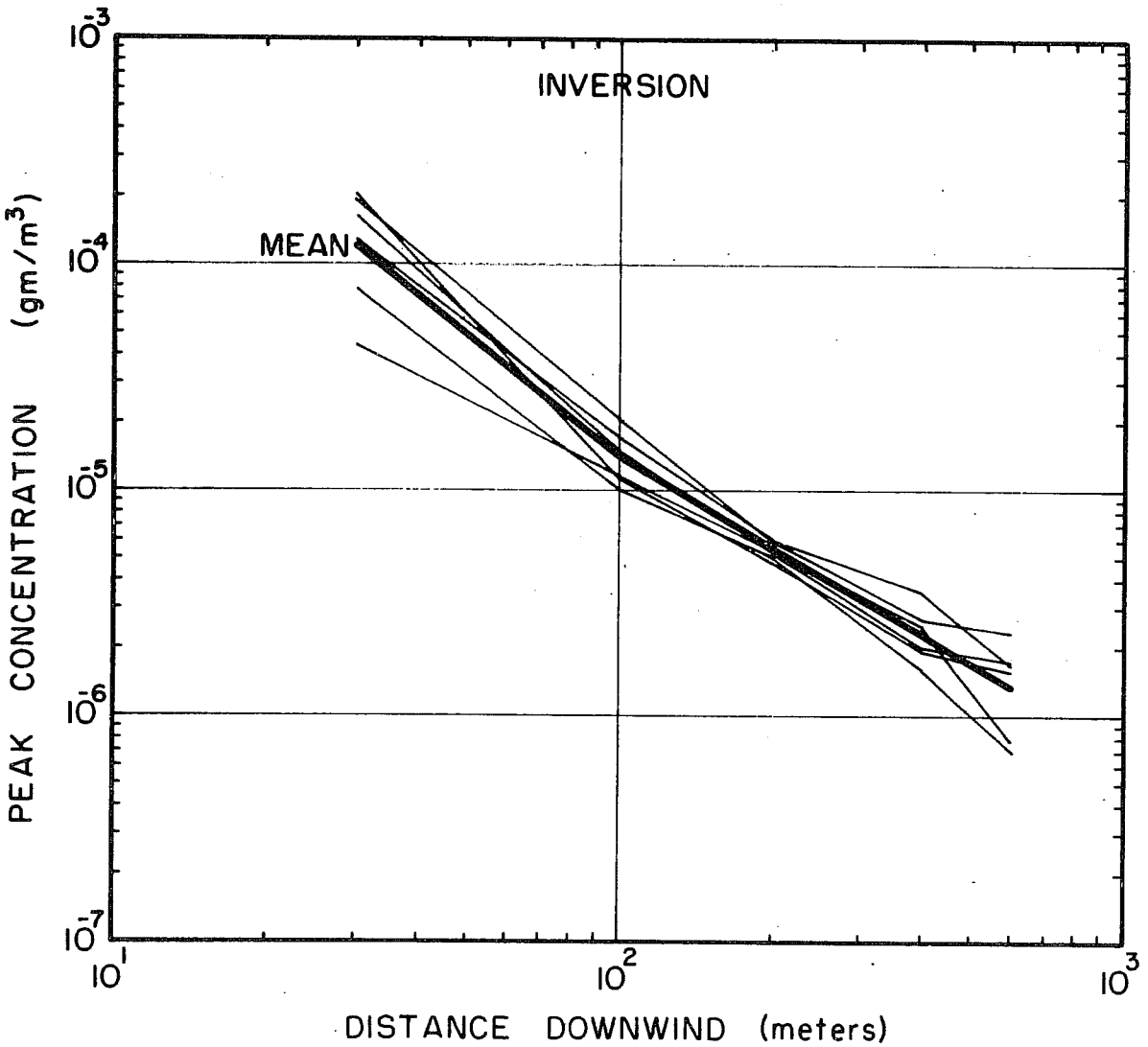

Fig. 18. Peak concentration vs downwind distance.

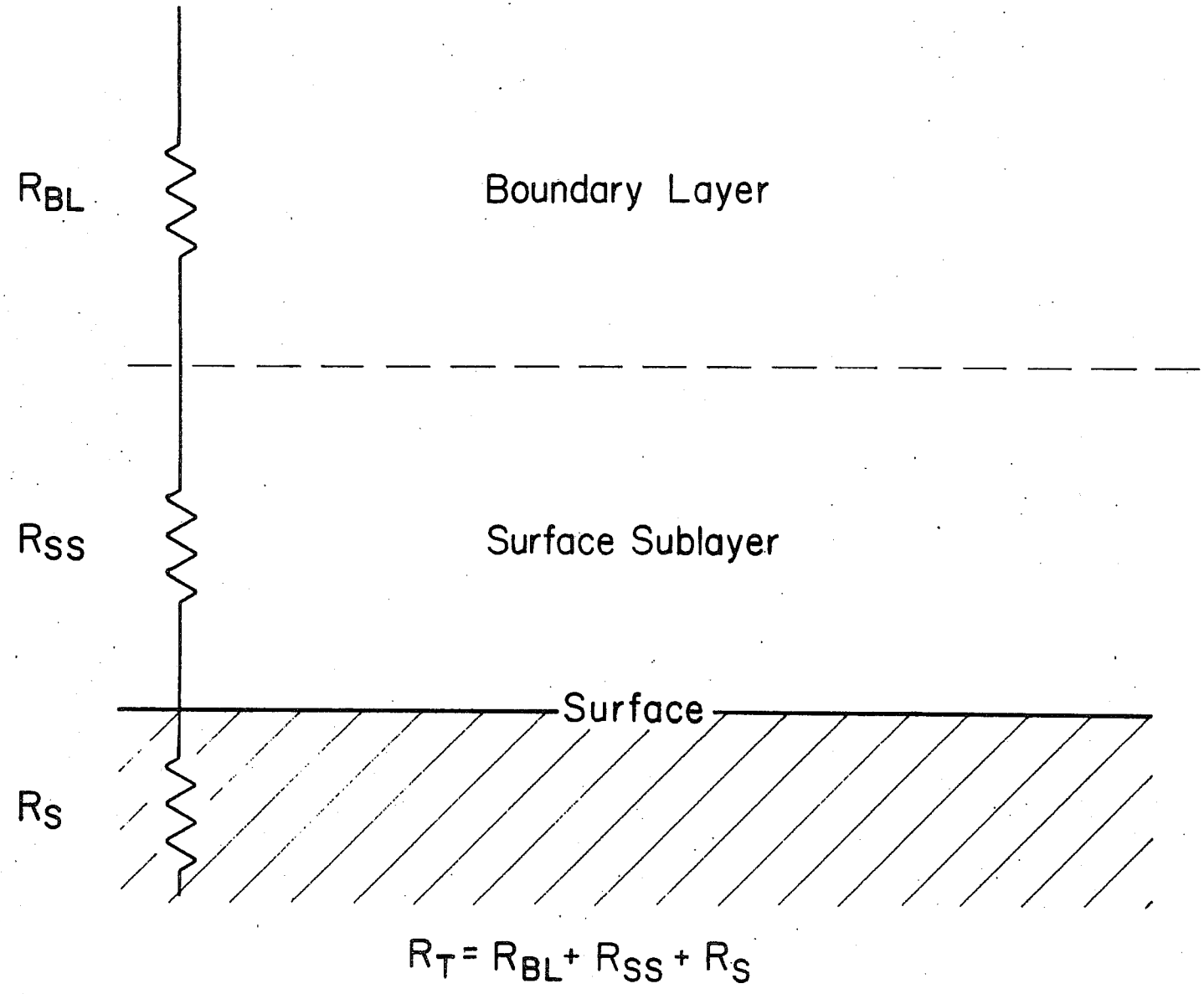

Fig. 19. Electrical resistance analogy.

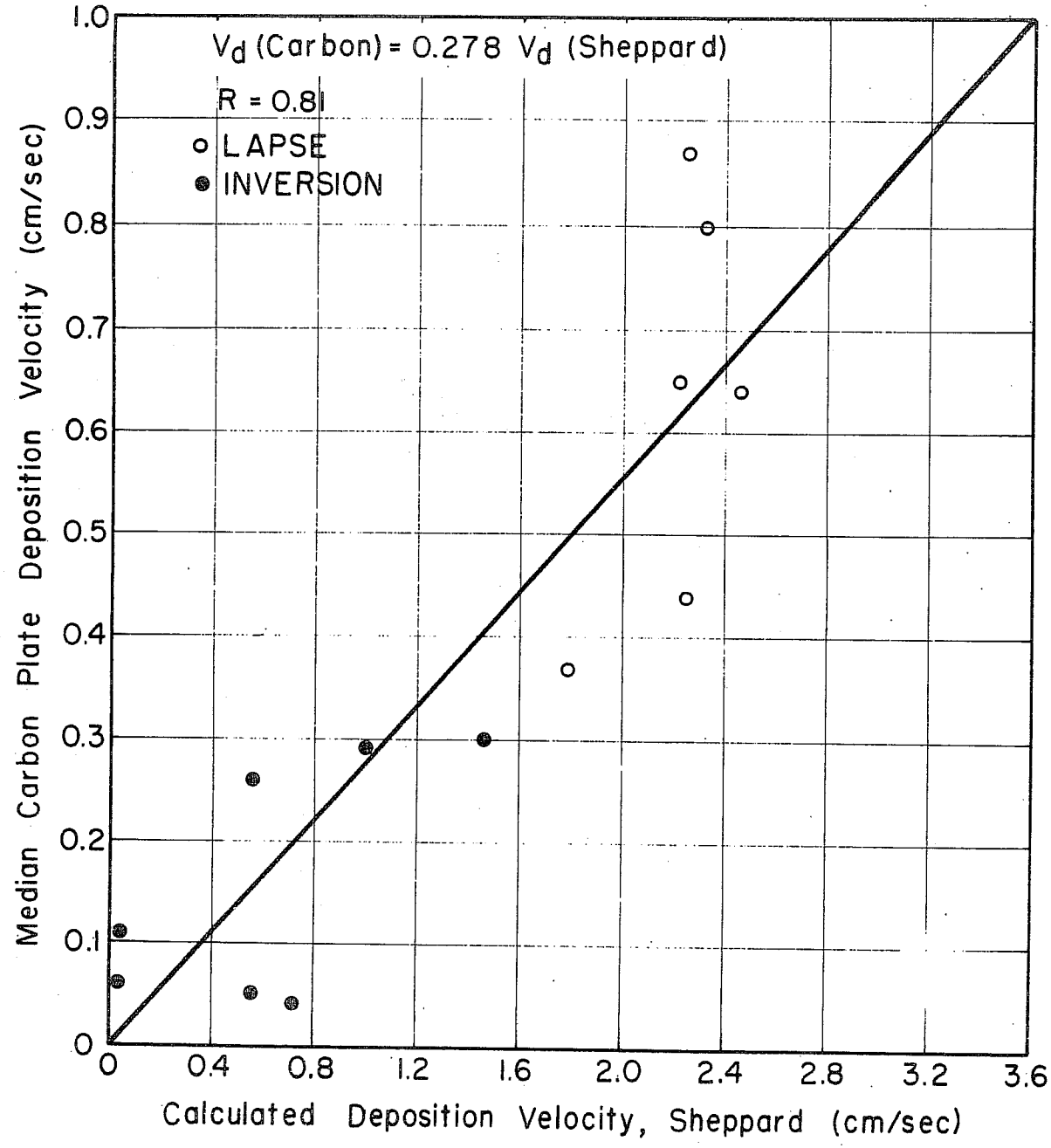

Fig. 20. Relationship between median carbon plate deposition velocities and Sheppard model calculations.

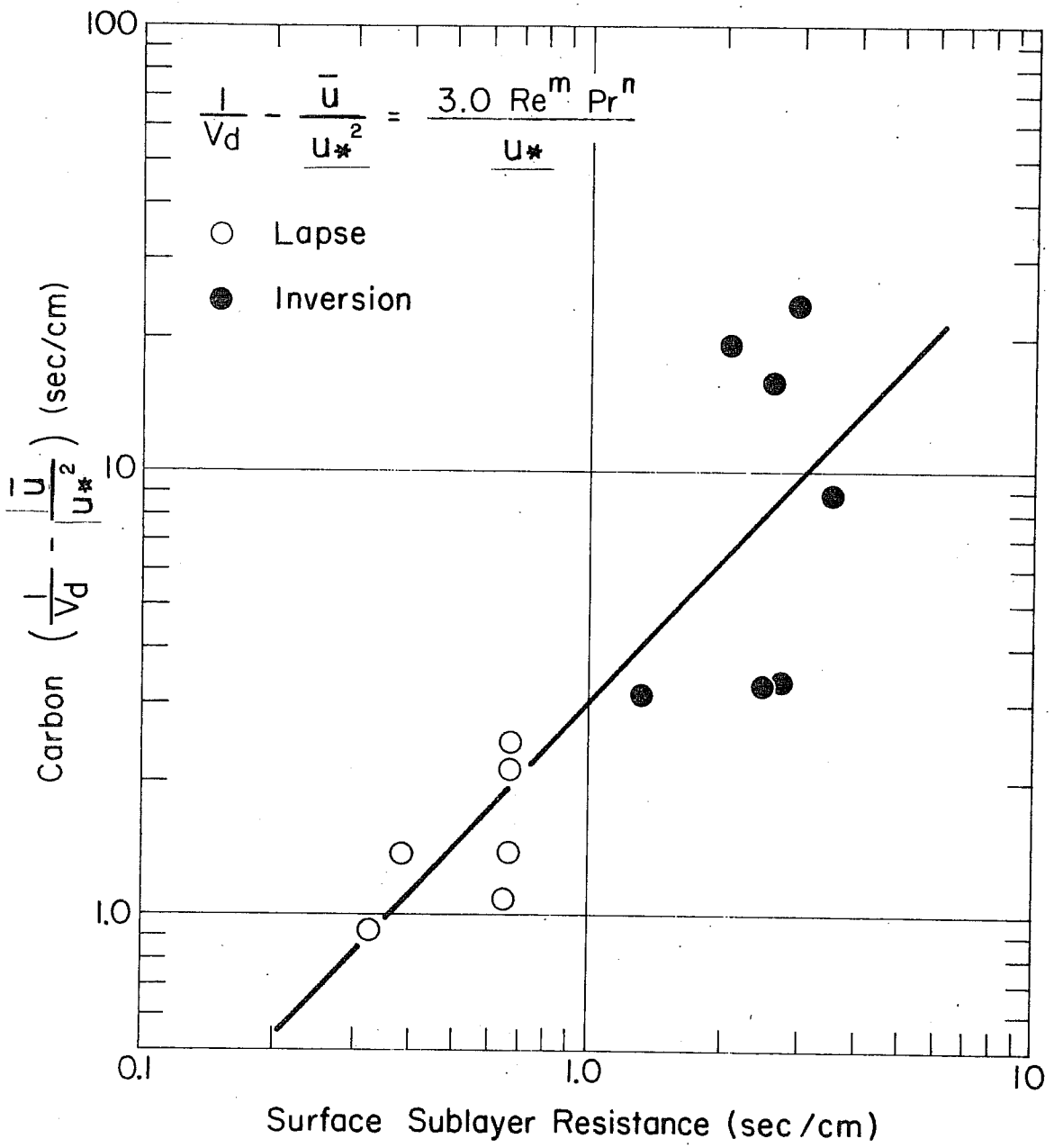

Fig. 21. Relationship between measured and calculated surface sublayer resistance - carbon plates.

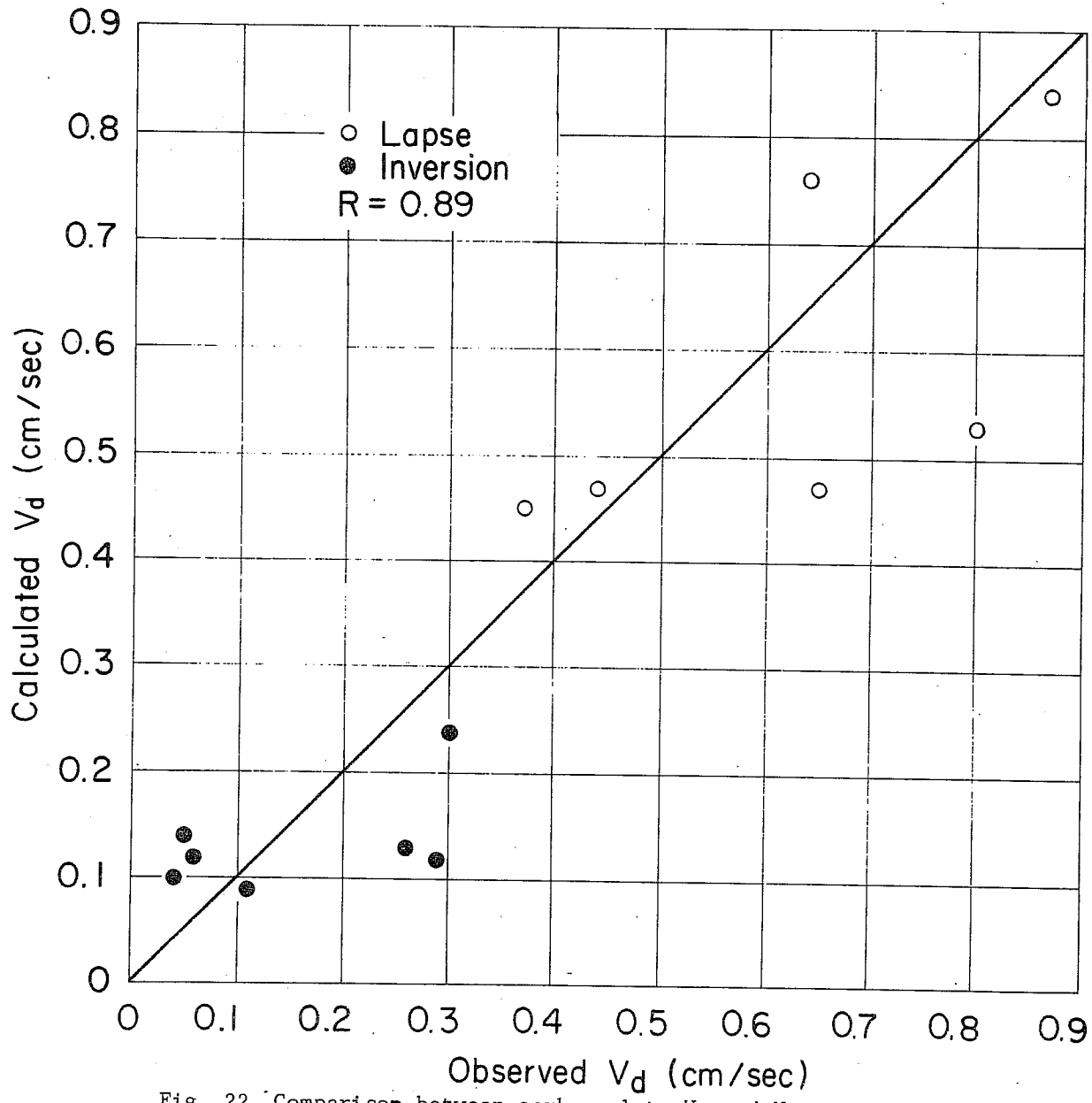

Fig. 22. Comparison between carbon plate V_d and V_d calculated from resistance analogy model.

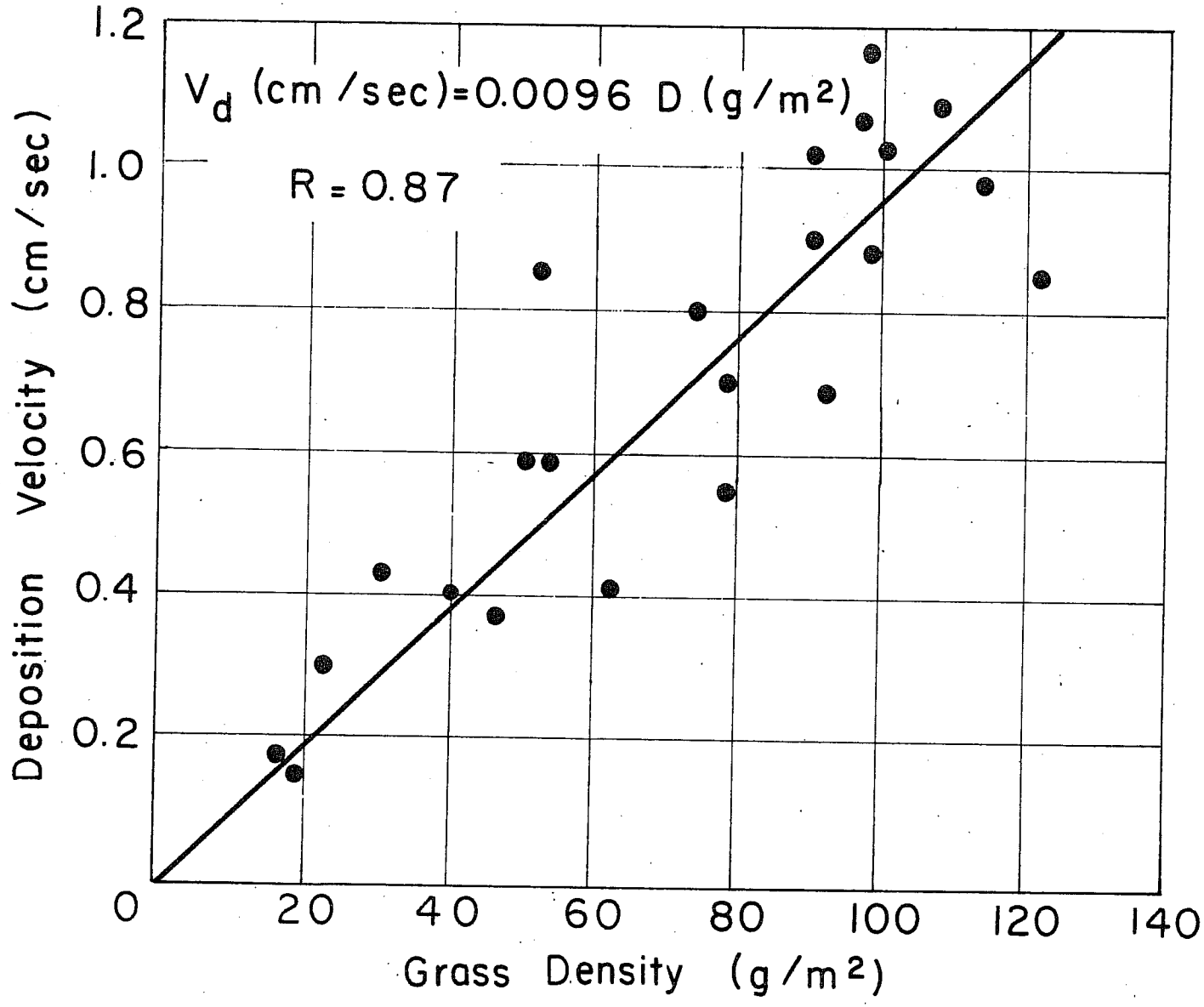

Fig. 23. Relationship between grass deposition velocity and grass density during one release.

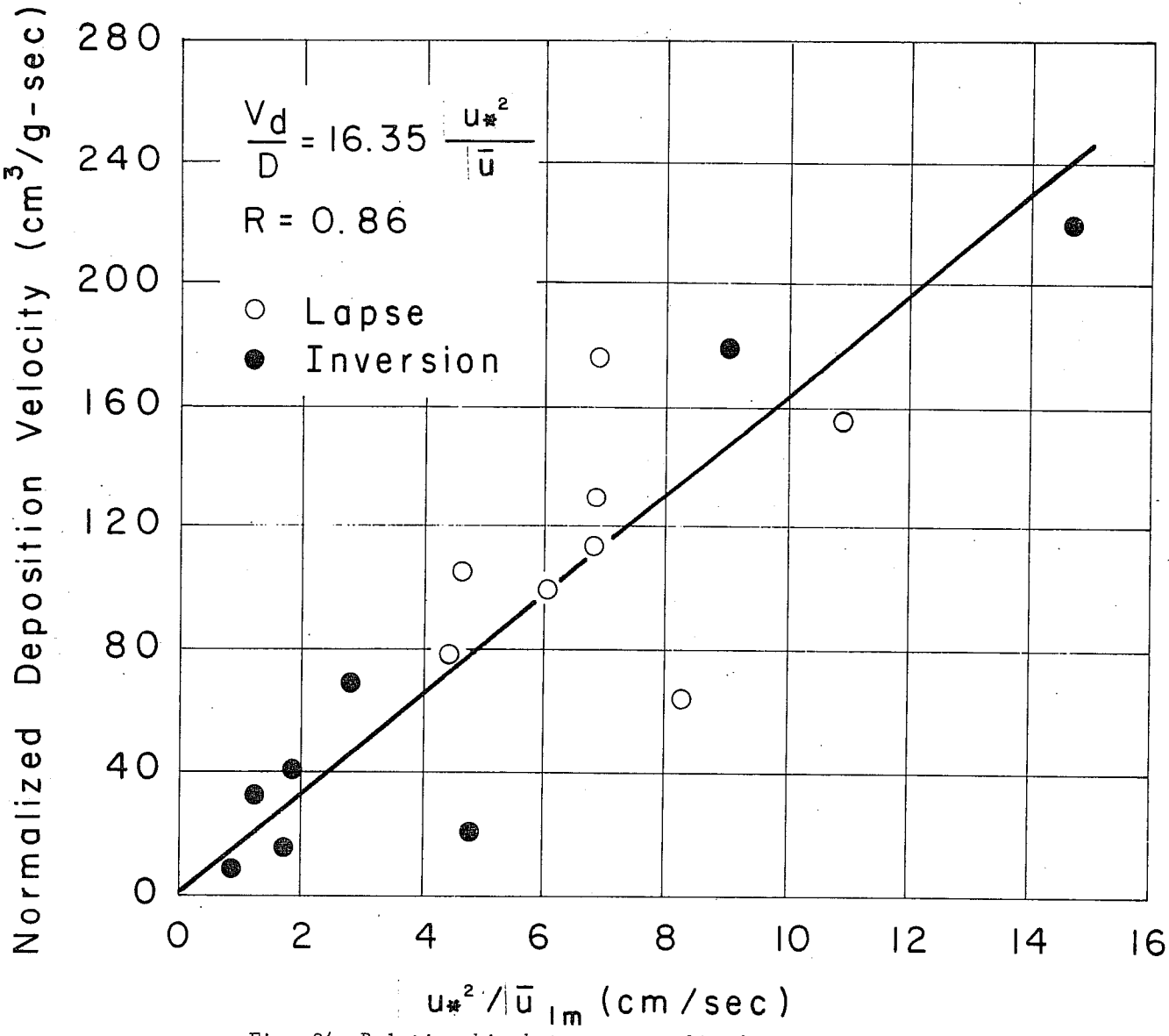

Fig. 24. Relationship between normalized grass V_d and boundary layer transfer velocity.

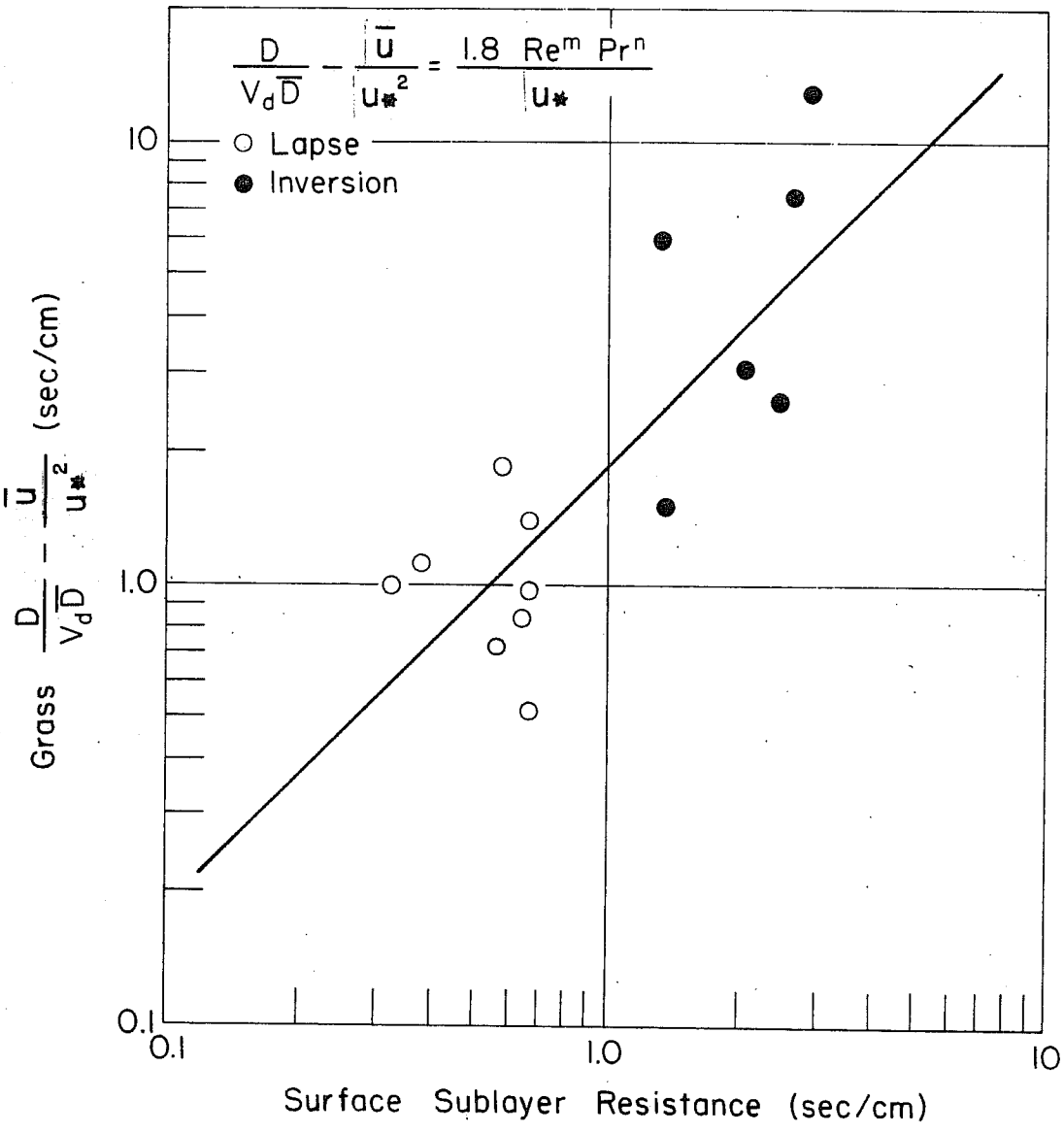

Fig. 25. Relationship between measured and calculated surface sublayer resistance - grass.

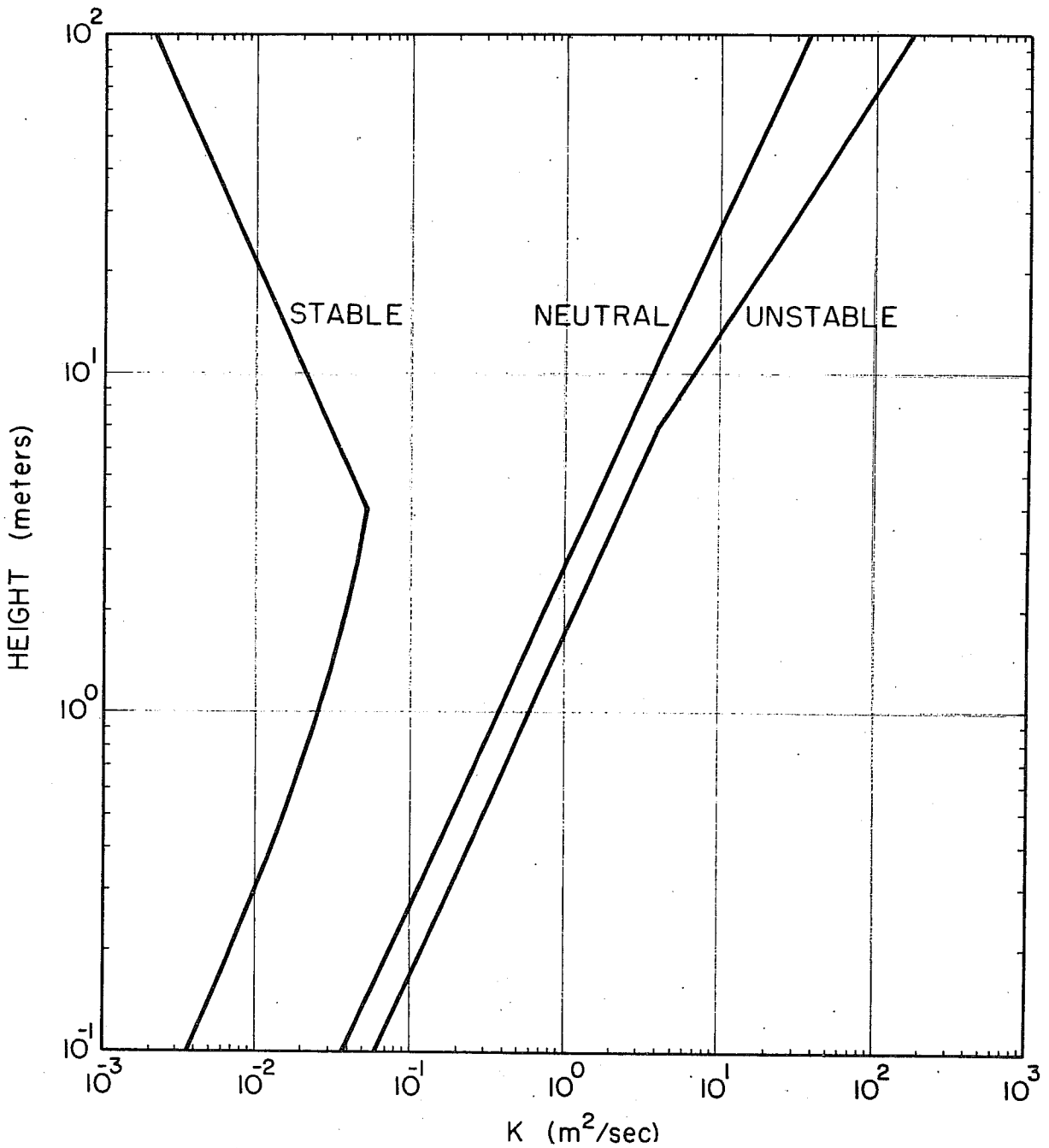

Fig. 26. Eddy diffusivity, K, profiles by stability class.

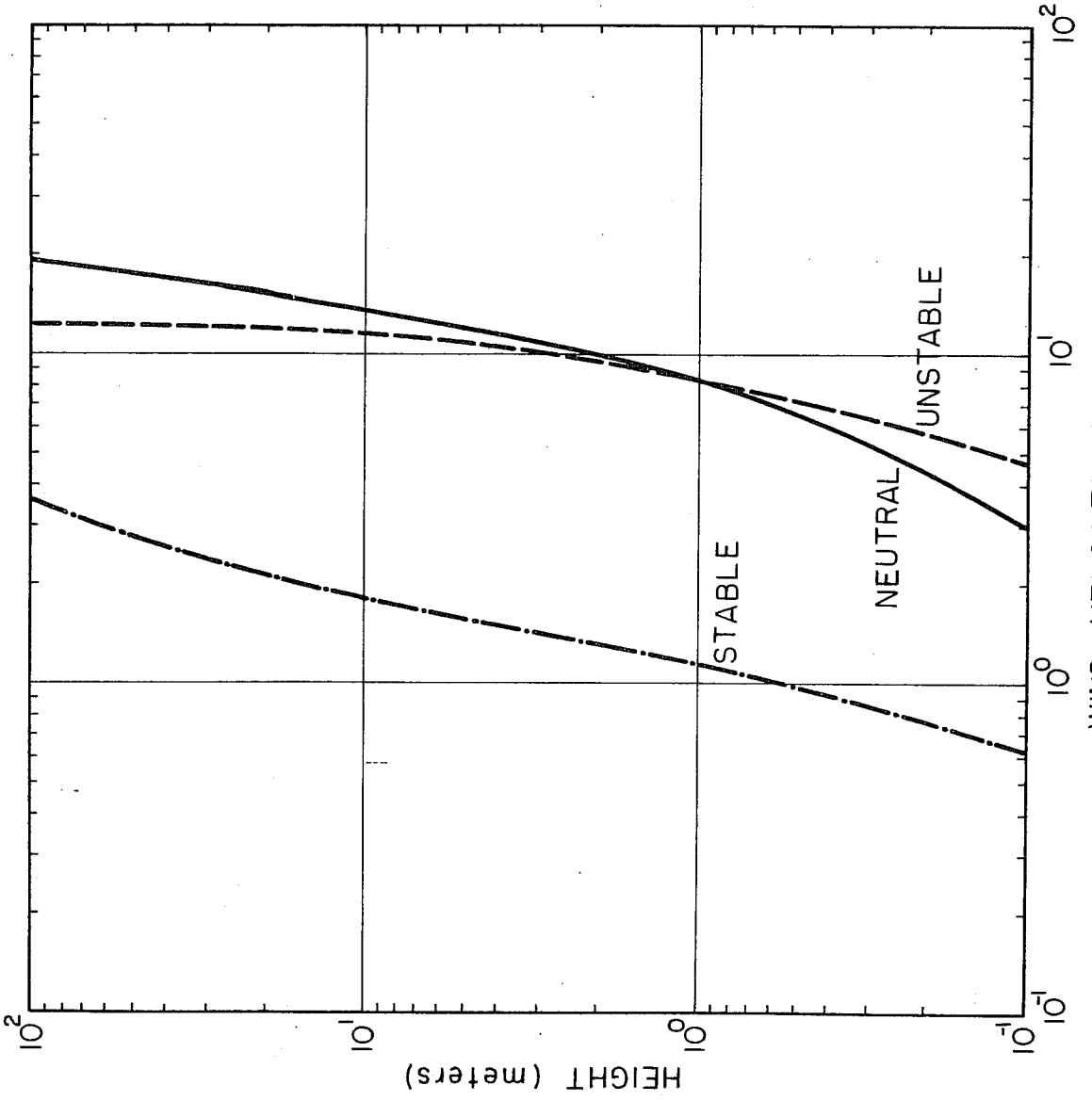

Fig. 27. Wind velocity profiles by stability class.

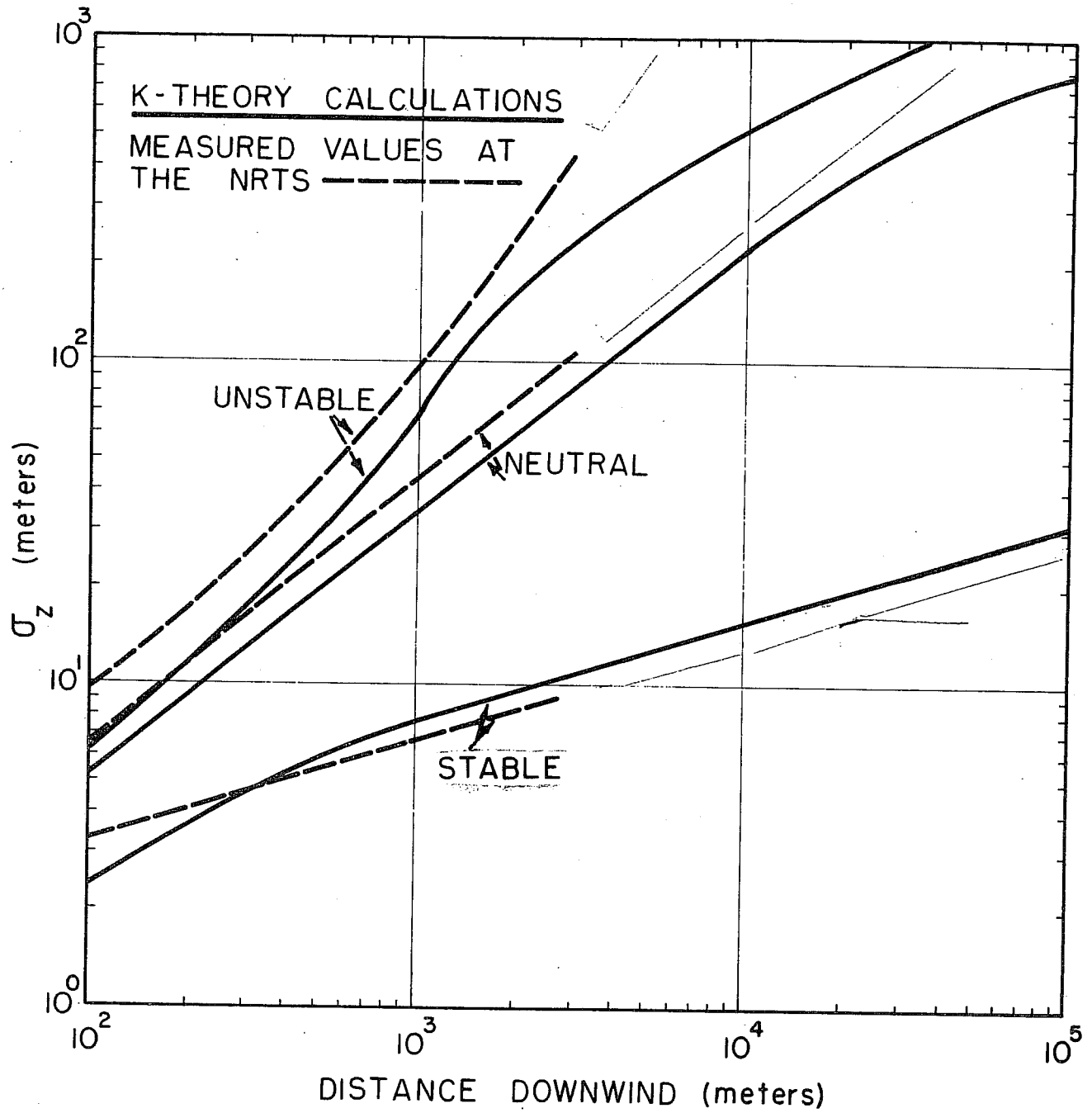

Fig. 28. Comparison of σ_z values by stability class and distance downwind.

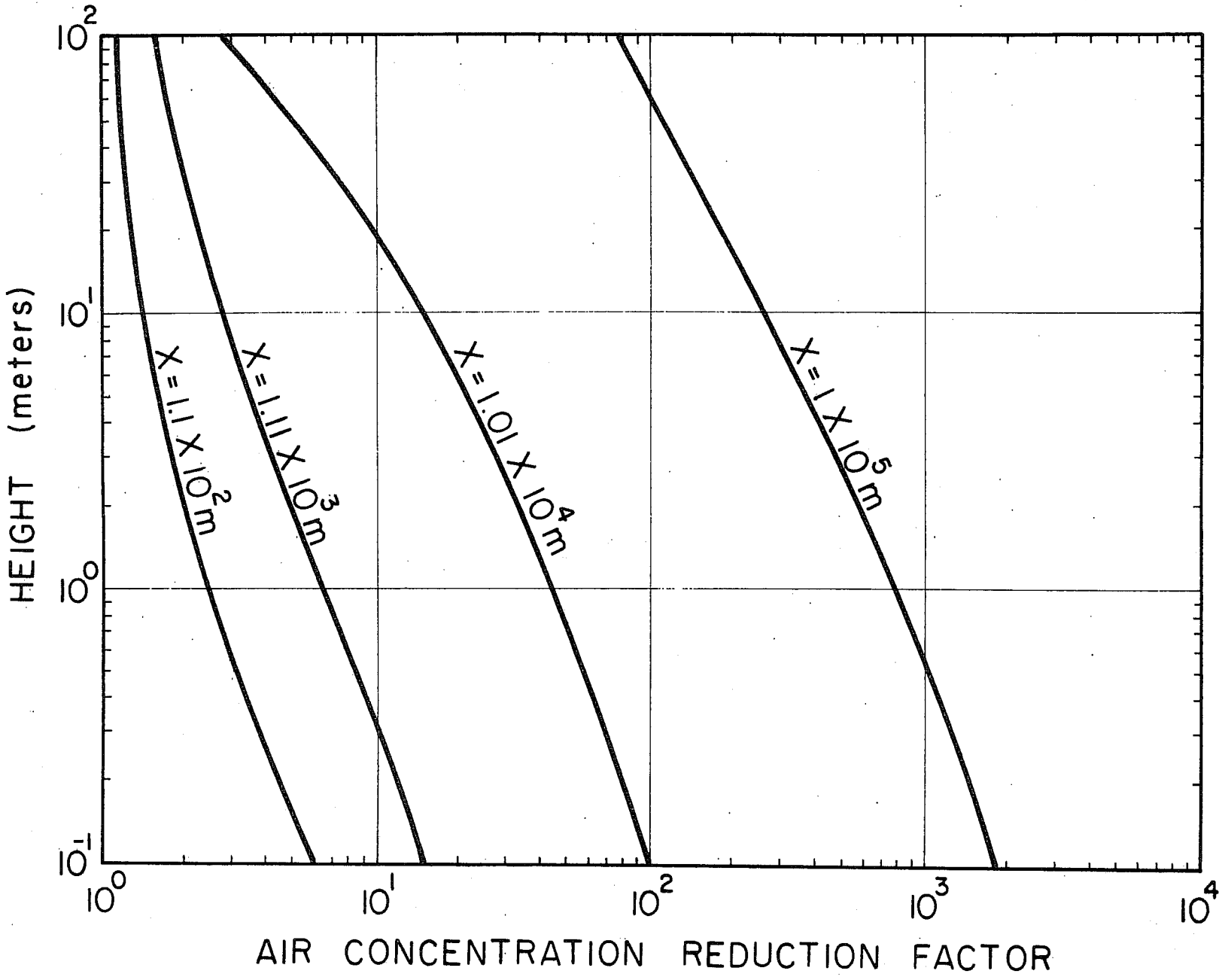

Fig. 29. Air concentration reduction factor variation with height for selected distance downwind - stable - perfect sink.

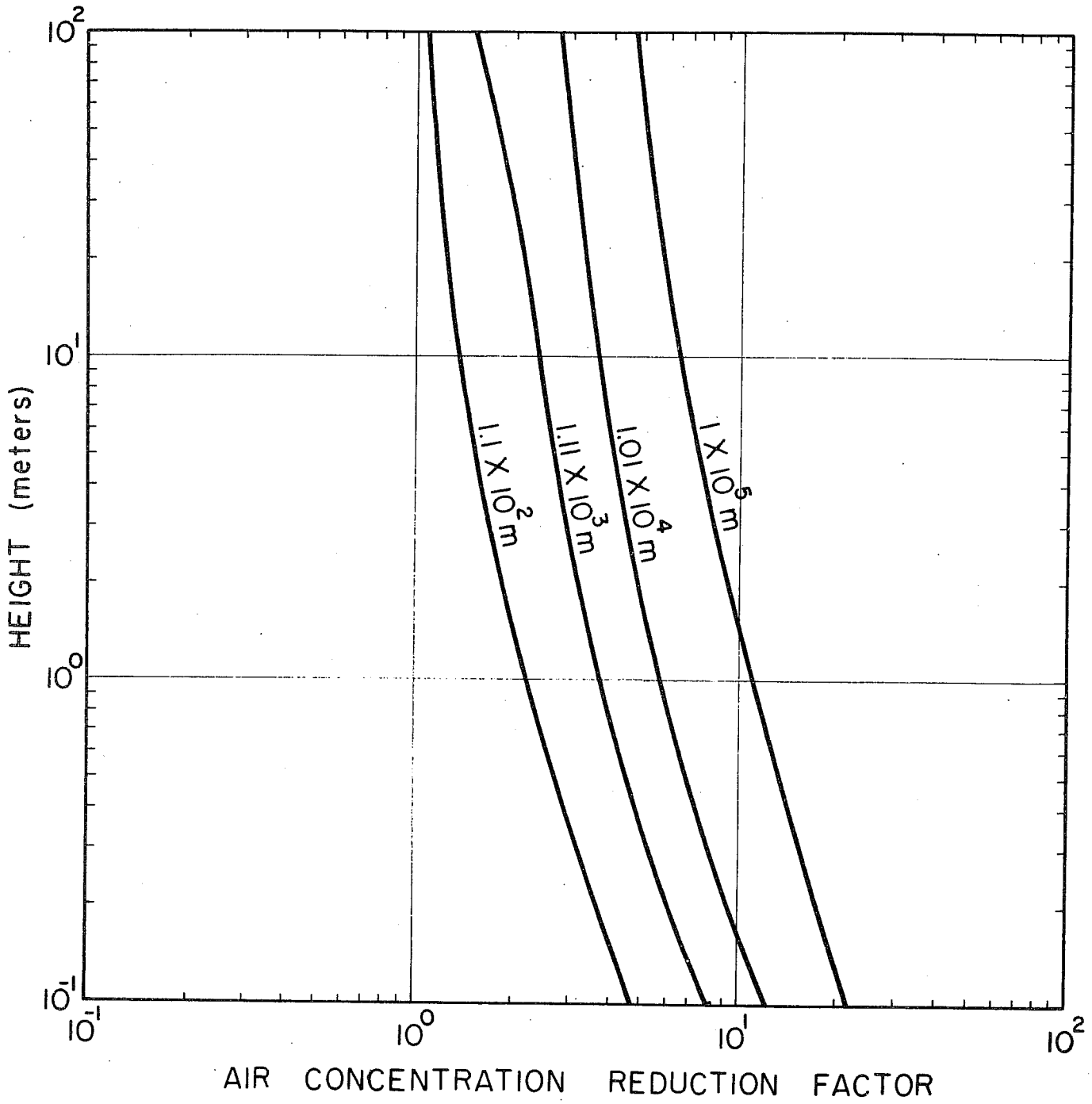

Fig. 30. Air concentration reduction factor variation with height for selected distances downwind - neutral - perfect sink.

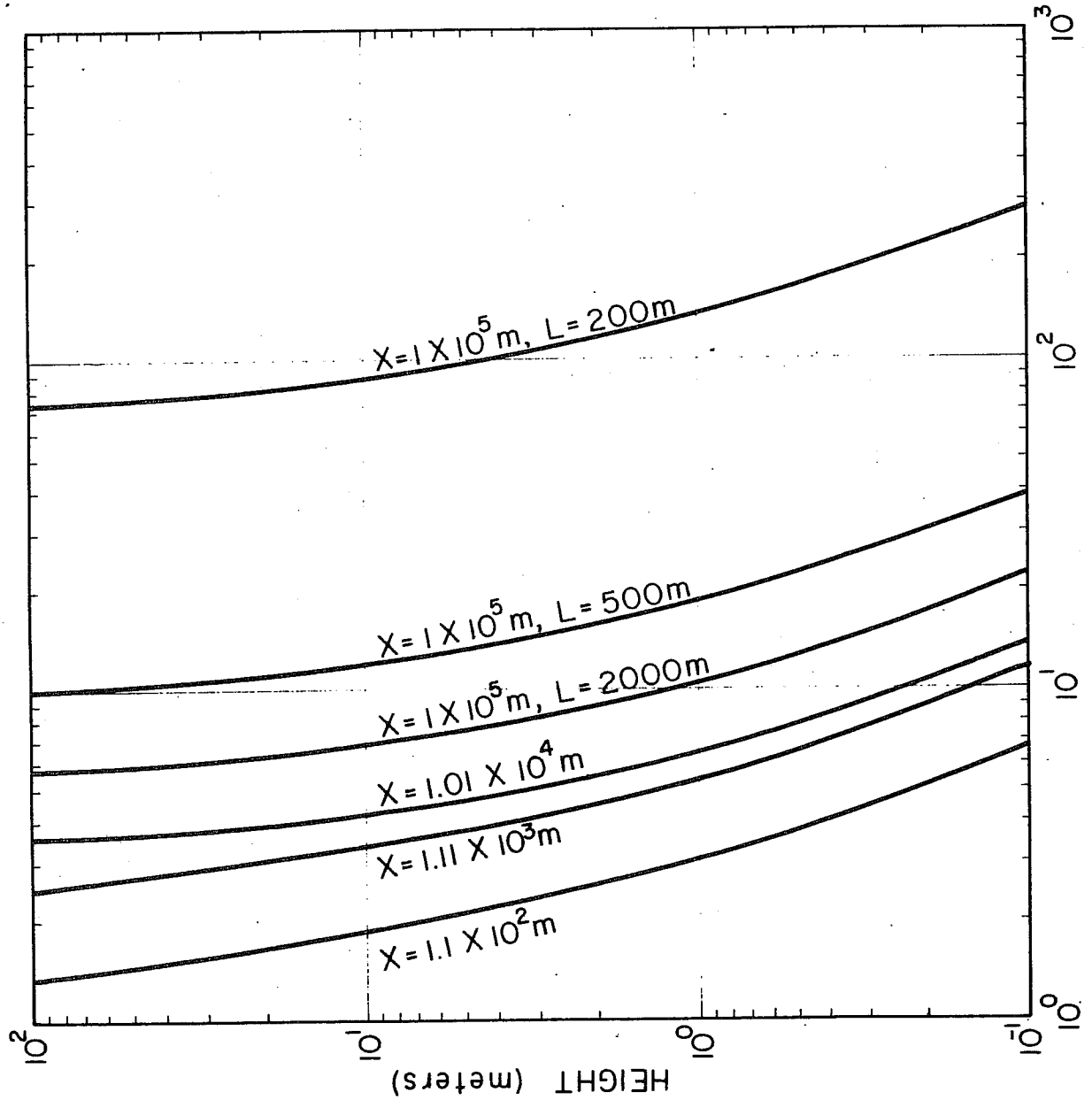

Fig. 31. Air concentration reduction factor variation with height for selected distances downwind - unstable - perfect sink.

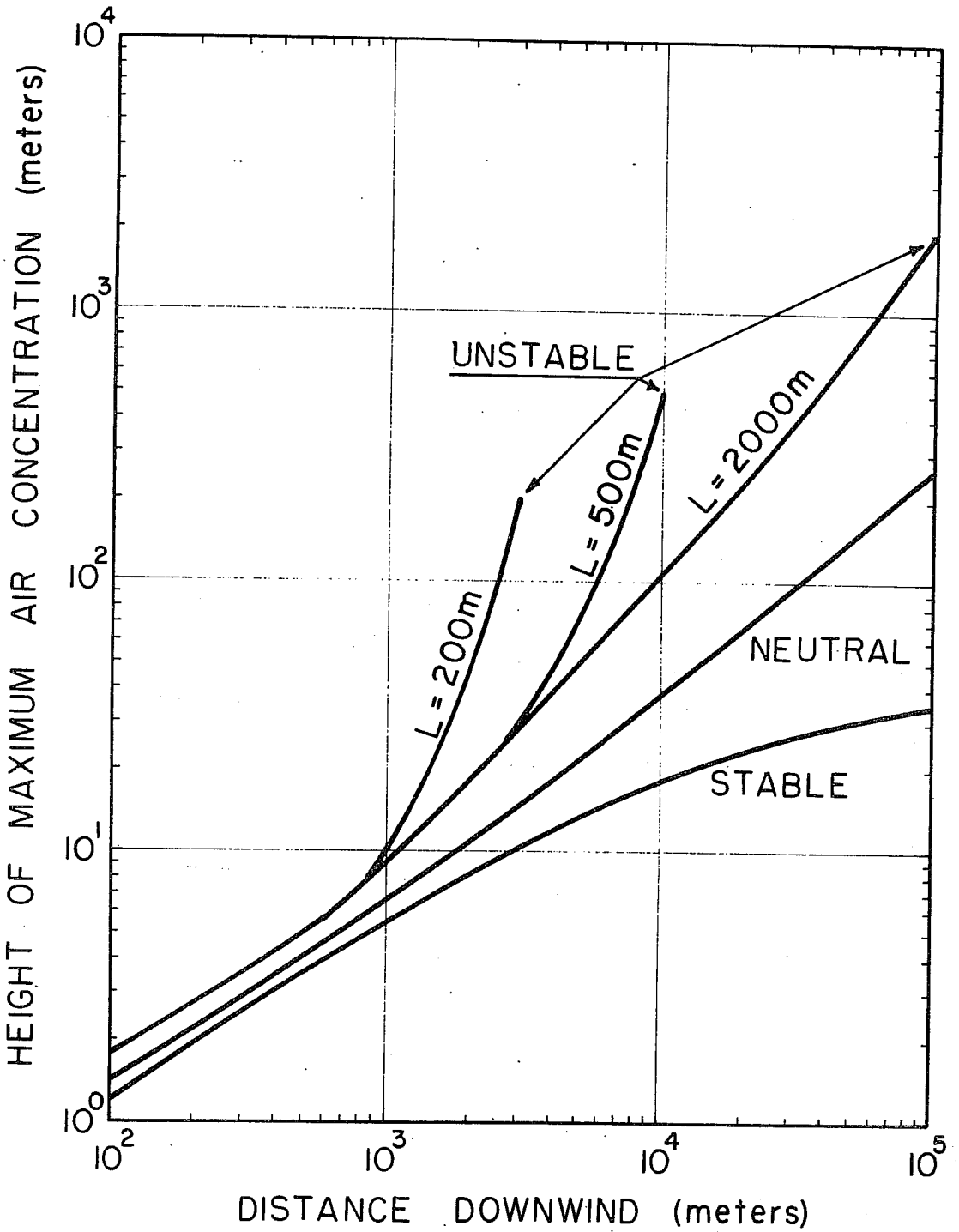

Fig. 32. Height of the maximum air concentration with distance downwind by stability class.

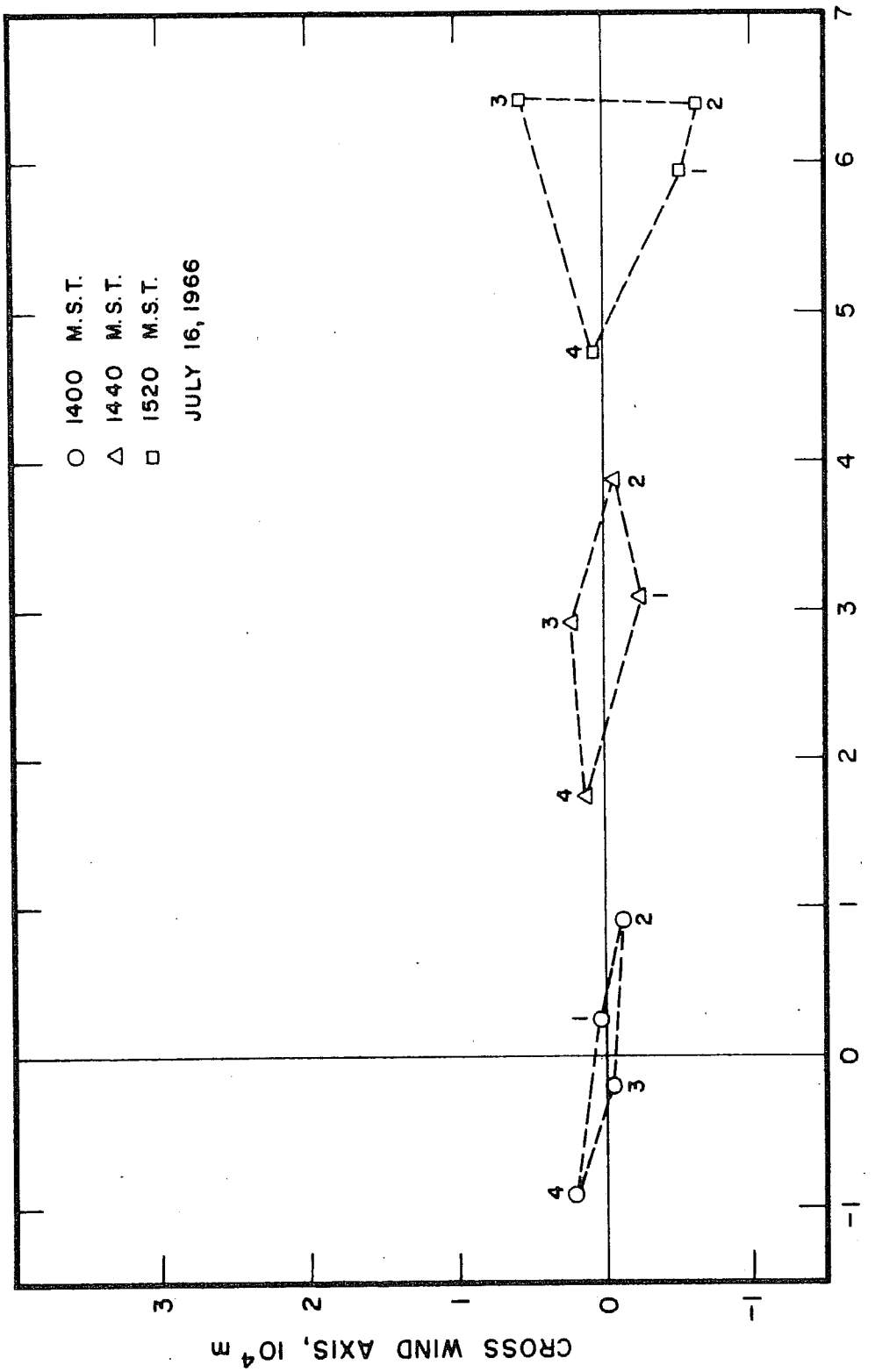

Fig. 33. Dispersion of a cluster of four tetroons in space and time.

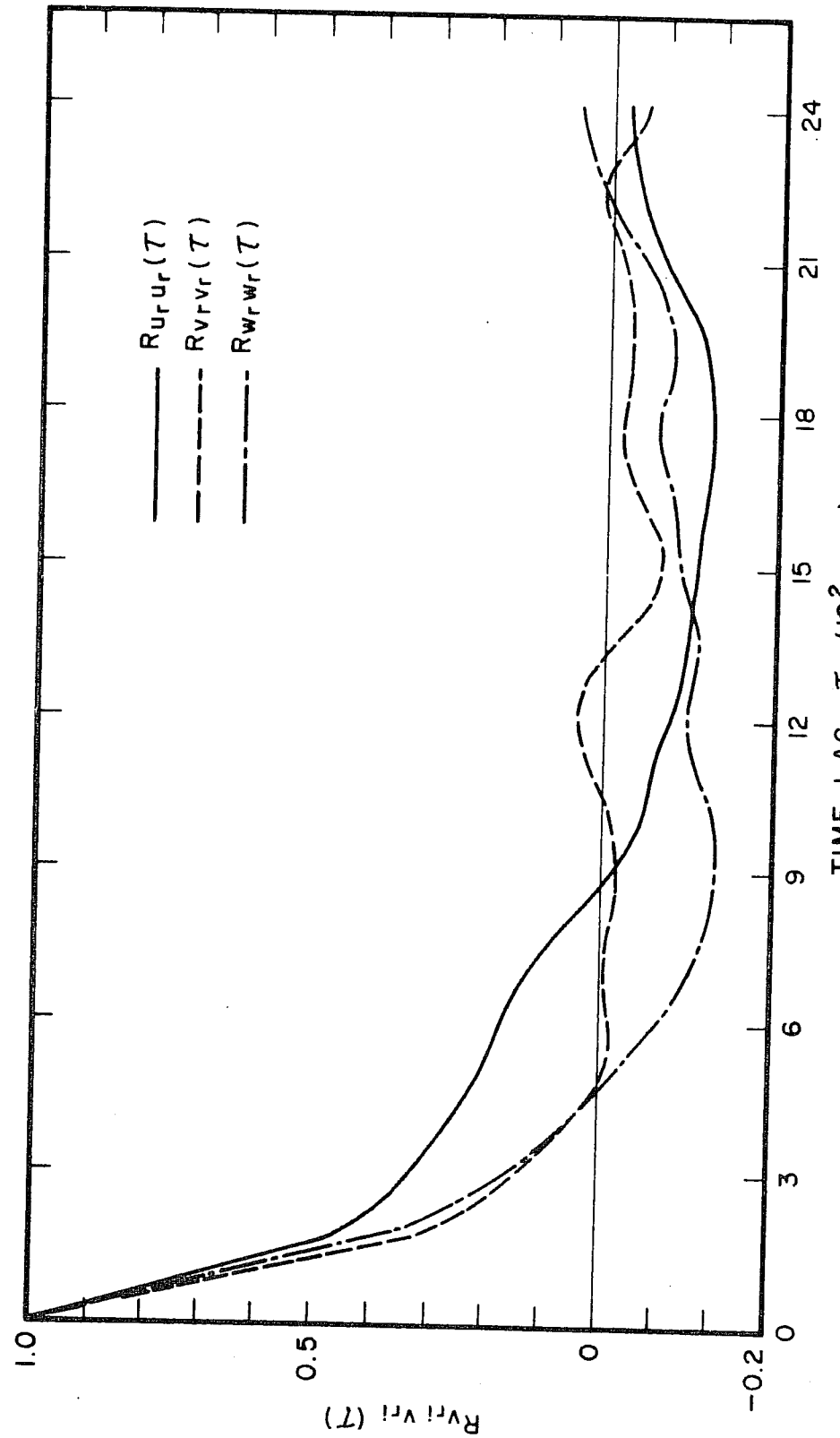

Fig. 34. Mean auto-correlation functions of the vertical, along- and cross-wind components of the relative velocities.

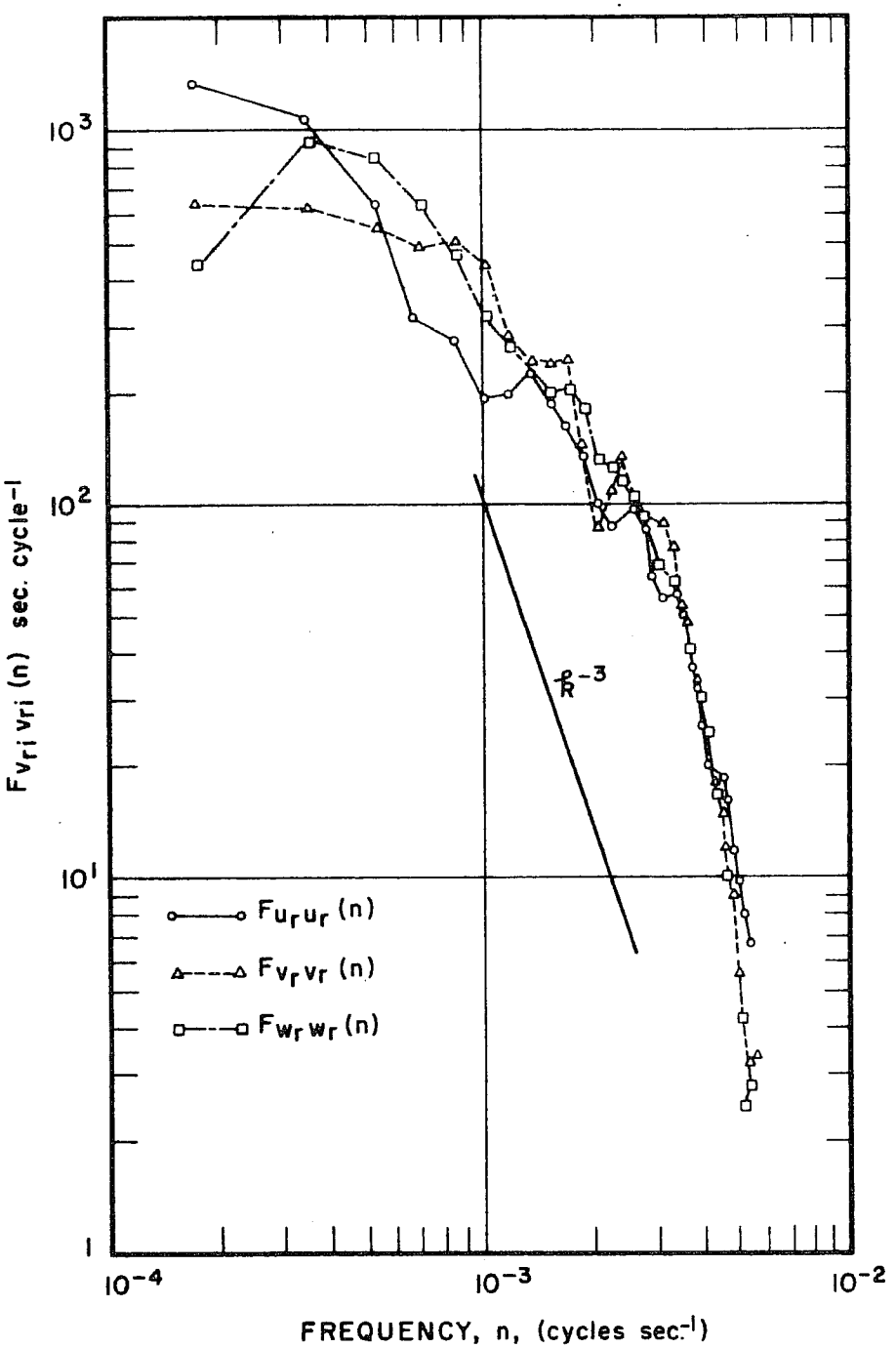

Fig. 35. Mean normalized power-spectra of the vertical, along- and cross-wind components of the relative velocities.

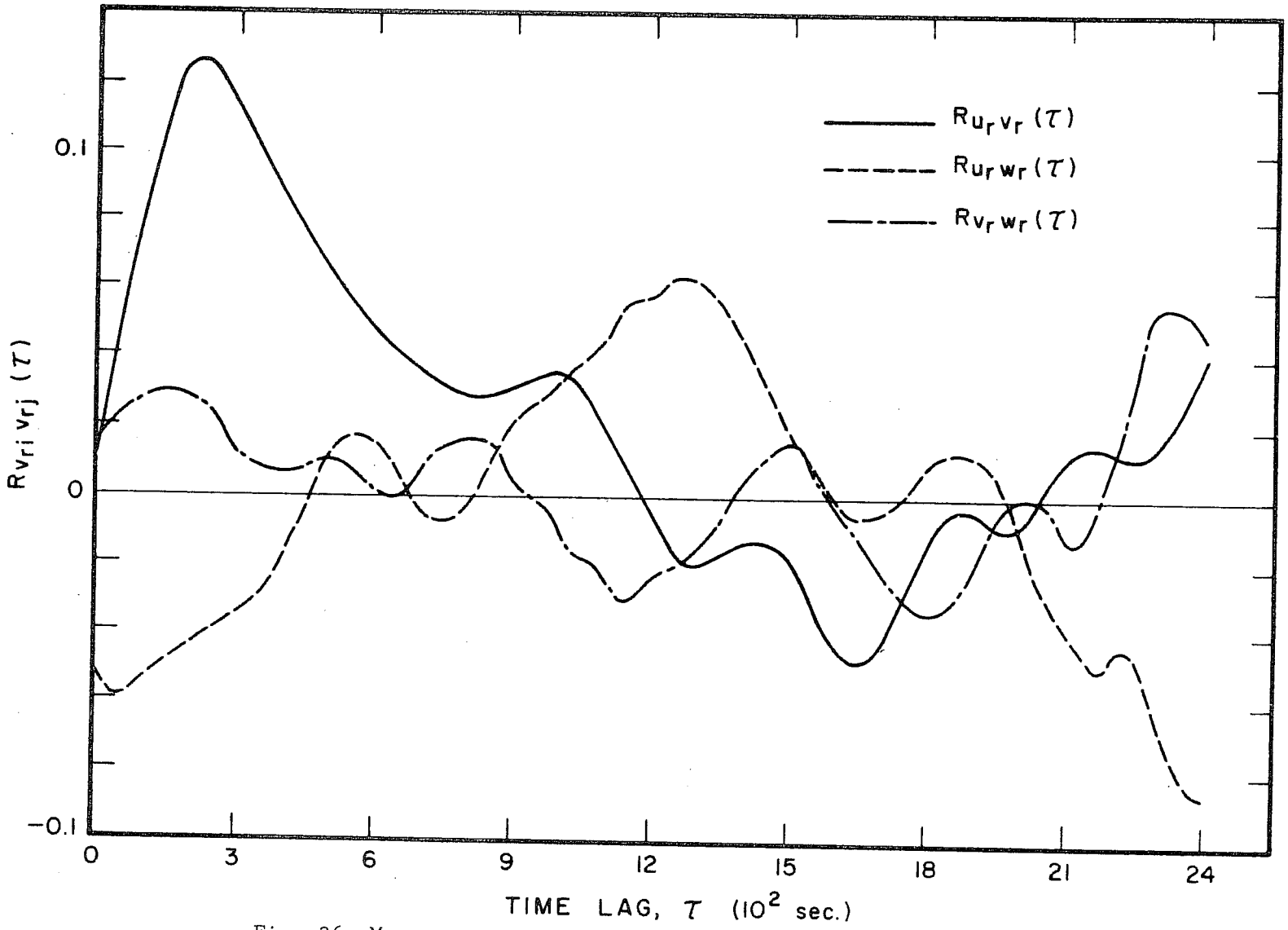

Fig. 36. Mean cross-correlation functions of the vertical, along- and cross-wind components of the relative velocities.

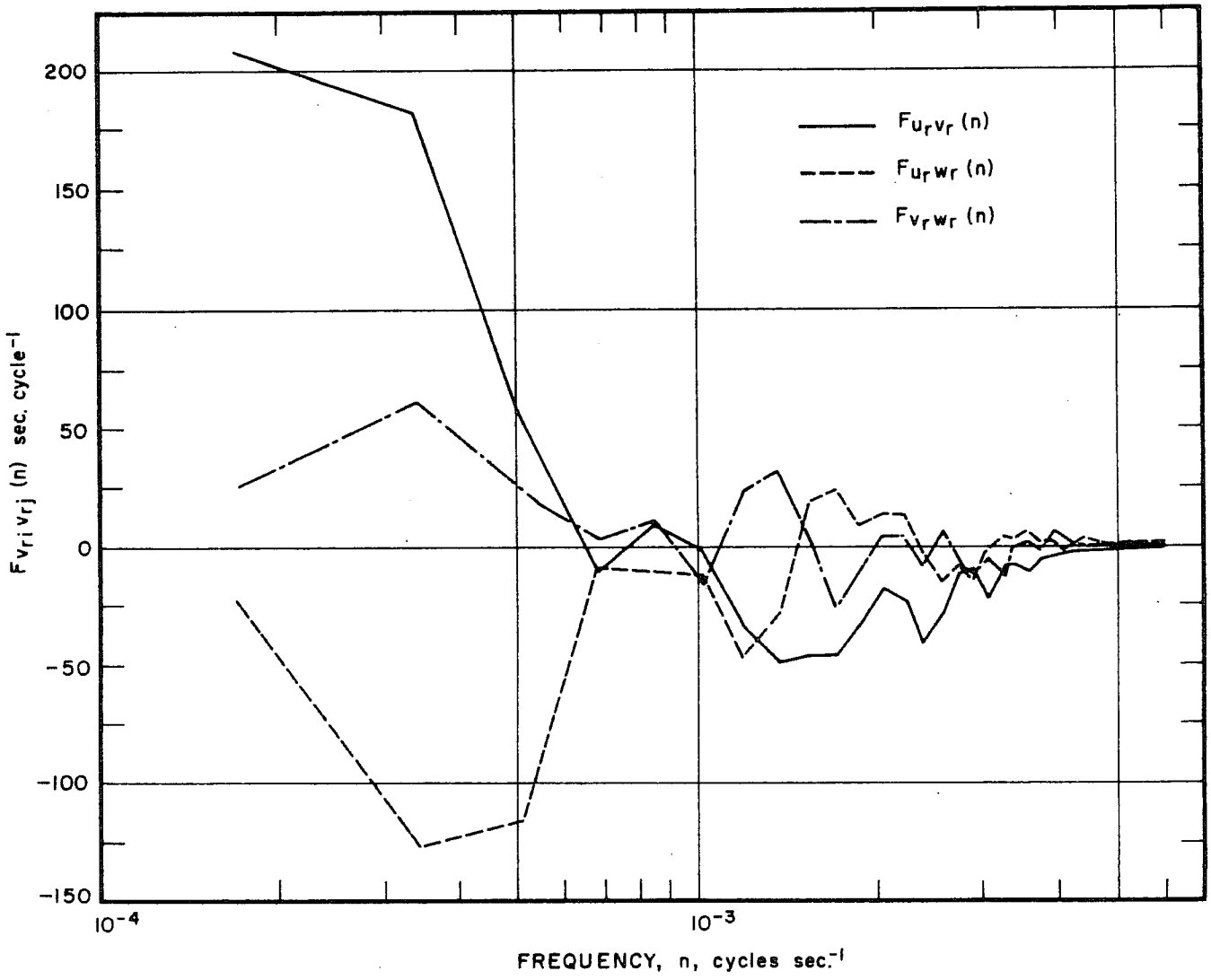

Fig. 37. Mean normalized cross-spectra of the vertical, along- and cross-wind components of the relative velocities.

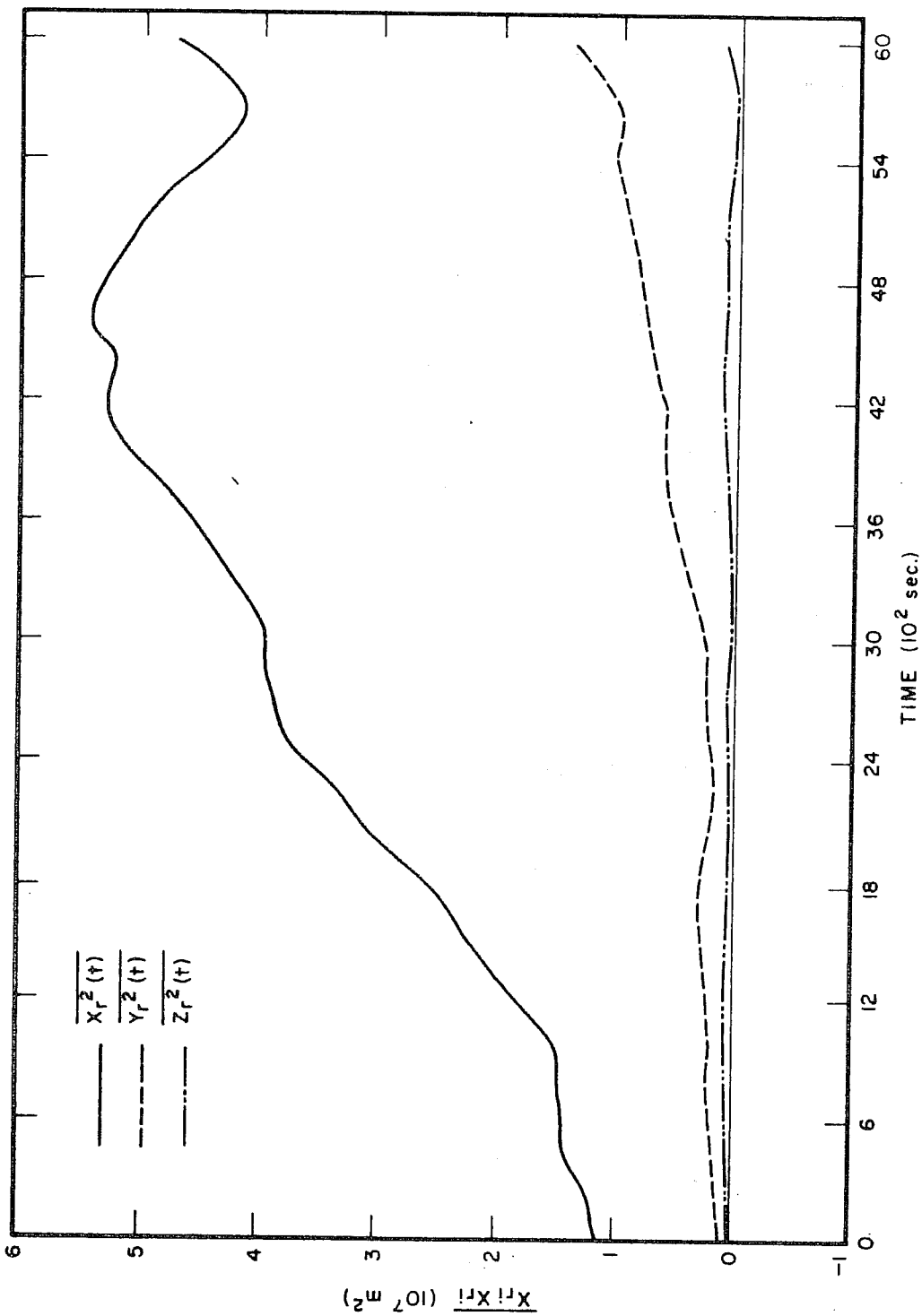

Fig. 38. Variances of vertical, along- and cross-wind components of the relative displacements.

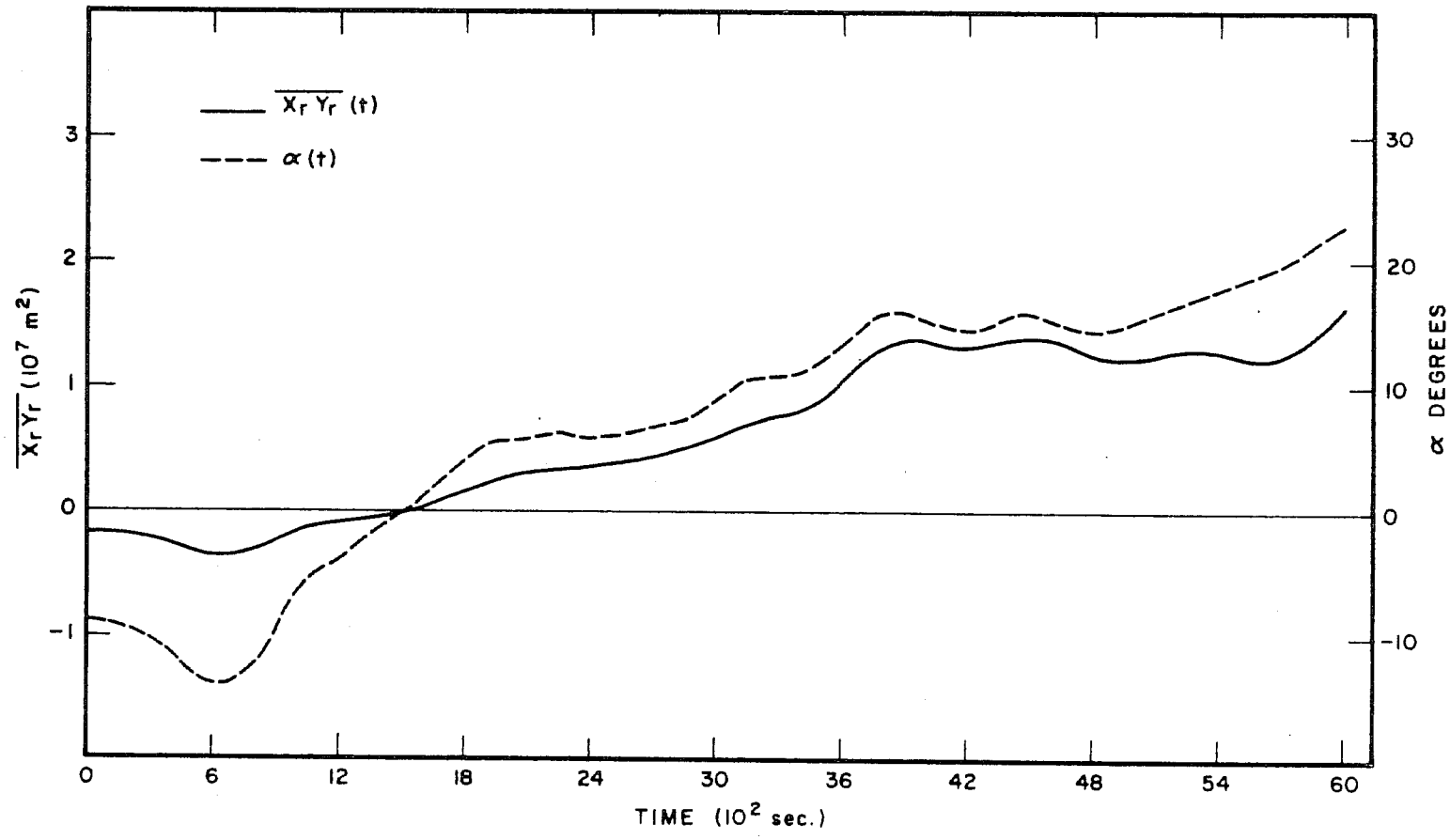

Fig. 39. Covariance of the along- and cross-wind components of the relative displacements, and the angle between the principal axis of diffusion and the direction of the mean wind.

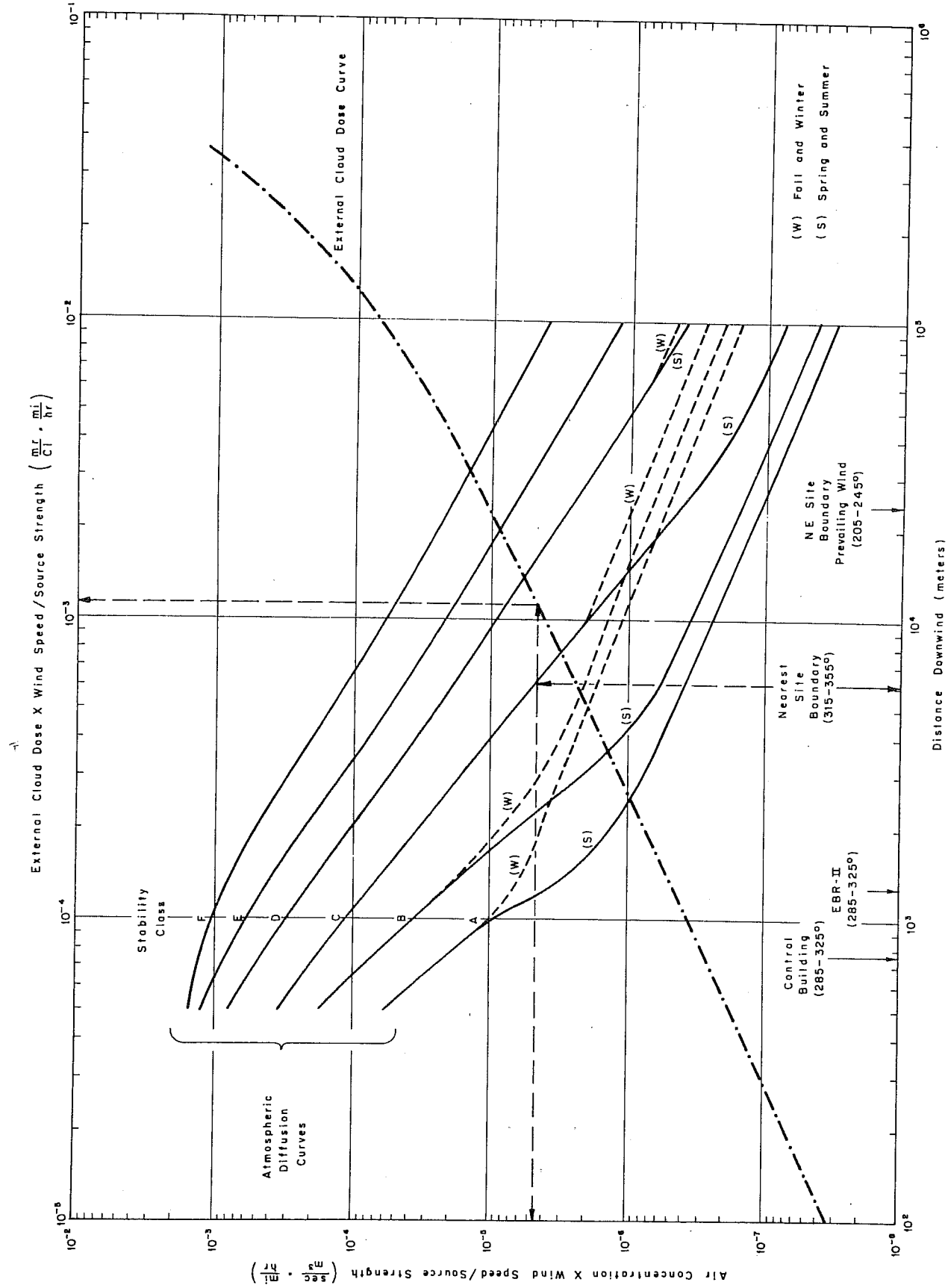

Fig. 40. Nomogram for environmental radiological calculations for TREAT.

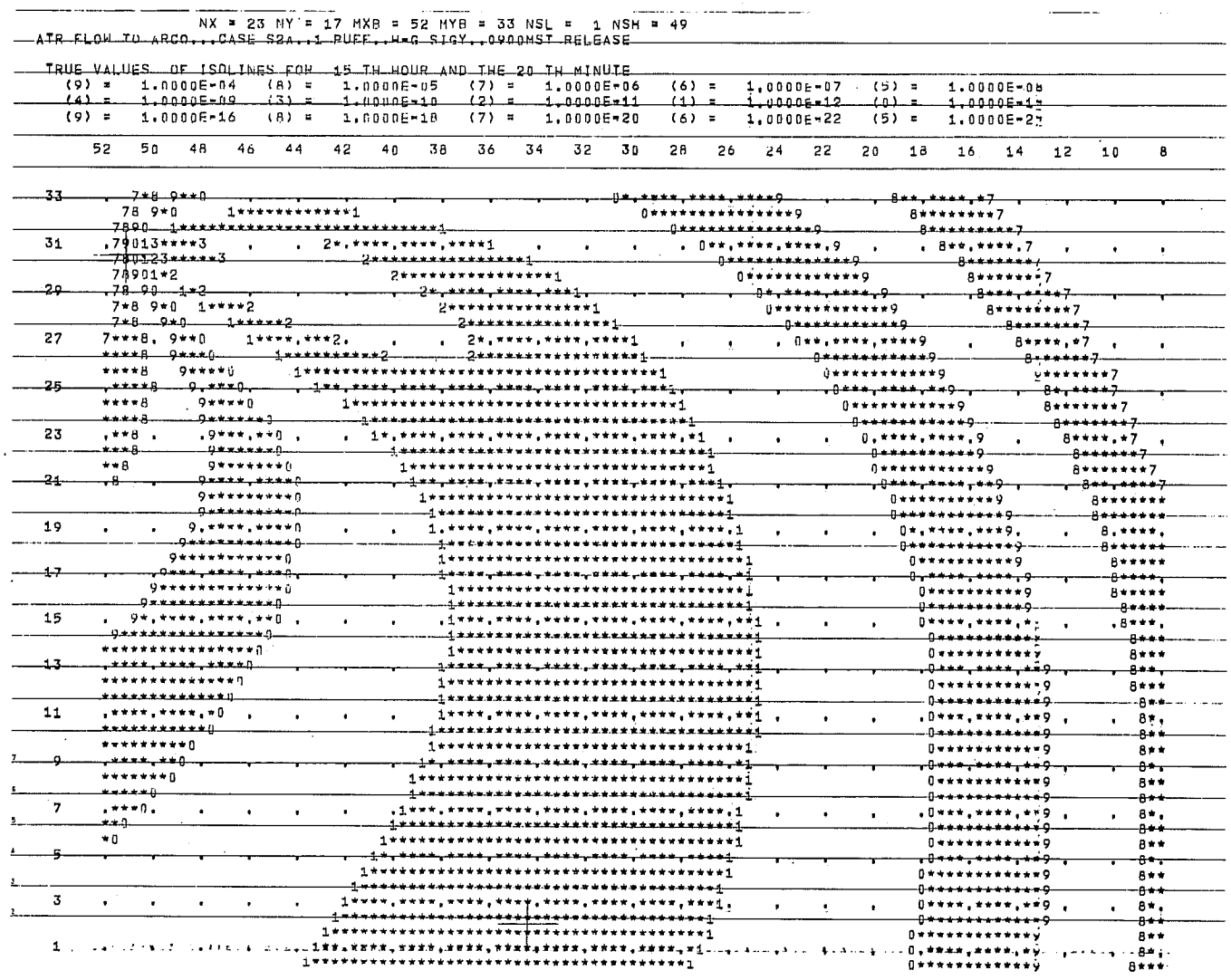

Fig. 41. Sample printout of computer analyzed concentration field.